# STUDY OF AN ABLE-MARS
# ENCOUNTER MISSION

NASW-246

(Review Draft)

August 31, 1962

SPACE TECHNOLOGY LABORATORIES, INC.
A Subsidiary of Thompson Ramo Wooldridge Inc.
One Space Park, Redondo Beach, California

# CONTENTS

I. SUMMARY OF STUDY . . . . . . . . . . . . . . . . . . . . . . . I-1

II. TRAJECTORY CONSIDERATIONS . . . . . . . . . . . . . . . . . II-1

III. MIDCOURSE GUIDANCE . . . . . . . . . . . . . . . . . . . . . III-1
  A. UNCORRECTED MISS . . . . . . . . . . . . . . . . . . . . . III-1
  B. MIDCOURSE PHILOSOPHY . . . . . . . . . . . . . . . . . . . III-1
  C. CORRECTION TIMES . . . . . . . . . . . . . . . . . . . . . III-6
  D. REORIENTATION EFFECTS . . . . . . . . . . . . . . . . . . III-7
  E. TIME-OF-FLIGHT CONTROL . . . . . . . . . . . . . . . . . III-16
  F. VELOCITY REQUIREMENTS . . . . . . . . . . . . . . . . . . III-17

IV. TRACKING STUDIES . . . . . . . . . . . . . . . . . . . . . . IV-1

V. THE ASTRONOMICAL UNIT AND PHYSICAL CONSTANTS . . V-1
  A. ASTRONOMICAL UNIT . . . . . . . . . . . . . . . . . . . . V-1

VI. RELATIVE EFFECTS OF ERROR SOURCES . . . . . . . . . . VI-1
  A. EXECUTION ERRORS . . . . . . . . . . . . . . . . . . . . VI-1
  B. TRACKING . . . . . . . . . . . . . . . . . . . . . . . . . VI-1
  C. PHYSICAL CONSTANTS . . . . . . . . . . . . . . . . . . . VI-2

VII. COMMUNICATIONS SUBSYSTEM . . . . . . . . . . . . . . . . VII-1
  A. REQUIREMENTS . . . . . . . . . . . . . . . . . . . . . . VII-1
  B. GENERAL DESCRIPTION . . . . . . . . . . . . . . . . . . VII-1
  C. TELEMETRY POWER BUDGET . . . . . . . . . . . . . . . . VII-3
  D. COMMAND POWER BUDGET . . . . . . . . . . . . . . . . . VII-5
  E. SPACECRAFT EQUIPMENT . . . . . . . . . . . . . . . . . . VII-9

VIII. MISS DISTANCE MEASUREMENT . . . . . . . . . . . . . . . VIII-1
  A. SENSING SYSTEM . . . . . . . . . . . . . . . . . . . . . VIII-2
  B. PROCESSING ELECTRONICS . . . . . . . . . . . . . . . . . VIII-5
  C. ACCURACY . . . . . . . . . . . . . . . . . . . . . . . . . VIII-6
  D. SIZE, WEIGHT, AND POWER . . . . . . . . . . . . . . . . VIII-6

IX. MARS ENCOUNTER SPACECRAFT DESIGN . . . . . . . . . . IX-1

# ILLUSTRATIONS

II-1 Launch Velocity and Transmission Distance Contours for 1964 II-2

II-2 V Infinity at Mars and Transmission Distance Contours for 1964 II-3

II-3 Launch Velocity and Transmission Distance Contours for 1966-67 II-4

II-4 V Infinity at Mars and Transmission Distance Contours for 1966-67 II-5

II-5 Maximum and Minimum Launch Velocities for 1964 II-7

II-6 Maximum and Minimum Launch Velocities for 1966-67 II-8

II-7 Heliocentric Plot of a 1964 Trajectory II-11

II-8 Heliocentric Plot of a 1967 Trajectory II-12

II-9 Approach Geometry for a 1964 Trajectory II-13

II-10 Approach Geometry for a 1967 Trajectory II-13

II-11 Definition of Impact Parameter Components II-14

III-1 Injection Sensitivities (1964) III-2

III-2 One-Sigma Uncorrected Miss Ellipse (1964) III-3

III-3 Midcourse Sensitivities (1964) III-4

III-4 Midcourse Sensitivities with Spin-Axis Pointed Away from the Sun (1964) III-8

III-5 Reorientation for Midcourse Guidance III-11

III-6 Angle Between Vernal Equinox and Projection of Spin Axis in the Ecliptic III-12

III-7 Definition of Rotations Required to Reorient the Spin Axis III-12

III-8 Possible Error in $\alpha_D$ as a Function of $\delta_D$ for Two Orientations III-14

III-9 Possible Error in $\delta_D$ as a Function of $\delta_D$ for Two Orientations III-14

III-10 Possible Error $\epsilon$ as a Function of $\delta_D$ for Two Different Orientations III-15

## ILLUSTRATIONS (Continued)

IV-1 One-Sigma Tracking Error Ellipses IV-4
IV-2 Tracking Errors as a Function of Time (no Midcourse Corrections) IV-5
IV-3 Impact Parameter Error as a Function of Time for Tracking after 80 Days IV-7
IV-4 AU Error as a Function of Time for Tracking after 80 Days IV-8
V-1 Change in Range Rate for an Error of Three Parts in $10^4$ Error in AU (1964 Trajectory) V-5
V-2 Change in $\dot{R}$ with AU Versus Time from Launch for Pioneer V V-6
V-3 Effects of a $3 \times 10^{-4}$ Change in AU with a 25 Mars Radii Nominal Impact Parameter V-7
VII-1 Communication Subsystem Simplified Block Diagram VII-2
VII-2 Transmitter Block Diagram VII-13
VII-3 Able-M Power Duty Cycle VII-15
VII-4 Receiver Block Diagram VII-17
VII-5 Block Diagram of Antenna Group for Able-M Bus Spacecraft VII-19
VII-6 Sketch Showing High-Gain Horn Antenna and Omni-Directional Sleeve-Dipole Antenna for use on the Able-M Bus Spacecraft VII-20
VII-7 Horn Antenna Gain Versus Look Angle and Relative Required Gain Versus Look Angle for the Able-M Bus Spacecraft VII-21
VII-8 Digital Telemetry Unit VII-24
VII-9 Command Decoder Block Diagram VII-26
IX-1 Mars Encounter Spacecraft IX-2

# TABLES

| | | |
|---|---|---|
| II-1 | Trajectory Characteristics | II-10 |
| III-1 | 1964 Injection Covariance Matrix | III-2 |
| III-2 | 1964 235-Day Trajectory Injection Sensitivities | III-3 |
| III-3 | Covariance Matrix of Impact Parameter and Time of Flight Errors | III-5 |
| III-4 | Midcourse Sensitivities with Nominal Spin Axis Orientation (for 1964) | III-5 |
| III-5 | Midcourse Sensitivities with Spin Axis Oriented Away from Sun at Each Firing (for 1964) | III-9 |
| III-6 | Midcourse Sensitivities with Spin Axis Oriented Away from Sun at 160 Days (for 1964) | III-17 |
| III-7 | Comparison of Flight Time Sensitivity to Impact Parameter Sensitivity | III-17 |
| III-8 | Covariance Matrix of Midcourse Correction Velocity (1964) | III-18 |
| III-9 | Midcourse Procedures | III-19 |
| IV-1 | Tracking Data Rates and Data Accuracies Assumed for 1964 | IV-2 |
| IV-2 | Covariance Matrices of Tracking Error In Impact Parameter and Time of Flight | IV-2 |
| IV-3 | Covariance Matrices of Velocity Measurement Error at Time of First Correction for 1964 | IV-3 |
| V-1 | Measurements of the AU in Terms of Solar Parallax | V-2 |
| VI-1 | Final Accuracy | VI-3 |
| VII-1 | Able-M Telemetry Power Budget | VII-6 |
| VII-2 | Able-M Command Power Budget | VII-8 |
| VII-3 | Spacecraft Equipment | VII-10 |
| IX-1 | Able-M Bus Plus NASA Capsule | IX-4 |

# I. SUMMARY OF STUDY

The results of a study by STL for NASA/Goddard to determine feasibility of using the Able-M spacecraft as a bus for a Mars entry capsule are reported here. The principal objective is to achieve an impact on Mars in 1964 and 1966-67. STL's primary task was to estimate the accuracy requirements and to determine the capability of the spin stabilized Able-M spacecraft for achieving them. Therefore, a considerable portion of this study has been devoted to trajectories, midcourse guidance, and the physical constants which affect accuracy. In addition, the required modifications to the Able-M spacecraft have been examined, a spacecraft communications system has been designed, and the problem of determining the distance by which the spacecraft misses Mars has also been considered.

In addition to these general objectives, the following specific constraints were placed on the study;

1) The capsule entry velocity at Mars should be less than 25,000 ft/sec

2) The communication distance should be minimized

3) The Deep Space Instrumentation Facility should be used

4) The miss distance should be measured

5) Mission opportunities in both 1964 and 1966-67 should be examined. A five shot set (2 in 1964 and 3 in 1966-67) were to be assumed. The earlier shots are intended largely to establish physical constants and confidence in the system.

Within these constraints, STL has examined the over-all mission to determine the minimum modifications to the Able-M spacecraft required to achieve an impact at Mars. A large number of trajectories were run analytically to discover those which met the launch velocity and communications distance requirements, and at the same time the required approach velocity for both the 1964 and the 1966-67 time eras. Two specific trajectories which met constraints were then searched in on a precise trajectory program and studied, one for 1964 and one for 1966. Once suitable runs were found by the search program, the miss coefficients for injection errors were derived and the statistics of the "uncorrected miss" determined using Atlas-Agena-ABL 248 burnout conditions. At the same time the orientation of the spin axis along the trajectory was determined and possible correction times studied. This is done by computing the effect of a velocity kick along the spin axis in the impact parameter plane-a hypothetical plane passing through the center of Mars and oriented perpendicular to the asymptotic approach velocity to Mars ($V_\infty$). Nominal correction times are then computed, that is times when thrusting along the spin axis will be most efficient both in terms of fuel consumption and accuracy. For the 1964 trajectory, the early correction at about 2 days tends to correct out the major components of errors. However, since there are execution errors, the spacecraft will be tracked for a few days and then a small vernier correction will be applied.

On a spin stabilized spacecraft, a second major correction is required later in the journey to correct out other components of miss. Trajectory sensitivities are computed to determine when another correction along the spin will reduce the remaining components of miss. This second correction for the 1964 trajectory will occur in about 60 days and will also be followed by a small vernier at about 80 days.

The attitude is not known precisely, and the first midcourse correction will be in error by the effect of the attitude error. Therefore, the spacecraft will be tracked between corrections, the error in attitude determined and this information utilized in computing the second correction. To evaluate the ultimate accuracy of this technique, execution errors and attitude errors were evaluated. Then tracking runs were made assuming the three DSIF tracking stations were used. In addition, the effect of the error in our knowledge of the astronomical unit (AU) was also evaluated. These errors were then considered in terms of the possible effect of the reorientation maneuver, used to increase communications capability, and also for alternate reorientation maneuvers in an attempt to increase impact probability.

The general conclusion is that the trajectories are slightly better in 1964 than they were in 1962 and that the probable miss exclusive of the AU error is less than 1.3 Mars radii ($3\sigma$). Since the uncertainty in our knowledge of the AU is possibly fairly large, we have assumed conservatively that it is good only to one part in $10^4$. Including this AU error, the $3\sigma$ miss may be as large as 7.5 Mars radii. However, the AU may be improved prior to the flight in 1964 (perhaps by Mariner R-2) and in any event it can be expected that the 1964 flights themselves should improve our knowledge of the AU by an order of magnitude.

Calculations were made of appropriate time of arrival correction after the reorientation maneuver (in 155 days), and it was determined that no difficulty would be encountered in insuring that Australia has the payload in sight as it impacts with Mars. Throughout the trajectory study primary effort was devoted to the 1964 mission since this presents the most difficult problems, particularly those associated with improving the AU. Specific powered flight trajectories were not analyzed nor effects of range safe azimuths investigated. However, these have small over-all effects.

A spacecraft communications system was studied which is compatible with the DSIF at 2300 mc. A number of alternative transmitters can be used which will supply the 25 watts required to transmit at least 1 bit/sec over 120,000,000 n mi (the required data for the spacecraft is 0.5 bits/sec excluding the data requirements of the miss distance indicator. A 30 percent efficient triode with a rather short lifetime, a modified TWT which is 25 percent efficient or the new Amplitron can be used as part of a recently designed STL transponder which will meet the tracking telemetry and command requirements with an excellent margin and with a very high probability success since the components are sufficiently light to be made redundant. In addition to two omni-directional antennas which provide approximately hemispheric coverage, an 8 lb horn antenna surrounds the aft hydrazine engine. This antenna, which has a 70 degree beam width, can provide coverage throughout most of the flight with a minimum gain of 5 lbs. Both the receiver and decoder are modified versions of equipment proven in the Able series. The digital telemetry unit, also the same as that proved on the Able series, will provide sufficient storage to take care of all miss distance data storage requirements.

Although tracking can be expected to provide a very accurate measure of miss, perhaps as good as ± one-tenth Mars radius, and perhaps so good as to make many other previously negligible errors predominant, an infrared miss distance indicator was also studied. It consists of thermistor bolometer mounted in the focal plane of a telescope with a $1^{\circ}$ field of view. The optical axis is rotated by the spinning of the spacecraft itself and by a constant speed revolving mirror which looks out the side of the spacecraft so that the field of view sweeps out $4\pi$ steradians. When it sweeps across Mars, a pulse whose width corresponds to the angular diameter is generated. It is expected that the accuracy of the measurement even at 15,000 n mi from Mars is less than one percent. It might be possible with a combination of tracking and the miss distance indicator to improve not only the AU measurement, but also the diameter of Mars at the same time. If two sensor units are used, one with a filter to detect $CO_2$ region and one at 6 to 11 microns, it appears reasonable to expect that the height of the Martian atmosphere may be measured and also the surface temperature.

## II. TRAJECTORY CONSIDERATIONS

The general characteristics of trajectories to Mars in the favorable periods of 1964 and 1966-67 were studied. The constraints placed on the trajectories for this mission are the following:

1) The transmission distance at impact should be minimized.
2) The approach velocity must be less than 24,000 feet per second, which is equivalent to 17,500 feet per second V infinity.

For a set of launch dates and times of flight, the resulting launch velocities, transmission distances, and approach velocities were calculated and plotted. These results were then cross-plotted to yield contours of constant launch velocity, constant transmission distance, and constant approach velocity, (V infinity) on coordinates of flight time and launch date. These contours are presented in Figures II-1 and II-2 for 1964 and in Figures II-3 and II-4 for 1966-67.

Figure II-1 shows that the minimum transmission distance for a 40,000 ft/sec injection velocity at 180 n mi altitude must be greater than 70,000,000 n mi. However, this velocity does not meet payload requirements. The maximum allowable injection velocity for a 450 lbs payload is about 38,800 ft/sec. In this velocity range, the minimum transmission distance is about 80,000,000 n mi. However, as can be seen from Figure II-2, a $V_\infty$ of 18,900, which corresponds to an approach velocity of 25,000 ft/sec, requires a minimum transmission distance of 100 million n mi. However, since midcourse corrections will affect the approach velocity substantially, a 24,000 ft/sec approach velocity has been used to insure that 25,000 ft/sec ($V_\infty$ 17,500 ft/sec) constraint will be met. Thus, the minimum transmission is always greater than 110 million n mi. Therefore, we have concentrated on trajectories which fall with the 110 to 120 million n mi trajectories. Referring to Figure II-1, we can see that there is a band of launch velocities and launch dates open for this

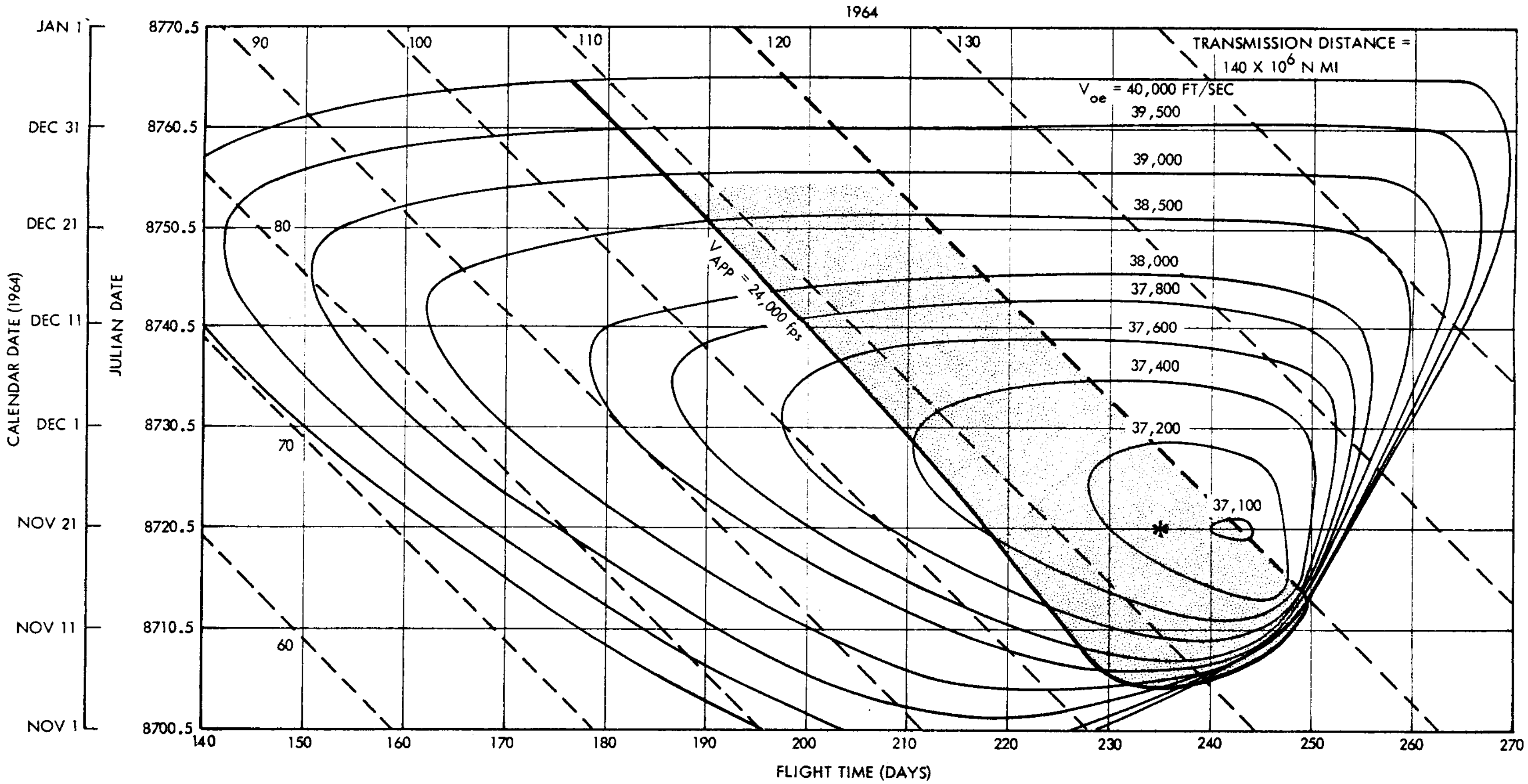

Figure II-1. Launch Velocity and Transmission Distance Contours for 1964

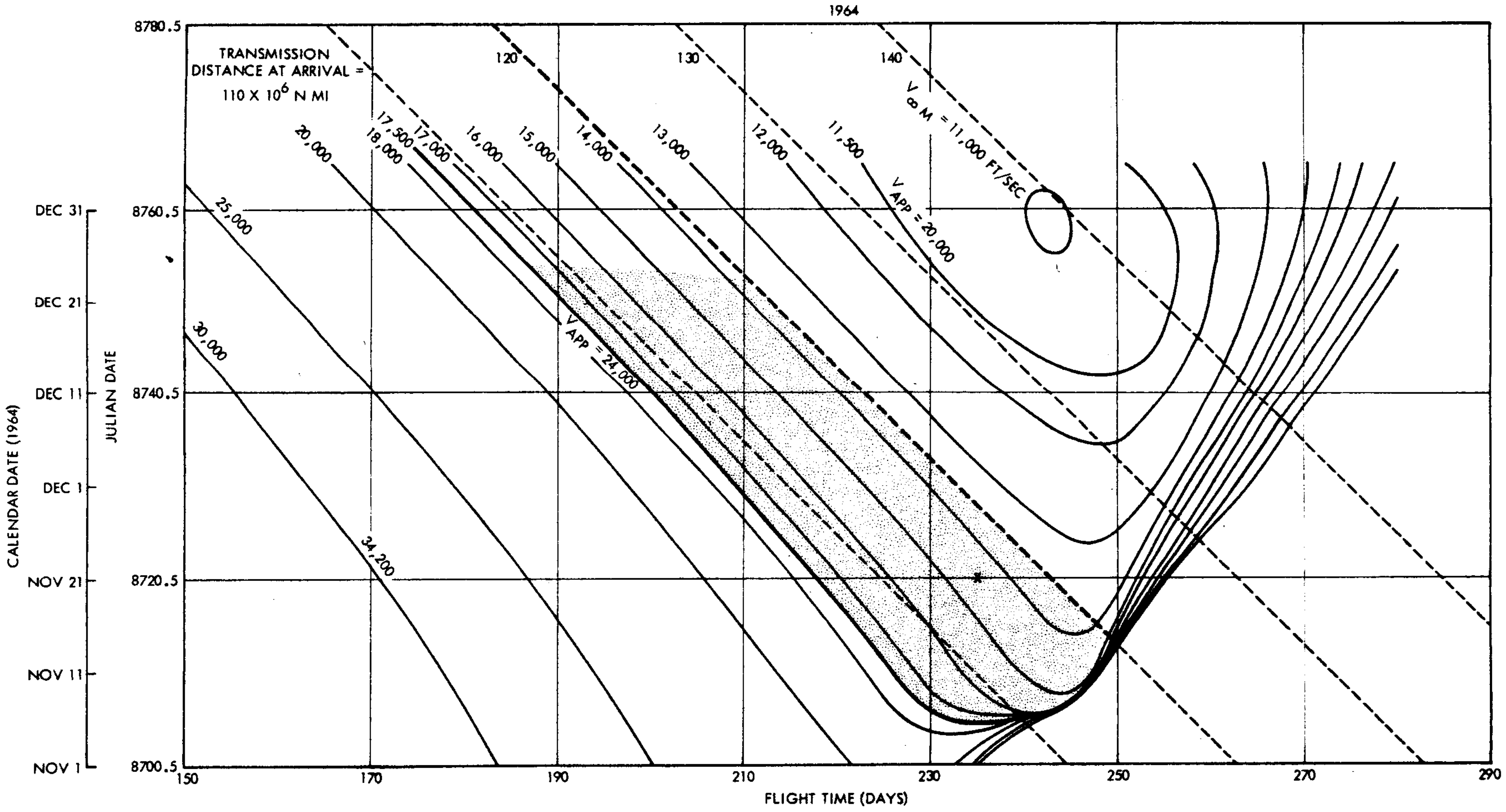

Figure II-2. Infinity at Mars and Transmission Distance Contours for 1964

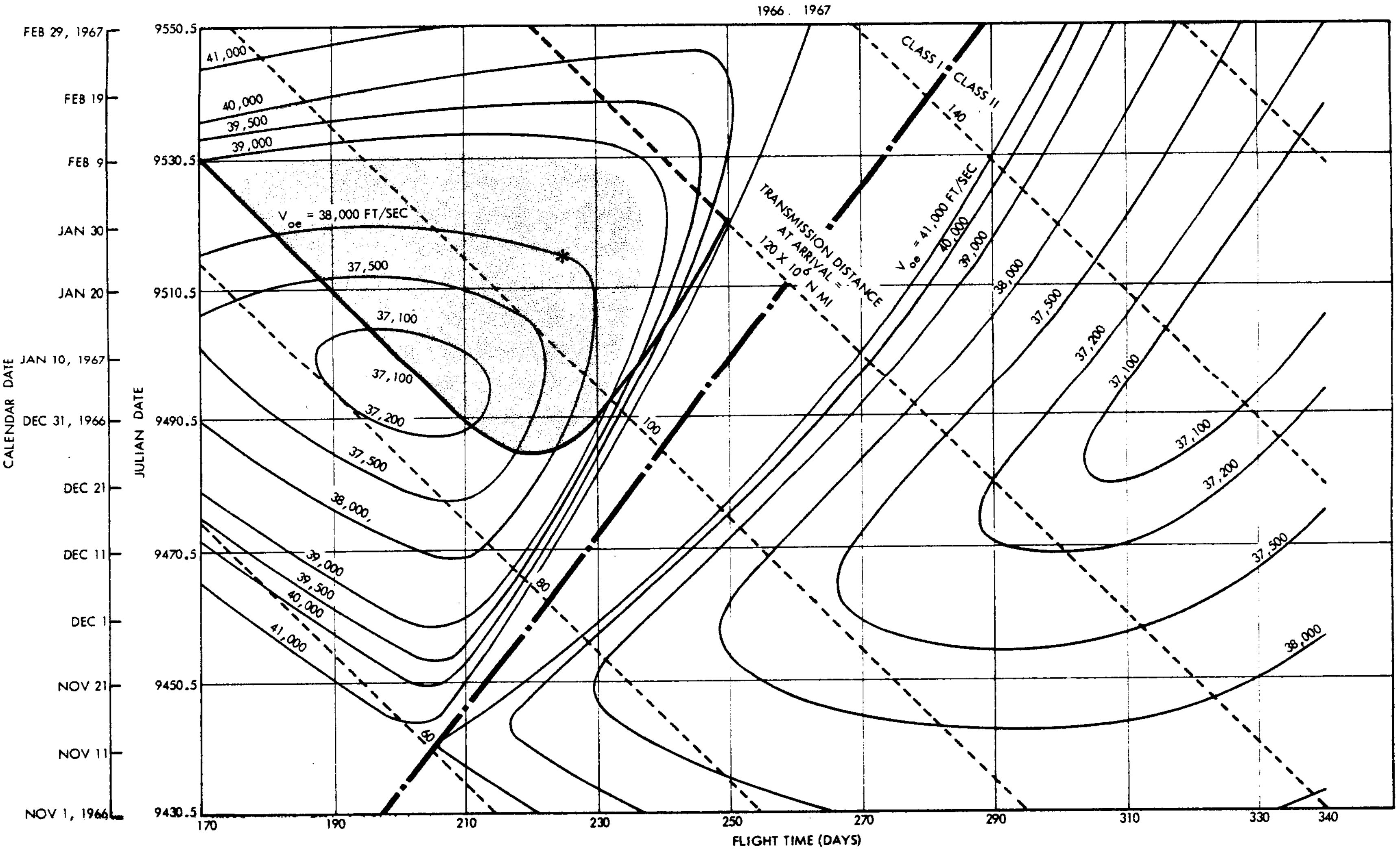

Figure II-3. Launch Velocity and Transmission Distance Contours for 1966-67

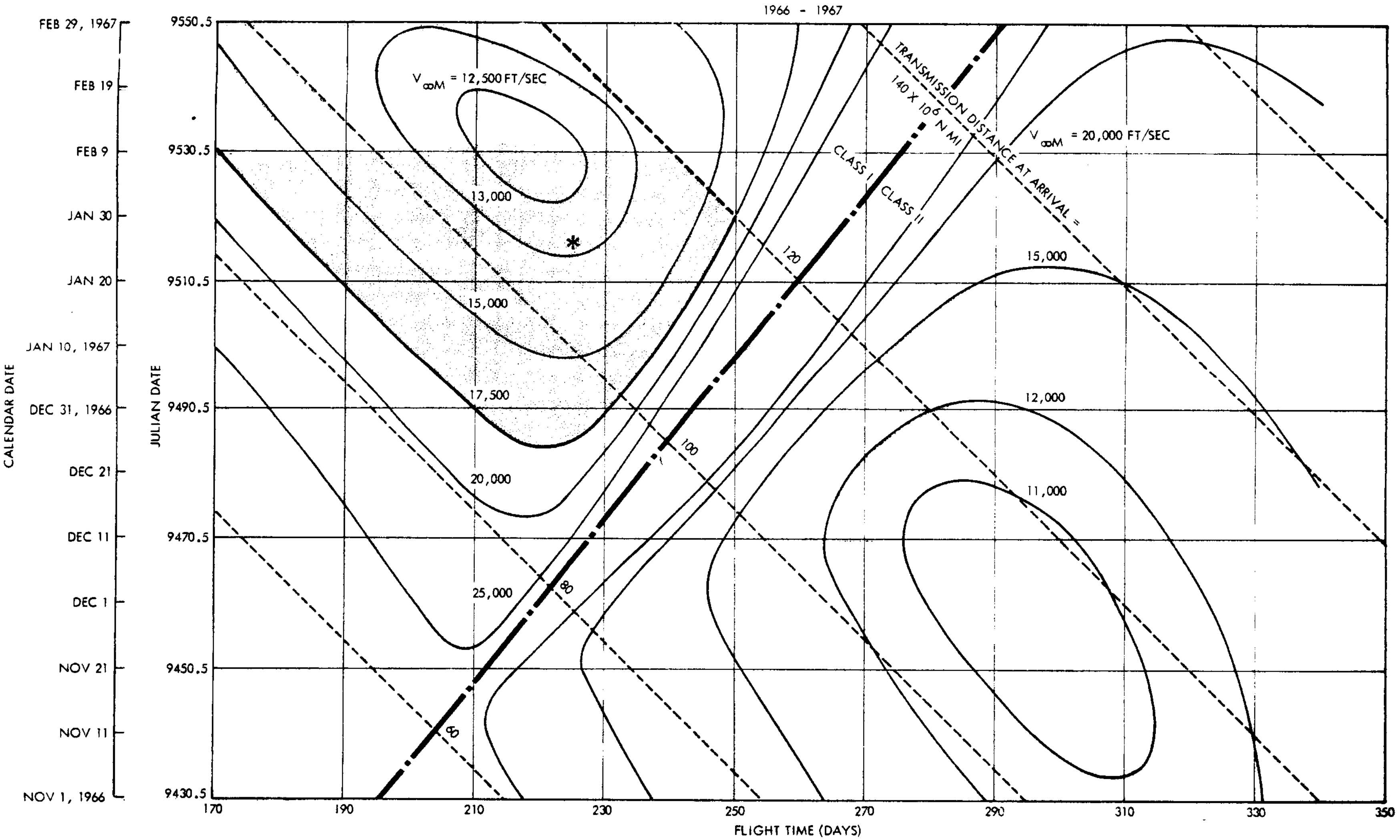

Figure II-4. V Infinity at Mars and Transmission Distance Contours for 1966-67

mission between November 10th and December 25th. As seen on Figure II-2, for these days, the minimum approach velocity is about 21,300 ft/sec.

The minimum energy trajectory does not produce the minimum approach velocity: that is, the 37,100 ft/sec launch velocity on November 21st gives an approach velocity of 21,600 ft/sec while the minimum approach velocity, launched December 30th, requires a launch velocity 39,300 ft/sec and this trajectory also results in a transmission distance of about 140 million n mi. These differences are largely the result of the three-dimensional effects.

For 1966-67 both the minimum approach velocity and minimum launch velocity fall within the tranmission distance constraint, but once again do not coincide, (see Figure II-3 and II-4). Although these figures show both Class I and II trajectories, (Class I is an intercept at the first crossing of the Mars orbit and a Class II is an intercept on the second crossing), only the Class I trajectories are of interest since for the Class II trajectories the approach velocity is too high, the mission duration is too great or the maximum transmission distance too great, although not the transmission distance at arrival.

Launch Window: When the 17,500 feet per second constraint curves are transferred to Figures II-1 and II-3, the minimum velocity required for each launch date can be determined and plotted as in Figures II-5 for 1964 and II-6 for 1966-67 to yield launch window curves. In 1964, launch is possible between November 5 and December 25 and in 1966 between December 25 and February 9. (It should be noted that the Atlas-Agena alone can launch a spacecraft to Mars for about 20 days.) In addition to the minimum launch velocity for each date, the maximum velocity for each date is also shown. If a launch window in excess of 10 days is required in 1964, it is not possible to launch with the same velocity on every day of the window and stay within the constraints. It will therefore be necessary to adjust the launch velocity to suit the particular launch date used. As mentioned earlier, a daily launch window for a

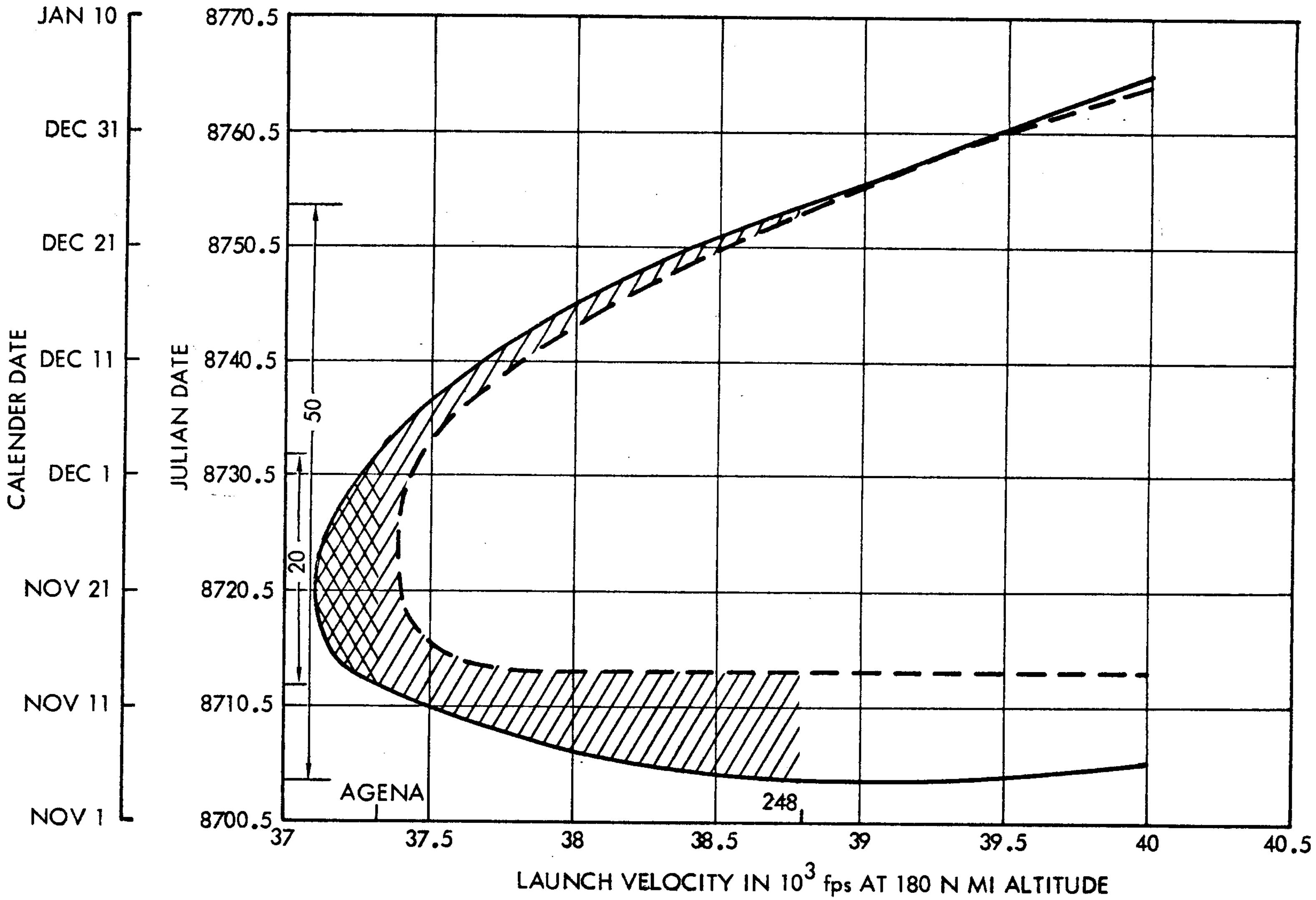

Figure II-5. Maximum and Minimum Launch Velocities for 1964

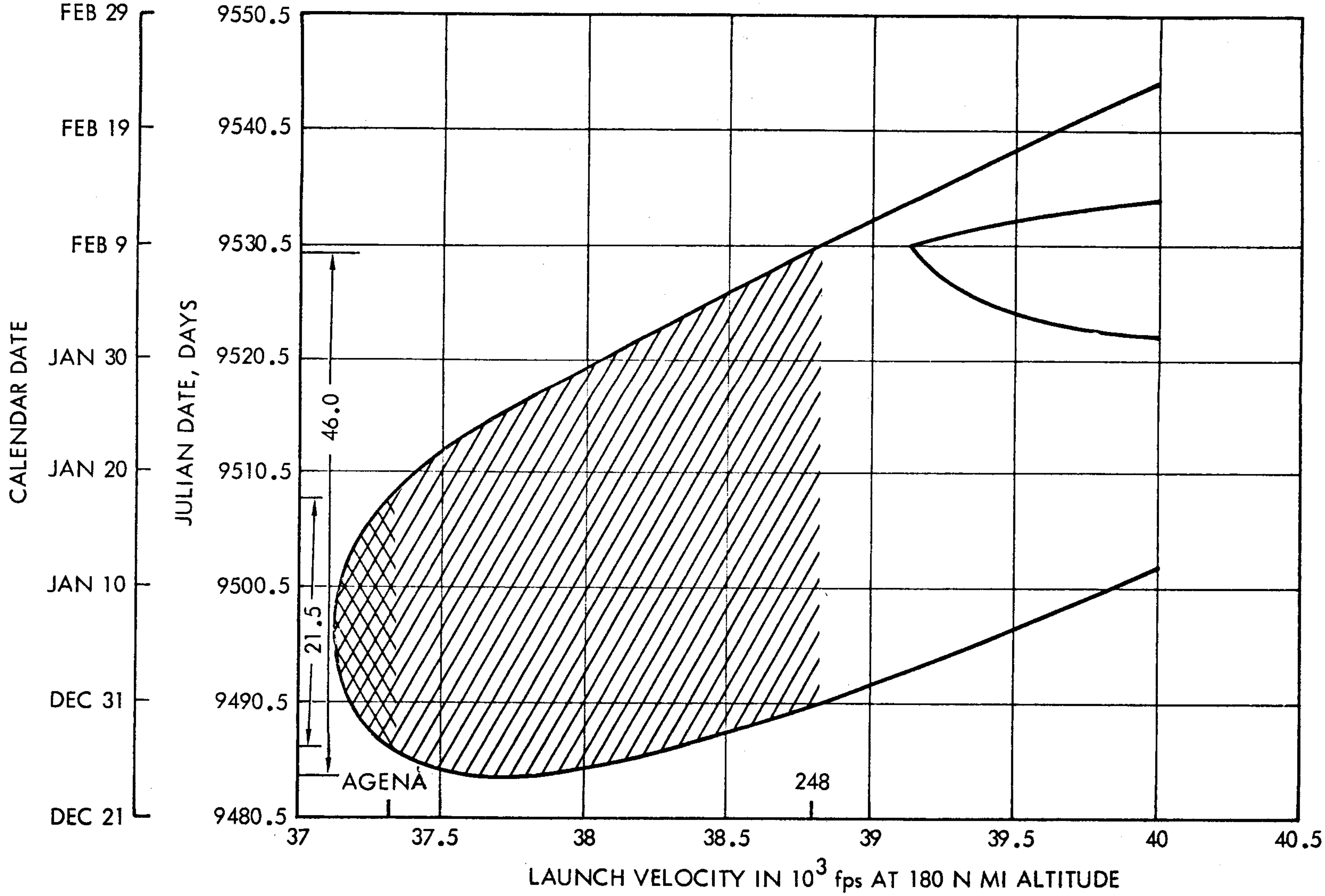

Figure II-6. Maximum and Minimum Launch Velocities for 1966-67

suitable launch azimuth (range safe) was not analyzed, but this will have little effect.

Typical Trajectories: Two trajectories were chosen as a basis for the analysis— one in 1964 and one in 1967. The launch dates and approximate injection conditions and other characteristics are given in Table II-1.

The heliocentric phases of the two trajectories are represented in Figures II-7 and II-8. The trajectories are shown circular in the plane of the ecliptic and are viewed from above (North). The transmission distance at various times is indicated by lines drawn from the spacecraft to the Earth. In 1964, the spacecraft is coming up to meet Mars since the spacecraft is approximately in the plane of the ecliptic and Mars is crossing the descending node. The reorientation for communications will be made at about 155 days when the spacecraft will turn toward the sun. The impact occurs approximately halfway between aphelion and perihelion in 1964. Since the Able-M spacecraft is designed for the 1962 launch when approach occurs much closer to aphelion, thermal and solar power problems will be somewhat improved. In 1966-67, the impact occurs even closer to perihelion, thus improving spacecraft performance even more.

The approach geometry for vertical impact is shown in Figures II-9 and II-10. The sunlit portion of the surface and the direction of the Earth are indicated. Since Mars is going faster than the spacecraft, essentially Mars impacts the spacecraft. This means that to impact, the spacecraft must first pass in front of Mars and Mars must then catch up. The possible impact area extends approximately 90 degrees in all directions away from the vertical impact site. The impact tends, therefore, to be on the sunlit side and facing Earth, although it is possible for the impact to occur on the dark side. The target area is defined by the impact parameter plane which is shown in Figure II-11.

## Table II-1. Trajectory Characteristics

| | Launch Date | January 25, 1967 | November 21, 1964 |
|---|---|---|---|
| Injection Conditions | R (Megameters) | 6.669 | 6.624 |
| | $\alpha$ (degrees) | 46.51 | 326.36 |
| | $\delta$ (degrees) | 30.40 | 24.40 |
| | V (km/sec) | 11.536 | 11.341 |
| | $\gamma$ (degrees) | 15.79 | -4.475 |
| | $A_z$ (degrees) | 105.68 | 11.40 |
| | a (Megameters) | -29.392 | -48.149 |
| | e | 1.211 | 1.136 |
| | i | 33.86 | 79.63 |
| | $\Omega$ | -72.51 | 321.60 |
| | $\omega$ | 85.96 | -326.7 |
| | $M_o$ | -0.03445 | -51.00 |
| | Declination of $V_{CO}$ infinity vector (degrees) | -25.89 | -4.77 |
| Heliocentric Elements: | | | |
| | a (Megameters) | $0.179582 \times 10^6$ | $0.89325 \times 10^6$ |
| | e | 0.1949 | 0.2195 |
| | i (degrees) | 3.78 | 1.69 |
| | $\Omega$ (degrees) | -56.77 | -122.20 |
| | $\omega$ (degrees) | 152.58 | -177.50 |
| | $M_o$ | 19.93 | 4.12 |
| | Approach speed at Mars (km/sec) | 3.99 | 4.12 |
| | Arrival date | September 7, 1967 | July 26, 1964 |
| | Flight time (days) | 225 | 247 |

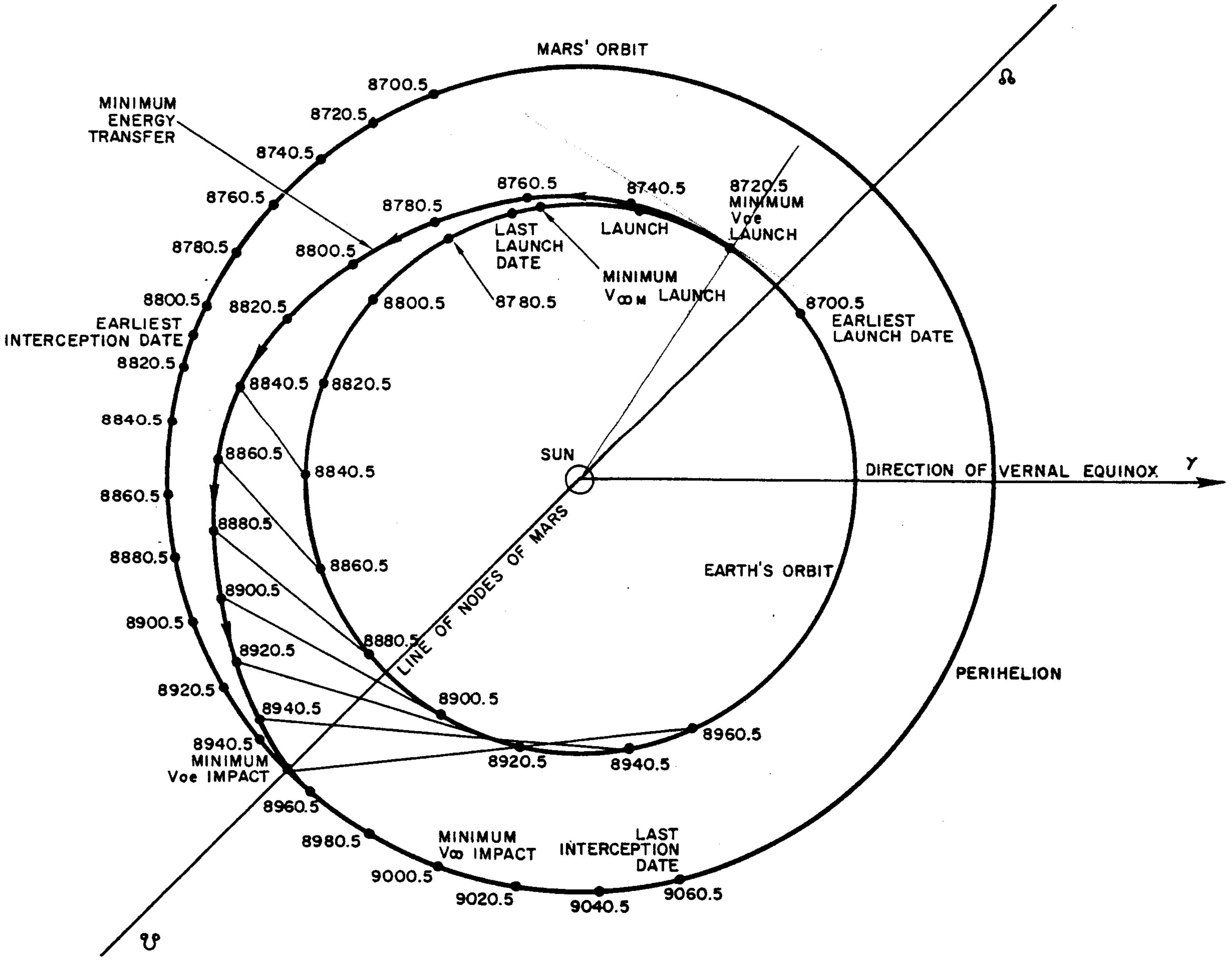
MARS' ORBIT
MINIMUM ENERGY TRANSFER
8700.5
8720.5
8740.5
8760.5
8780.5
8800.5
EARLIEST INTERCEPTION DATE
8820.5
8840.5
8860.5
8880.5
8900.5
8920.5
8940.5
MINIMUM Voe IMPACT
8960.5
8980.5
9000.5
MINIMUM V∞ IMPACT
9020.5
9040.5
LAST INTERCEPTION DATE
9060.5
8760.5
8740.5
8720.5
MINIMUM Voe LAUNCH
LAUNCH
8780.5
LAST LAUNCH DATE
MINIMUM V∞M LAUNCH
8800.5
8820.5
8780.5
8800.5
8840.5
8820.5
8860.5
8840.5
8880.5
8860.5
8900.5
8880.5
8920.5
8900.5
8940.5
8920.5
8940.5
8960.5
8700.5
EARLIEST LAUNCH DATE
SUN
DIRECTION OF VERNAL EQUINOX
♈
LINE OF NODES OF MARS
EARTH'S ORBIT
PERIHELION
☊
☋

Figure II-7. Heliocentric Plot of a 1964 Trajectory

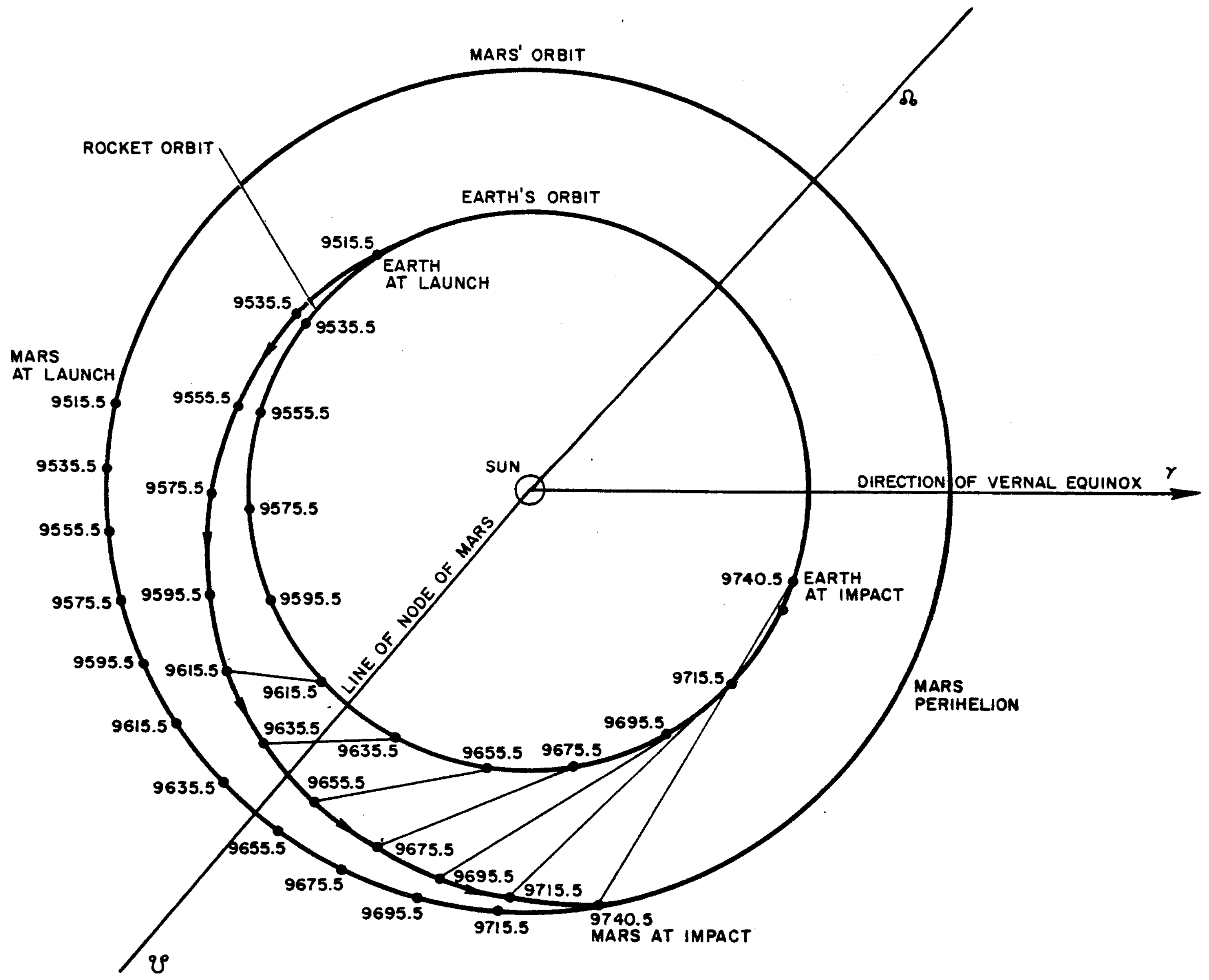
MARS' ORBIT
ROCKET ORBIT
EARTH'S ORBIT
☊
9515.5
EARTH
AT LAUNCH
9535.5
9535.5
MARS
AT LAUNCH
9515.5
9555.5
9555.5
9535.5
SUN
9575.5
9575.5
DIRECTION OF VERNAL EQUINOX
♈
9555.5
LINE OF NODE OF MARS
9575.5
9595.5
9595.5
9740.5
EARTH
AT IMPACT
9595.5
9615.5
9615.5
9715.5
MARS
PERIHELION
9615.5
9635.5
9695.5
9635.5
9655.5
9675.5
9635.5
9655.5
9655.5
9675.5
9675.5
9695.5
9715.5
9695.5
9715.5
9740.5
MARS AT IMPACT
☋

Figure II-8. Heliocentric Plot of a 1967 Trajectory

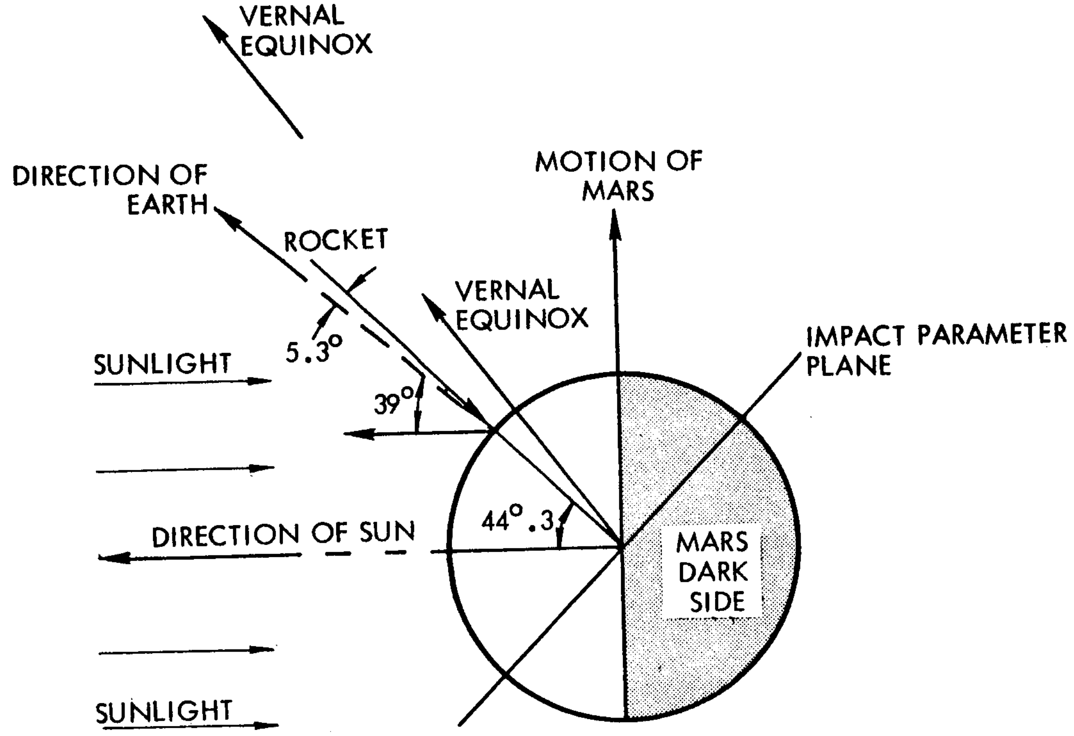
VERNAL EQUINOX
DIRECTION OF EARTH
ROCKET
MOTION OF MARS
VERNAL EQUINOX
IMPACT PARAMETER PLANE
SUNLIGHT
5.3°
39°
44°.3
DIRECTION OF SUN
MARS DARK SIDE
SUNLIGHT

Figure II-9. Approach Geometry for a 1964 Trajectory

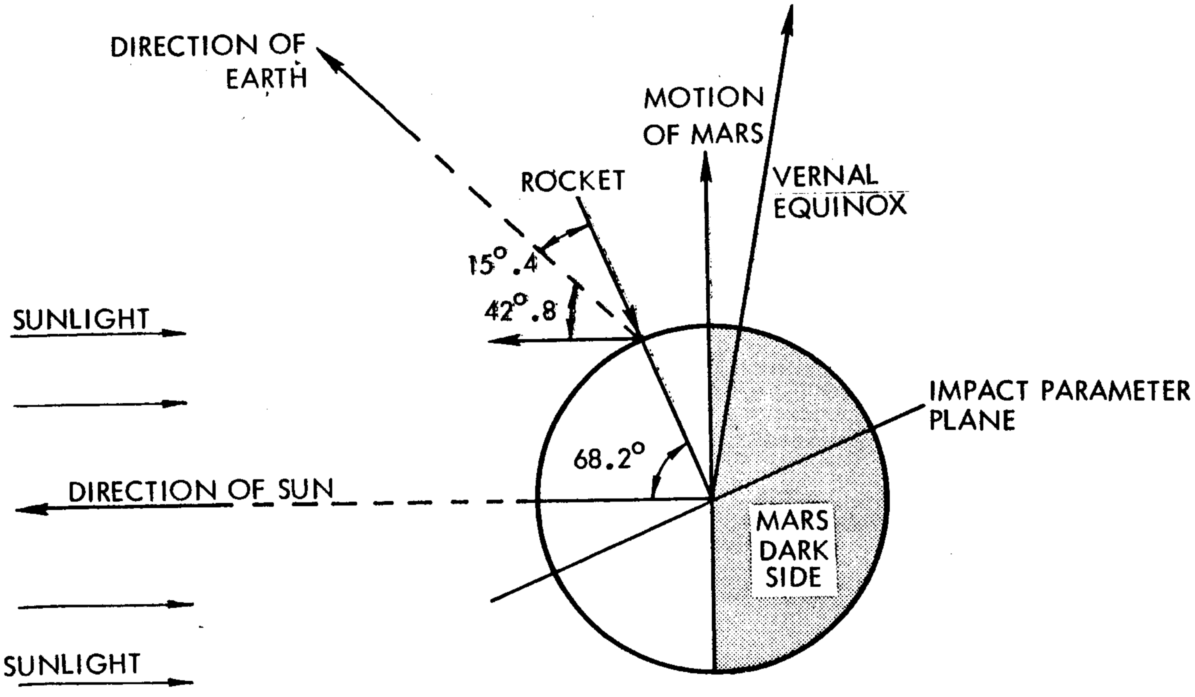
DIRECTION OF EARTH
MOTION OF MARS
ROCKET
VERNAL EQUINOX
15°.4
42°.8
SUNLIGHT
IMPACT PARAMETER PLANE
68.2°
DIRECTION OF SUN
MARS DARK SIDE
SUNLIGHT

Figure II-10. Approach Geometry for a 1967 Trajectory

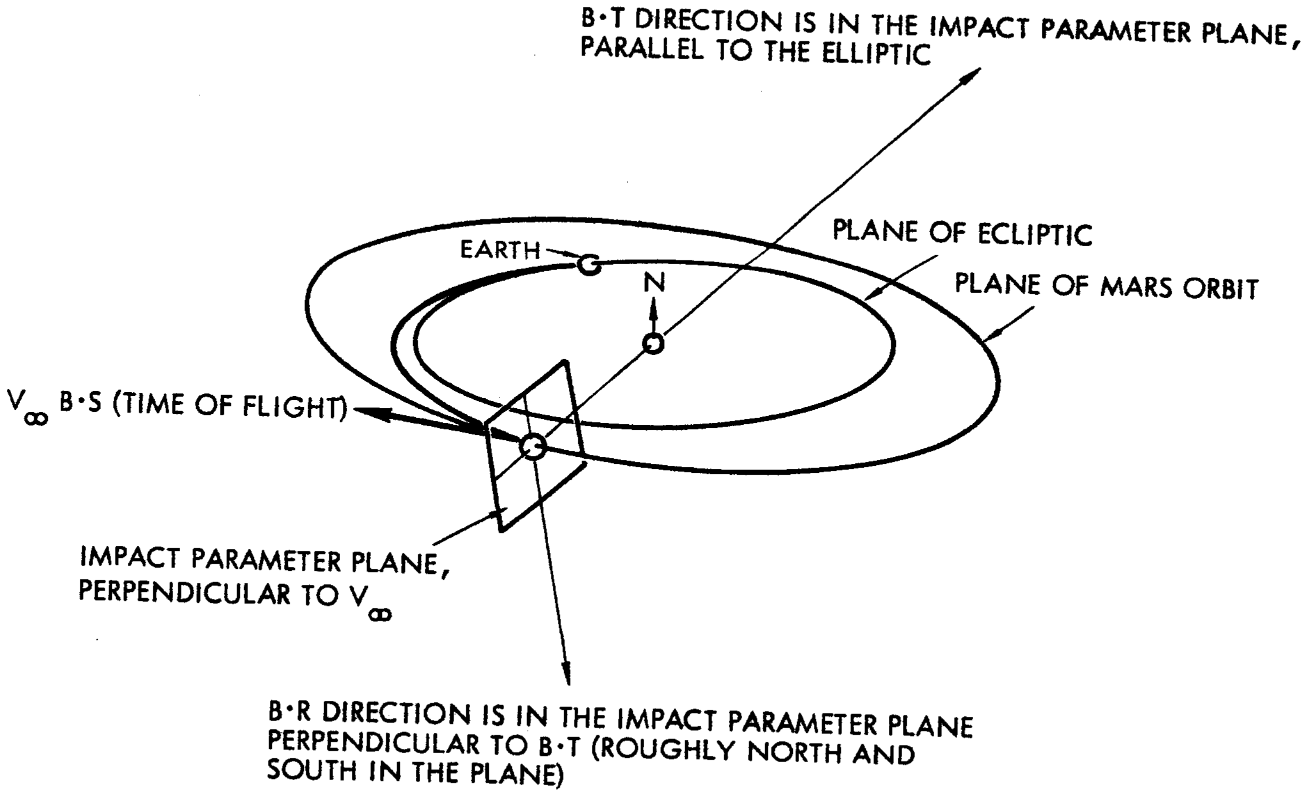
B·T DIRECTION IS IN THE IMPACT PARAMETER PLANE, PARALLEL TO THE ELLIPTIC
PLANE OF ECLIPTIC
PLANE OF MARS ORBIT
EARTH
N
$V_\infty$ B·S (TIME OF FLIGHT)
IMPACT PARAMETER PLANE, PERPENDICULAR TO $V_\infty$
B·R DIRECTION IS IN THE IMPACT PARAMETER PLANE PERPENDICULAR TO B·T (ROUGHLY NORTH AND SOUTH IN THE PLANE)

Figure II-11. Definition of Impact Parameter Components

# III. MIDCOURSE GUIDANCE

## A. UNCORRECTED MISS

The miss for the 1964 trajectory before midcourse corrections was calculated from the injection errors and sensitivities. The covariance matrix of injection errors is listed in Table III-1 and the sensitivities to injection errors are listed in Table III-2. The sensitivities are also represented graphically in Figure III-1. As can be seen, the dominant errors are altitude and velocity, but these two errors tend to be negatively correlated since the guidance laws used are based upon guiding to be specified energy. If we compare the 1964 coefficients with the 1962 coefficients, we find that the velocity coefficient is slightly more in 1964 but, in general, they are both very similar. The resulting covariance matrix of impact parameter and time-of-flight error is listed in Table III-3. The one-sigma ellipse (40% ellipse) in the impact parameter plane is shown in Figure III-2. The size of this ellipse compared to the radius of Mars showing a miss of two orders of magnitude clearly indicates that midcourse guidance is necessary.

## B. MIDCOURSE PHILOSOPHY

The basic philosophy of midcourse guidance for a spin-stabilized vehicle is to use two firings to correct two components of miss. This scheme depends on the fact that the vector effect of firing a correction along the spin axis, viewed in the impact parameter plane, usually rotates in the impact parameter plane as the time of firing is varied. For the sample 1964 trajectory this effect is shown in Figure III-3 and the corresponding numerical values are listed in Table III-4. The sensitivities at any two times can be used as basis vectors to decompose the impact parameter error into two components, which can then be removed by firing the appropriate velocities at the two chosen times. If the two firings could be made with complete accuracy, the error in impact parameter would be eliminated. The fact that there is always error in the firings leads to modifications of the basic scheme to improve the resulting accuracy.

The error made in firing the first correction can be essentially removed by varying the time of the second correction to make its sensitivity

Table III-1. 1964 Injection Covariance Matrix*

| | α Right Ascension | δ Declination | β Flight Path Angle | A Azimuth | R Injection Radius from Center of Earth | V Velocity |
|---|---|---|---|---|---|---|
| α | 0.1333 | -0.217 ($10^{-1}$) | 0.22 ($10^{-2}$) | -0.927 ($10^{-1}$) | -0.845 ($10^{-1}$) | 7.36 |
| δ | | 0.1513 ($10^{-1}$) | -0.286 ($10^{-5}$) | -0.331 ($10^{-1}$) | 0.985 ($10^{-2}$) | -1.98 |
| β | | | 0.1368 ($10^{-1}$) | -0.256 ($10^{-2}$) | -0.530 ($10^{-2}$) | -0.649 |
| A | | | | 0.348 | 0.738 ($10^{-1}$) | -2.55 |
| R | | | | | 0.0567 | -4.13 |
| V | | | | | | 708 |

---

*Angles are in degrees

R is in $10^5$ ft

V is in ft/sec

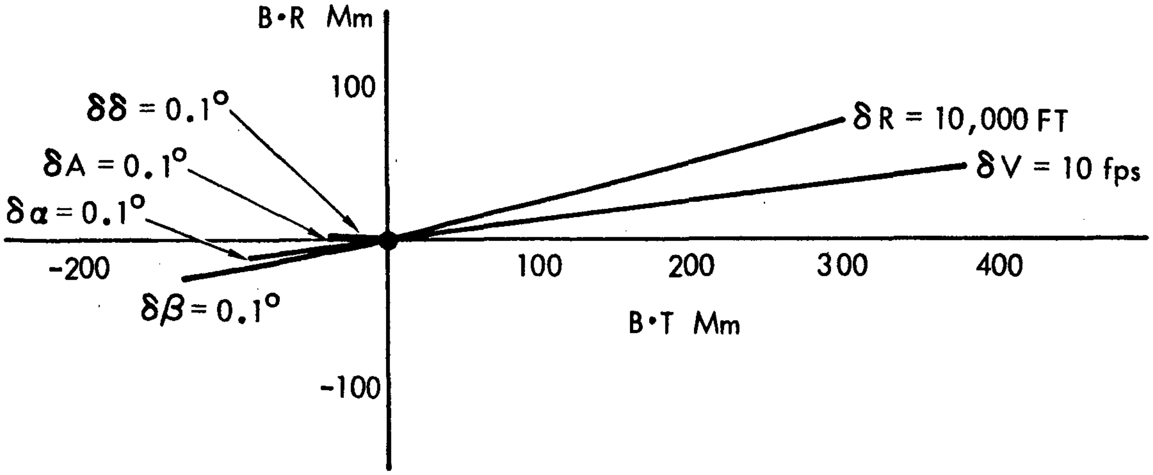

Figure III-1. Injection Sensitivities (1964)

Table III-2. 1964 235-Day Trajectory Injection Sensitivities

| | | $\delta$ Initial Conditions | $\delta B \cdot T$ Mm | $\delta B \cdot R$ Mm | $\delta t_f$ (Time of Flight) (days) |
|---|---|---|---|---|---|
| Right Ascension | $\alpha$ | +0.1° | -90.21 | -11.53 | 0.18283 |
| Declination | $\delta$ | +0.1° | -36.86 | 2.32 | 0.04985 |
| Flight Path Angle | $\beta$ | +0.1° | -133.56 | -24.27 | 0.29571 |
| Azimuth | A | +0.1° | -36.40 | -0.36 | 0.05449 |
| Injection Radius from Center of Earth | R | +3,048 km (10,000 ft) | 303.55 | 78.26 | -2.75868 |
| Velocity | V | +3 m/sec (10 ft/sec) | 382.92 | 98.57 | -1.74560 |

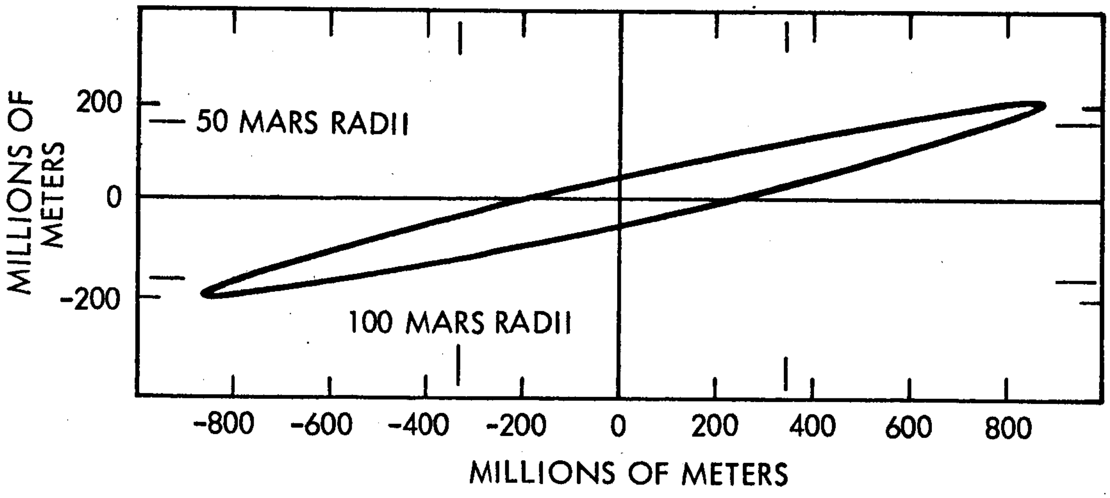

Figure III-2. One-Sigma Uncorrected Miss Ellipse (1964)

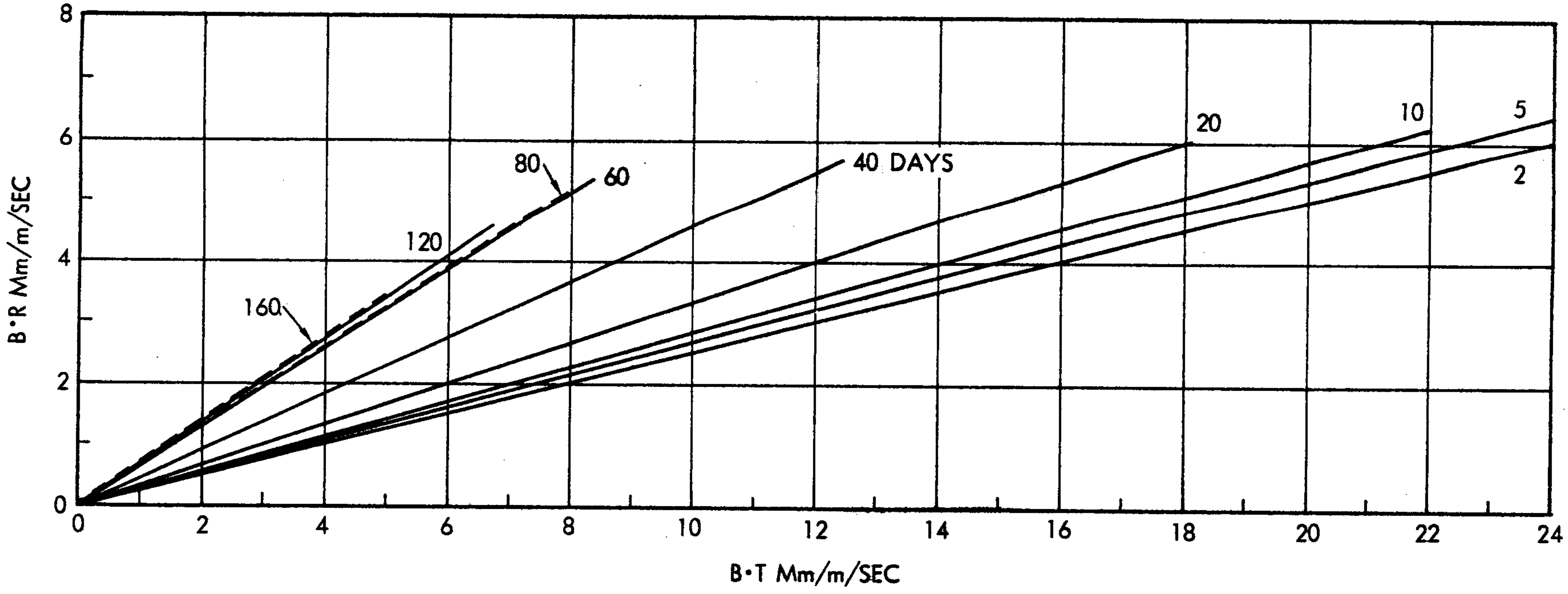

Figure III-3. Midcourse Sensitivities (1964)

Table III-3. Covariance Matrix of Impact Parameter and Time of Flight Errors

| | B•T | B•T | $t_f$ |
|---|---|---|---|
| B•T (Mm) | $0.7056393 \times 10^6$ | $0.1756395 \times 10^6$ | $-0.3904821 \times 10^4$ |
| B•R (Mm) | | $0.4540758 \times 10^5$ | $-0.2722126 \times 10^3$ |
| $t_f$ (days) | Symmetric | | $0.2909398 \times 10^2$ |

Table III-4. Midcourse Sensitivities with Nominal Spin Axis Orientation (for 1964)

Spin axis: $C_x = -0.17285$ Equatorial
$C_y = 0.95896$
$C_z = -0.22444$

| Time (days) | $\frac{\partial B \cdot T}{\partial V} \frac{Mm}{m/sec}$ | $\frac{\partial B \cdot R}{2V} \frac{Mm}{m/sec}$ | $\frac{\partial t_f}{\partial V} \frac{hr}{m/sec}$ |
|---|---|---|---|
| 0 | 125.517 | 33.267 | -823.378 |
| 2 | 25.842 | 6.478 | -138.96 |
| 5 | 24.171 | 6.330 | -128.61 |
| 10 | 21.956 | 6.230 | -116.03 |
| 20 | 18.091 | 6.052 | -92.867 |
| 40 | 12.439 | 5.695 | -52.187 |
| 60 | 9.337 | 5.405 | -38.955 |
| 80 | 7.931 | 5.178 | -4.907 |
| 120 | 6.694 | 4.575 | +6.813 |
| 160 | 4.994 | 3.428 | +4.098 |

lie along the impact parameter error remaining after the first correction. The final error in this case is then essentially the error associated with the second correction. The success of this method depends on having sufficient rotation of the sensitivity vector with time in order to reduce the amount of rotation required, the accuracy of the first firing can be improved by making a vernier firing as soon after the first correction as there is sufficient tracking data. This firing cannot remove all of the error associated with the first correction since the direction of its effect is essentially fixed, but it can reduce the effect of the magnitude error in the first correction. It cannot remove the components' miss due to attitude error effects since these are perpendicular to the nominal sensitivity vector.

The attitude error for the second correction can be reduced by measuring the attitude with tracking after the first correction. The change in velocity at the time of firing the first correction determined from tracking is compared with the predicted value using the nominal attitude. The difference gives the attitude during the first correction. This measured attitude is then used in calculating the time and magnitude of the second correction.

## C. CORRECTION TIMES

The selection of nominal correction times for midcourse corrections depends on tracking accuracy and midcourse velocity (fuel) requirements. Sufficient time must be allowed before the first correction to determine the orbit accurately, but since the midcourse sensitivity normally decreases with time, it is possible to trade-off fuel for accuracy. Choosing the first correction time so that the effect vector lies along the major axis of the uncorrected miss ellipse in the impact parameter plane, tends to minimize the required velocity. Fortunately this axis tends to be near the early sensitivities so that we are able to do this.

Once the first correction time is chosen, the optimum time (from the velocity or fuel standpoint) for the second correction is the one that maximizes the component of sensitivity perpendicular to the first correction in the impact parameter plane.

The vernier times are chosen as soon after the main corrections as sufficient tracking is available.

Applying the above criteria, the main-correction times chosen for the 1964 trajectory are 2 to 60 days, with verniers at 5 and 80 days.

## D. REORIENTATION EFFECTS

The effects of orienting the spin-axis along a radial line from the Sun immediately before firing a correction, were determined for 1964. The impact parameter sensitivities resulting from this scheme are plotted in Figure III-4, and the complete sensitivities are listed in Table III-5.

Comparison of Figure III-4 with Figure III-3 shows that the sensitivities early in the flight are greater with the nominal attitude then after reorientation, but that a greater rotation of sensitivity occurs when the spin-axis always points away from the Sun.

Comparison of Table III-5 with Table III-4 shows that the sensitivity of time-of-flight relative to impact parameters is greater with the reorientation than with the nominal spin-axis. This fact is useful in correcting time-of-flight, as is shown later.

### 1. Midcourse Corrections

For the 1964 trajectory the first correction sensitivity essentially lies along the major axis of the uncorrected miss ellipse. This allows the high early sensitivity to be used to remove the larger component of miss (in a statistical sense), and tends to minimize the total midcourse velocity required. For some trajectories, however, the spin-axis orientation is such that the early sensitivities do not lie near the major axis of the miss ellipse. This was the case for 1962 until the powered flight was modified to give a better orientation.

An alternate and more flexible way of changing the orientation for the first correction is described below. The closed-loop operation of the attitude control system can only point the spin-axis toward the Sun, but an open-loop reorientation to any direction can be accomplished. Naturally, the open-loop maneuver has more error than the closed-loop maneuver — 6 percent of the reorientation angle as opposed to one degree ($3\sigma$). The largest reorientation that could be required is 90 degrees. This would

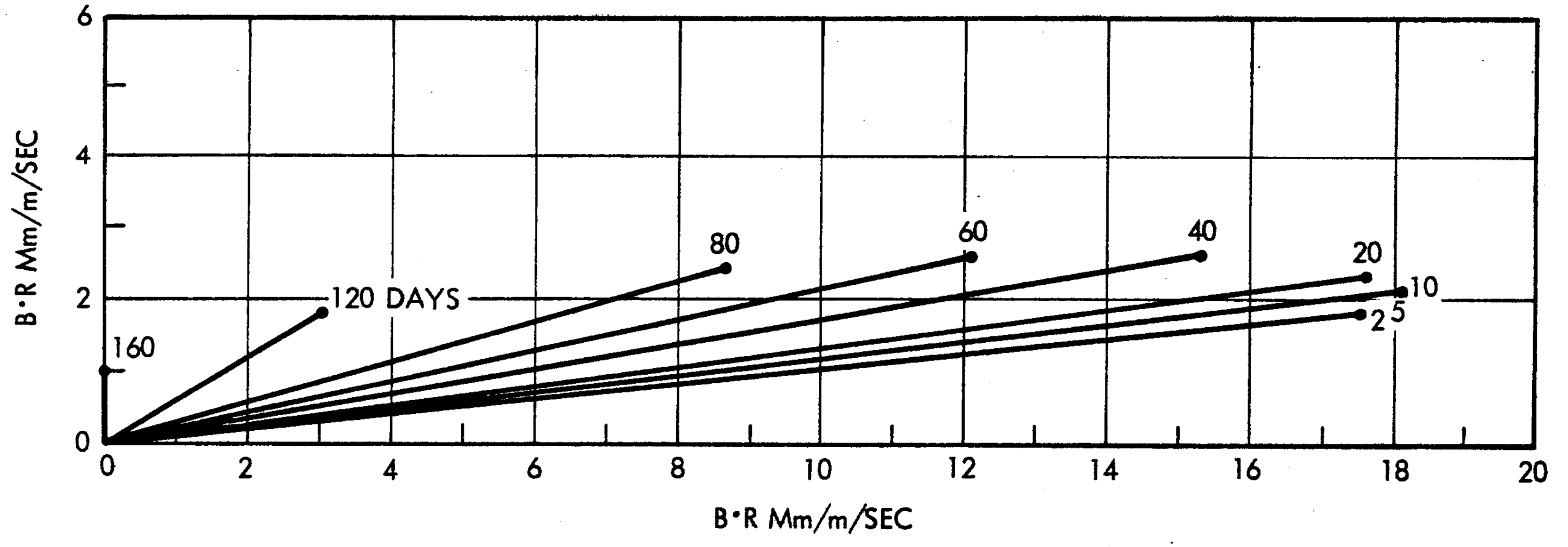

Figure III-4. Midcourse Sensitivities with Spin-Axis Pointed Away from Sun (1964)

Table III-5. Midcourse Sensitivities with Spin Axis Oriented Away from Sun at Each Firing (for 1964)

Spin axis away from sun

| Time (days) | $\frac{\partial B \cdot T}{\partial V} \frac{\text{Mm}}{\text{m/sec}}$ | $\frac{\partial B \cdot R}{2V} \frac{\text{Mm}}{\text{m/sec}}$ | $\frac{\partial t_f}{\partial V} \frac{\text{hr}}{\text{m/sec}}$ |
|---|---|---|---|
| 0 | 76.69527 | 19.84178 | -497.2150 |
| 2 | 17.90901 | 1.878015 | -44.50518 |
| 5 | 18.15589 | 1.987486 | -47.32055 |
| 10 | 18.13652 | 2.139776 | -51.33610 |
| 20 | 17.61116 | 2.390335 | -58.08032 |
| 40 | 15.34145 | 2.677833 | -66.26693 |
| 60 | 12.10109 | 2.680114 | -67.26030 |
| 80 | 8.671850 | 2.479275 | -62.94657 |
| 120 | 3.024065 | 1.791127 | -46.35862 |
| 160 | -0.1190563 | 1.061260 | -28.20235 |

occur if the spin-axis were perpendicular to the critical plane (a low-probability occurrence). The error from this reorientation would be 5.4 degrees.

The procedure when the open-loop reorientation is used is to orient the spin-axis in the critical plane in the direction that corresponds to the major axis of the uncorrected miss ellipse. The attitude would then be determined accurately from tracking before and after the first correction, and the correction logic would be standard from that point to the end.

This method of making midcourse corrections has not been studied in detail, since it is not needed for 1964. However, it is obvious that in all cases it can save fuel and, for trajectories with a very poor spin-axis orientation with respect to midcourse sensitivities, such a reorientation could make the mission possible.

### 2. Midcourse Guidance Reorientation Technique

A reorientation maneuver for improvement of the midcourse guidance was studied. The attitude errors derived here are only those caused by reorientation, and are only valid under the assumptions made.

The results obtained must be modified to include the effects of initial error and the spin-axis not contained in the ecliptic plane after the reorientation is defined.

The reorientation would be performed in two phases. In Phase I, the spacecraft is rotated in the plane determined by the spin-axis and vehicle sun line until the spin-axis has the proper angle with the sun line. At this time, a null sensor (the angle has been precalculated for a particular orientation and the null sensor mounted in the spacecraft to measure the required angle) will stop Phase I, and Phase II can be started. Phase II torques the spin-axis perpendicular to the plane formed by the spin-axis sun line. Since the plane is constantly changing while being torqued, the spin-axis moves around the sun line on a conical surface. The spin axis is rotated until the desired orientation is achieved. Since the angle between the sun line and the spin-axis is fixed and the use of earth sensors is deemed too complicated (expensive, and unreliable), this rotation is best accomplished by an open-loop correction. That is by rotating at a predetermined rate for a fixed period of time. This method of correction results in an error in spin-axis orientation discussed later. This error is removed when the vehicle is reoriented to the sun to increase the antenna gain. A diagram of the reorientation for midcourse guidance is shown in Figure III-5.

Although there are several valid coordinate systems that may be used to describe the spin-axis attitude, the one most suited for the description of the reorientation system consists of two angles. The first angle measured in the ecliptic and is the angle between the vernal equinox and the projection of the spin-axis in the ecliptic ($\alpha$). The second is the angle between ecliptic projection and the spin-axis ($\delta$) as shown in Figure III-6 . Let the subscript D represent the desired orientation for the midcourse correction and o the starting position. In general, two rotations will be necessary to obtain the desired location. One in the plane formed by the spin-axis and sun line and the second around the sun line as shown in Figure III-7 , where H is the momentum vector, $\theta$ is the first rotation, $\phi$ is the second rotation, $\Omega$ is the angle between the vernal equinox and sun line, $\psi$ is the desired angle between the sun line

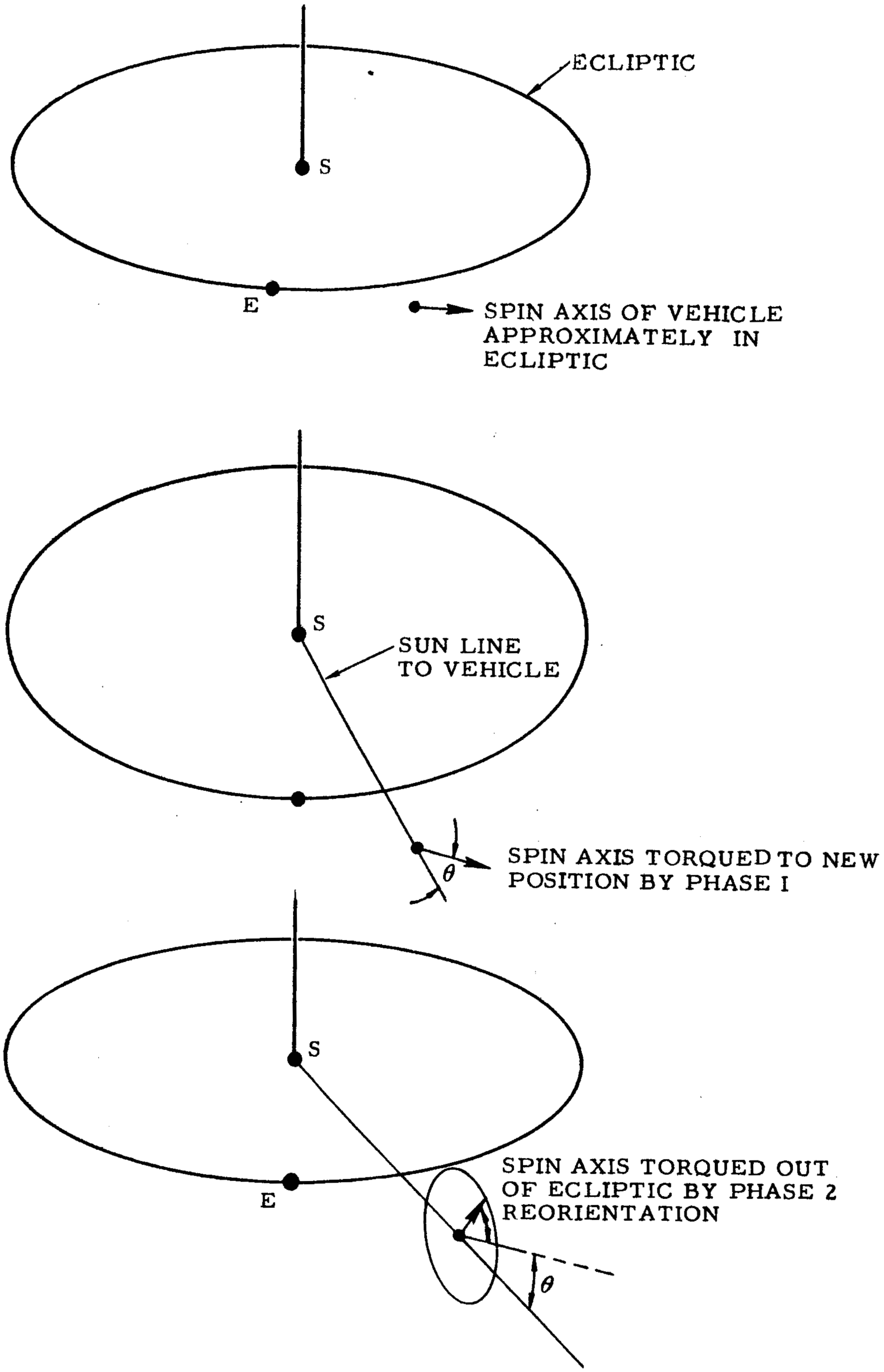
ECLIPTIC
S
E
SPIN AXIS OF VEHICLE APPROXIMATELY IN ECLIPTIC
S
SUN LINE TO VEHICLE
SPIN AXIS TORQUED TO NEW POSITION BY PHASE I
θ
S
E
SPIN AXIS TORQUED OUT OF ECLIPTIC BY PHASE 2 REORIENTATION
θ

Figure III-5. Reorientation for Midcourse Guidance

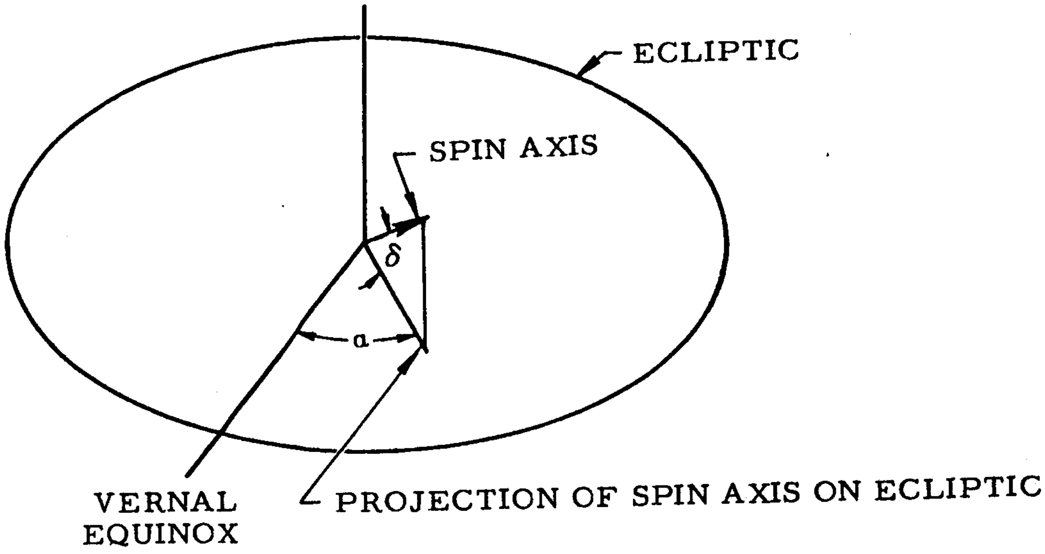
ECLIPTIC
SPIN AXIS
δ
α
VERNAL EQUINOX
PROJECTION OF SPIN AXIS ON ECLIPTIC

Figure III-6. Angle Between Vernal Equinox and Projection of Spin Axis in the Ecliptic

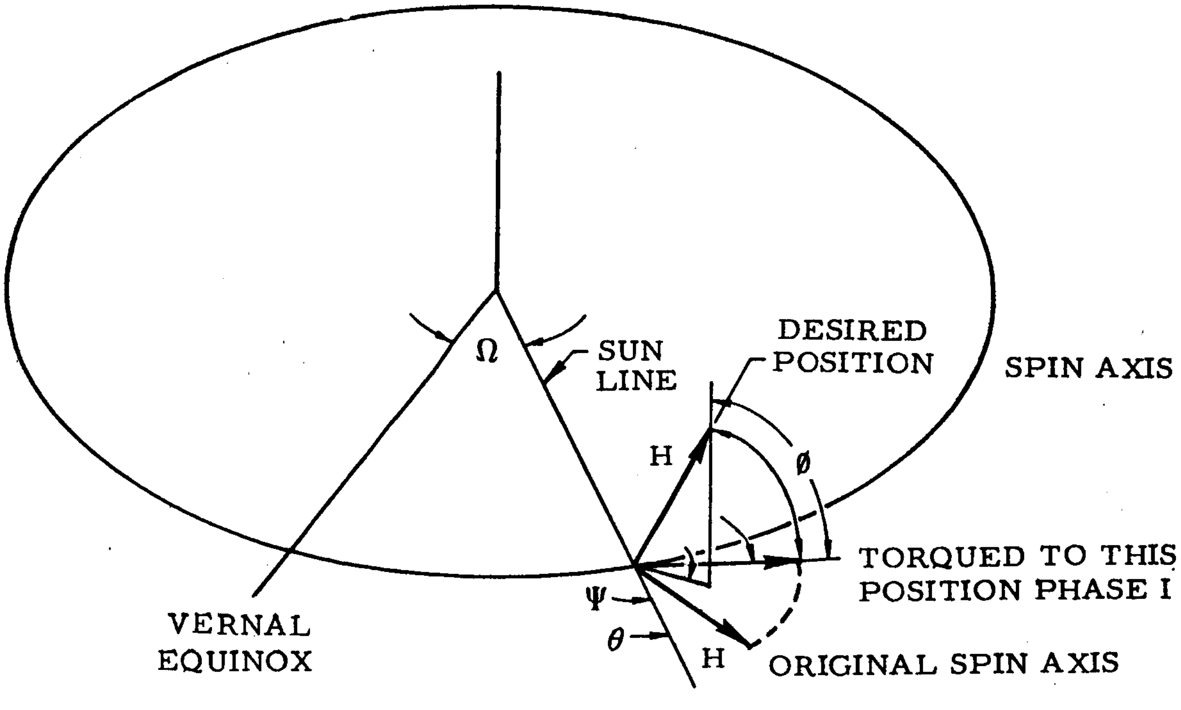
Ω
SUN LINE
DESIRED POSITION
SPIN AXIS
H
ø
TORQUED TO THIS POSITION PHASE I
Ψ
θ
H
VERNAL EQUINOX
ORIGINAL SPIN AXIS

Figure III-7. Definition of Rotations Required to Reorient the Spin Axis

and the spin axis projection, and assuming the original momentum vector lies in the ecliptic plane. The required angles $\phi$ and $\theta$ may be determined from the following equations:

$$\psi = \alpha_D - \Omega$$

$$\psi = \sin^{-1} \frac{\sin\theta \cos\phi}{\sqrt{1 - \sin^2\theta \sin^2\phi}}$$

$$\delta_D = \sin^{-1} (\sin\theta \sin\phi)$$

Prior studies of this technique indicate that the variation in $\theta$ can be controlled to at least ±1 degree by using a null sensor, while the angle $\phi$ can vary ±0.06 of the desired $\phi$ due to primarily the variation in jet thrust. The partial deviatives of the above equations can be taken resulting in:

$$\frac{\partial \delta_D}{\partial \theta} = \frac{\sin\theta \cos\phi}{\sqrt{1 - \sin^2\theta \sin^2\phi}}$$

$$\frac{\partial \delta_D}{\partial \phi} = \frac{\cos\phi \sin\theta}{\sqrt{1 - \sin^2\theta \sin^2\phi}}$$

$$\frac{\partial \alpha_D}{\partial \theta} = \cos\phi \left[1 + \tan^2 \delta_D\right]$$

$$\frac{\partial \alpha_D}{\partial \phi} = -\sin\phi \tan\theta \left[1 - \tan^2 \delta_D \cos^2 \phi\right]$$

Figures III-8 and III-9 are plots of the spin-axis attitude error for typical desired orientations and Figure III-10 is the total resultant error. The attitude errors presented in the figures are due only to reorientation; that is, any error present in the attitude before the reorientation maneuver is started must be considered and will modify the results. However, these can be measured quite accurately after the midcourse corrections. (See Section V.) Also the spin-axis was assumed to be in the ecliptic, and the equations would have to be modified if this is not the case. Refinements of this nature are better performed after a particular orientation has been selected.

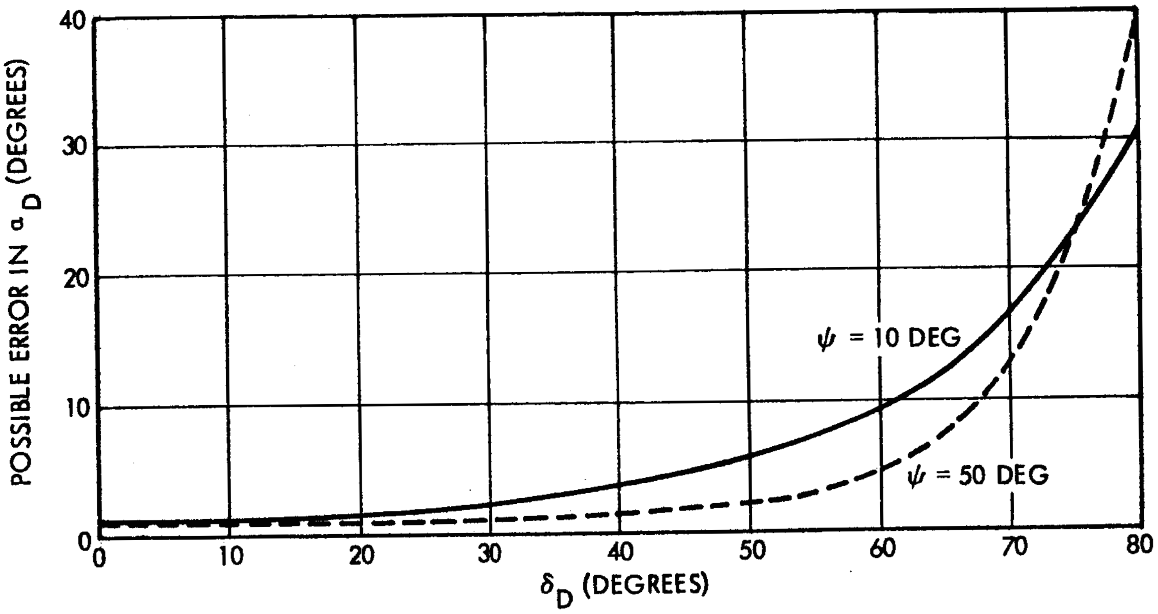

Figure III-8 Possible Error in $a_D$ as a Function of $\delta_D$ for Two Orientations

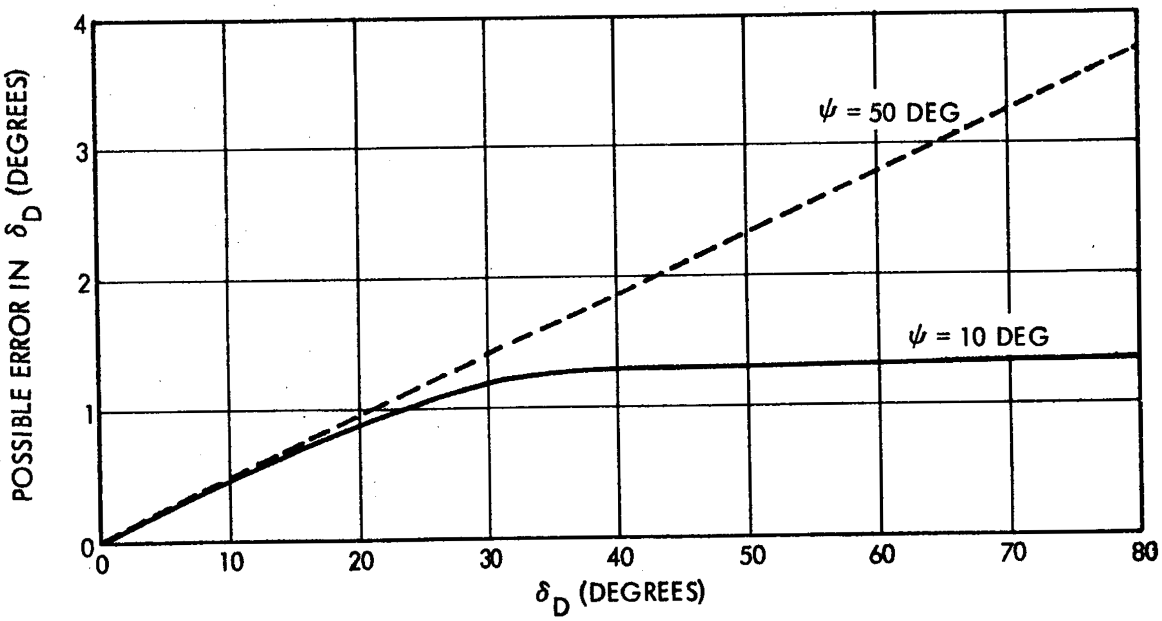

Figure III-9. Possible Error in $\delta_D$ as a Function of $\delta_D$ for Two Orientations

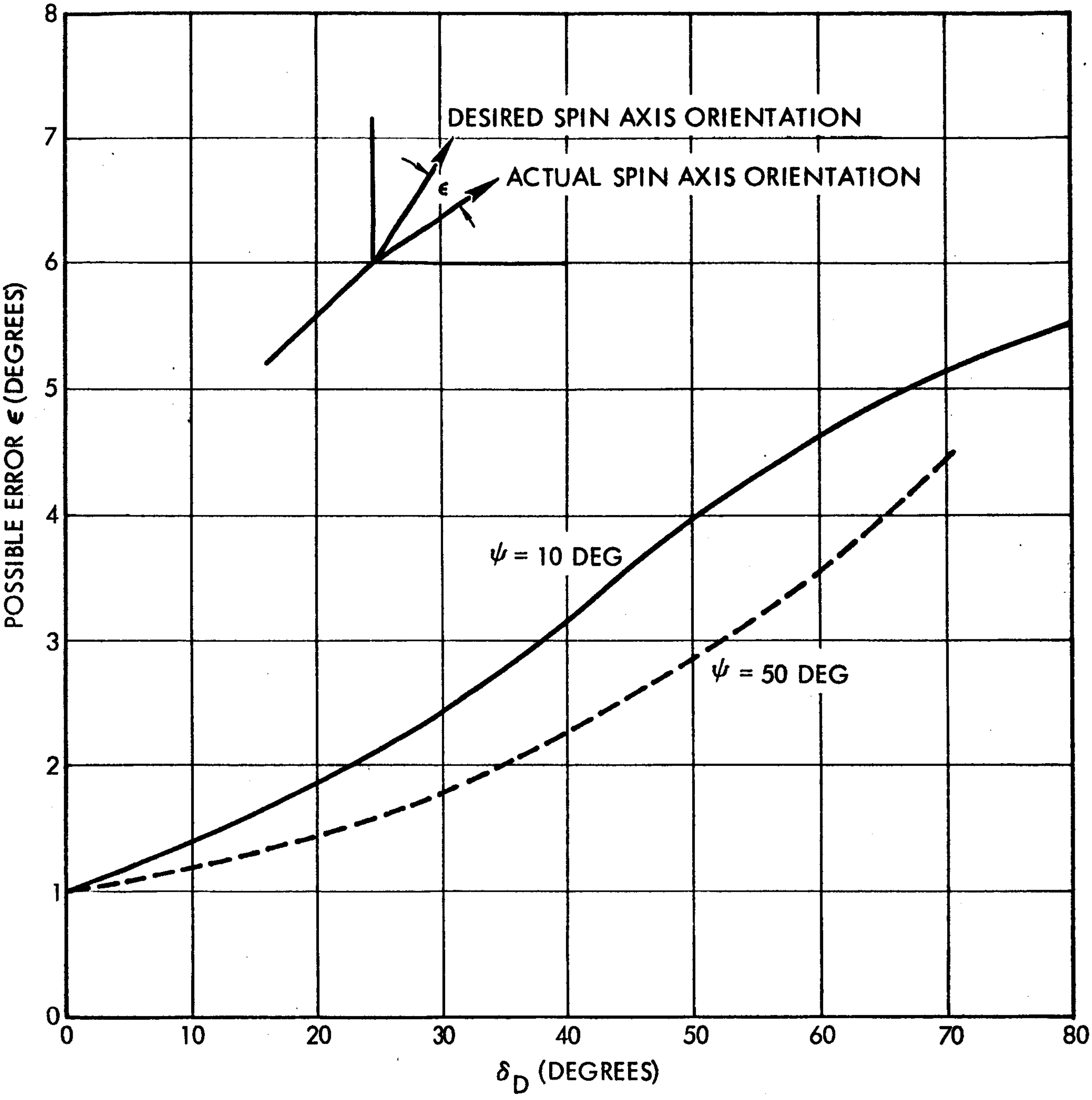

Figure III-10 Possible Errors $\epsilon$ as a Function of $\delta_D$ for Two Different Orientations

A major trade-off in the consideration of the reorientation technique described here is the weight added to the vehicle for the reorientation. This weight is dependent upon the particular orientation required and initial orientation of the spacecraft. While specific numbers for any orientation are not available, number for a typical rotation would be 3.46 pounds.* This does not include the extra weight required for the bottle which would be approximately 4.5 pounds for the above gas or does it include any additional gas requirements for the reorientation to improve antenna gain.

## E. TIME-OF-FLIGHT CONTROL

It is possible to control time of flight by using three correction times to provide a three-dimensional set of basis vectors. This scheme is formally similar to the basic two-correction scheme except for the number of dimensions.

In order to correct flight time to its nominal value with this scheme, excessively large correction velocities are required for the 1964 trajectory. For example, the correction velocity was calculated for correction times of 2, 40, and 80 days. One-sigma velocities 99 and 282, and 246 meters per second are required. These can be compared to 33 and 13.4 meters per second for correcting impact parameter only.

These large velocities lead to correspondingly large execution errors. It is therefore desirable to use some other scheme to control flight time.

It has been found from the reorientation investigation that a correction fired late in the flight can change flight time enough to control the time of day (as opposed to day and time of day) at impact without disturbing the impact parameter significantly. The sensitivities after reorientation for communications (at 160 days) are shown in Table III-6. From these, the correction required for a 12-hour time of flight correction is shown in Table III-7 with the corresponding miss coefficients for corrections at three times.

---

*Rotation of the angular momentum by 45° considers an inertia 2.31 slug/ft$^2$, a spin rate of 2.86 revolutions/sec, a 19.50inch moment arm, and a gas with a specific impulse of 60 lb-sec/lb.

Table III-6. Midcourse Sensitivities with Spin Axis Oriented Away from Sun at 160 Days (for 1964)

| Time (days) | $\frac{\partial B\cdot T}{\partial V}$ $\frac{Mm}{m/sec}$ | $\frac{\partial B\cdot R}{\partial V}$ $\frac{Mm}{m/sec}$ | $\frac{\partial t_f}{\partial V}$ $\frac{hr}{m/sec}$ |
|---|---|---|---|
| 160 | -0.1190563 | 1.061260 | -28.20235 |
| 180 | -0.03095806 | 0.7103651 | -19.25537 |
| 200 | -0.03333426 | 0.4411343 | -12.03637 |
| 220 | -0.09071587 | 0.1426888 | -4.468672 |
| 230 | -0.01813986 | 0.02966654 | -1.278563 |
| 233 | -0.04221030 | 0.009801805 | -0.3719742 |

Table III-7. Comparison of Flight Time Sensitivity to Impact Parameter Sensitivity

| Time | Vel. for 12 hr (m/sec) | $\delta B\cdot T$ (Mm) | $\delta B\cdot R$ (Mm) |
|---|---|---|---|
| 233 | 32.2 | 1.36 | 0.316 |
| 230 | 9.39 | 0.170 | 0.279 |
| 220 | 2.68 | 0.244 | 0.382 |

The velocity required for this correction is about 10 meters per second 5 days before impact for a 12-hour change in time of flight. This is sufficiently small to require no extra fuel, but is large enough to be fired accurately.

With this late correction the flight time will not be corrected to nominal, but the impact can be adjusted to occur when it is in view of a particular tracking station.

## F. VELOCITY REQUIREMENTS

The velocity required by the basic spin-stablized scheme is calculated from the sensitivities at the two correction times and the uncorrected miss. For the corrections at 2 and 60 days, the covariance matrix of velocity required is listed in Table III-8.

A conservative estimate of the velocity required for verniers is five percent of the main-correction velocity which is essentially negligible.

The maximum velocity required for controlling impact time is the amount required to make a 12-hour change, which is about 10 meters per second for 1964. Table III-9 gives the midcourse procedures for the nominal 1964 mission.

Table III-8. Covariance Matrix of Midcourse Correction Velocity (1964)

| | $V_1$ | $V_2$ |
|---|---|---|
| $V_1$ (m/sec) | 1091.478 | -80.95772 |
| $V_2$ (m/sec) | -80.95772 | 180.513 |

$3\sigma$ Values

$V_1$ 99.0 m/sec

$V_2$ 40.2 m/sec

## Table III-9. Midcourse Procedures

1. Track from injection to 2 days.

   Calculate velocity $V_1$ required with nominal spin axis orientation.

   Fire first midcourse.

2. Track from 2 days to 5 days.

   Improve estimate of spin axis with tracking data.

   Calculate vernier velocity with new spin axis.

   Fire first vernier.

3. Track from 5 days to nominally 60 days.

   Select precise time for second correction (60 days nominal).

   Calculate velocity $V_2$.

   Fire second correction.

4. Track 20 days more.

   Calculate second vernier velocity.

   Fire second vernier.

5. Track

6. If impact seems improbable, make no more firings, and continue tracking.

7. If impact seems probable, fire a time of flight correction at 5 days before the predicted time of impact.

# IV. TRACKING STUDIES

Tracking simulations were carried out assuming that the DSIF stations, Goldstone, Woomera, and Johannesburg, would be used. The observations used are range rate, azimuth, and elevation. The data rates and accuracies used depend on the tracking interval and are listed in Table IV-1 for the 1964 trajectory. The data rates in each case were chosen to give sufficient tracking accuracy, but are low enough to be consistent with practical data handling. The limiting factor for the data near Mars, however, is not data handling, but the duty cycle of the transponder. A duty cycle of 20 minutes every 6 hours was assumed. Data accuracy is a function of distance and therefore can be different for different tracking intervals.

There are three uses which will be made of tracking data in real time:

1) Tracking between midcourse corrections, or from injection to the first correction, is used to measure the existing miss in the impact parameter plane and compute the next midcourse correction.

2) Tracking before and after any midcourse correction, is used to measure the vehicle spin axis at the time of that correction. This is done by comparing the effect of the correction on the velocity vector as indicated by tracking with the effect which had been predicted.

3) Tracking after the last midcourse correction will be used to estimate both the miss at the target and the astronomical unit (AU). In cases of planetary impact, this tracking data will be used to compute the "time of arrival correction," made 5 days before impact. (This is discussed further in Section III.) In non-impacting cases, the space bus will be tracked for 5 days after planetary encounter and the combined tracking data used to estimate the AU. (This technique is discussed further in Section V.)

Results of tracking simulations are listed in the accompanying tables and figures. Table IV-2 shows the covariance matrices of tracking errors in the impact parameter for 1964; the corresponding $1\sigma$ error ellipse (40 percent ellipses) are shown in Figure IV-1. Tracking in each of the pertinent intervals is handled independently of all other data--in other words no a priori data is used. By contrast, Figure IV-2 shows how tracking errors decrease with with tracking time if there is continous tracking with no interruption for mid-course maneuvers. The curves, in Figure IV-1, showing the semi-major and semi-minor axes of the uncertainty ellipse in the impact parameter plane, constitute

Table IV-1: Tracking Data Rates and Data Accuracies Assumed for 1964.

| Interval (days) | Data Rate (pt/min) | $\sigma_R$ (fps) | $\sigma_A$ | $\sigma_E$ (deg) | Number of Observations |
|---|---|---|---|---|---|
| 0-2 | 0.1 | 0.2 | 0.06 | 0.06 | 1296 |
| 2-5 | 0.1 | 0.2 | 0.06 | 0.06 | 1944 |
| 5-60 | 0.02 | 0.4 | 0.03 | 0.03 | 7128 |
| 60-80 | 0.02 | 0.4 | 0.03 | 0.03 | 2592 |
| 230-240 | 0.3 | 0.4 | 0.03 | 0.03 | 19440 |

Table IV-2. Covariance Matrices of Tracking Error In Impact Parameter and Time of Flight

|  | B·T | B·R | $t_f$ |
|---|---|---|---|
|  |  | 0 to 2 days |  |
| B·T (Mm) | .1649712 | $.4726328 \times 10^{-2}$ | $-.4317268 \times 10^{-1}$ |
| B·R (Mm) |  | $.3519836 \times 10^{-2}$ | $-.1815996 \times 10^{-2}$ |
| $t_f$ (min) | Symmetric |  | $.2758052 \times 10^{-2}$ |
|  |  | 2 to 5 days |  |
| B·T (Mm) | $.1539556 \times 10^{1}$ | .9773596 | -.1463136 |
| B·R (Mm) |  | $.4956680 \times 10^{-1}$ | $-.1932438 \times 10^{-1}$ |
| $t_f$ (min) | Symmetric |  | $.1933903 \times 10^{-1}$ |
|  |  | 5 to 60 days |  |
| B·T (Mm) | .5664292 | .1187881 | -.1623880 |
| B·R (Mm) |  | $.2675030 \times 10^{-1}$ | $-.3490216 \times 10^{-1}$ |
| (min) | Symmetric |  | $.4764792 \times 10^{-1}$ |

Table IV-2. Covariance Matrices of Tracking Error In Impact Parameter and Time of Flight (Continued)

| | B·T | B·R | $t_f$ |
|---|---|---|---|
| | | 60 to 80 days | |
| B·T (Mm) | .6196000 x $10^{-1}$ | .2005474 x $10^{-1}$ | -.2549503 x $10^{-1}$ |
| B·R (Mm) | | .8537336 | -.2354486 |
| $t_f$ (min) | Symmetric | | .3401498 |
| | | 230 to 240 days | |
| B·T (Mm) | .1170998 x $10^{1}$ | .1474244 x $10^{1}$ | -.2134248 x $10^{1}$ |
| B·R (Mm) | | .2042405 x $10^{1}$ | -.2830538 x $10^{1}$ |
| $t_f$ (min) | Symmetric | | .4071728 x $10^{1}$ |

Table IV-3. Covariance Matrices of Velocity Measurement Error at Time of First Correction for 1964

| | | | |
|---|---|---|---|
| | | 0 to 2 days | |
| $\dot{x}$(fps) | 0.36883753 x $10^{-1}$ | 0.30092992 x $10^{-1}$ | 0.46493368 x $10^{-1}$ |
| $\dot{y}$(fps) | | 0.52451780 x $10^{-1}$ | -0.12761218 x $10^{-1}$ |
| $\dot{z}$(fps) | | | 0.17134702 |
| | | 2 to 5 days | |
| $\dot{x}$(fps) | 0.22684370 | 0.26820352 | 0.24395061 |
| $\dot{y}$(fps) | | 0.56806384 | -0.14950696 |
| $\dot{z}$(fps) | | | 1.10136622 |

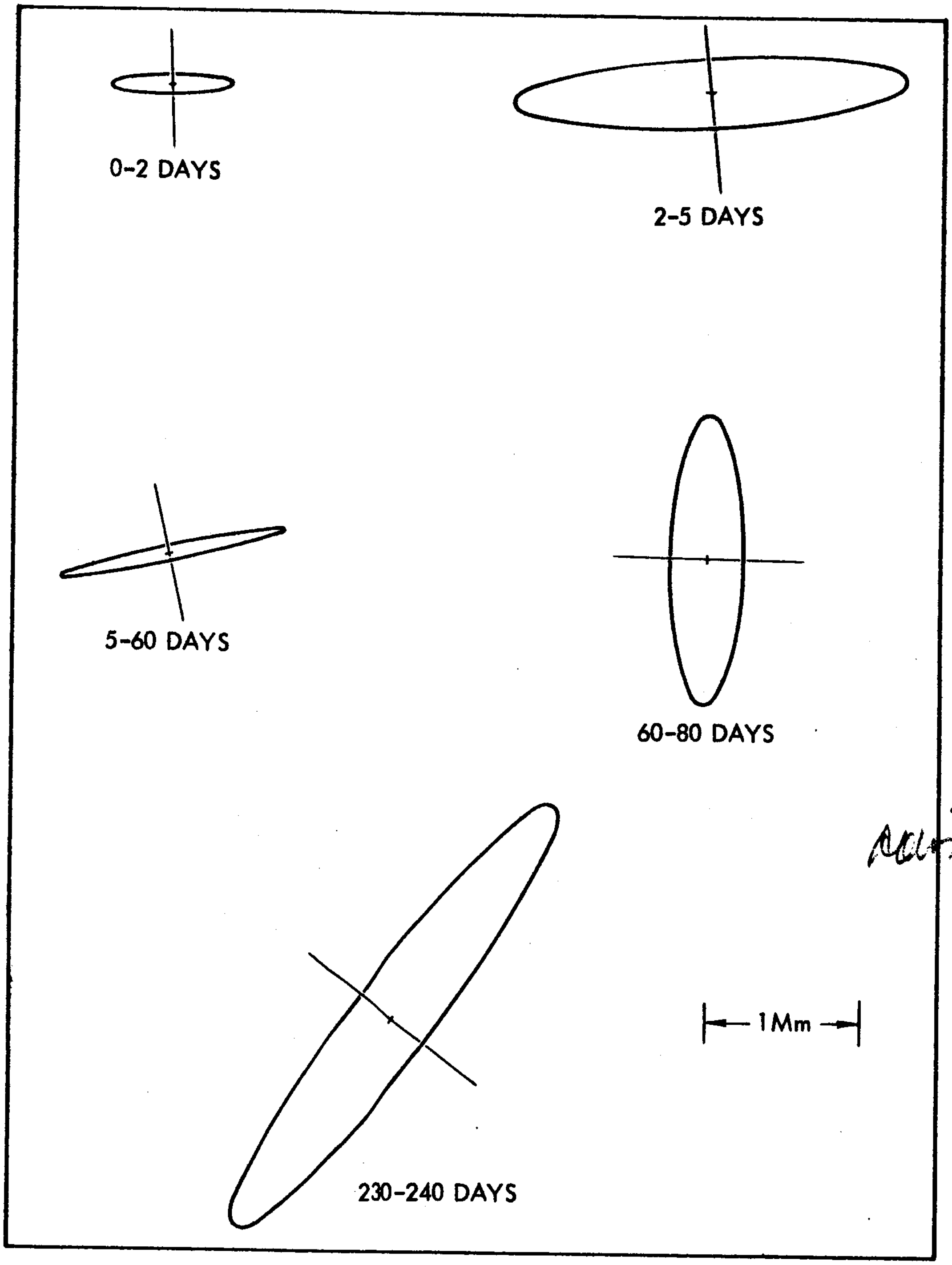

accost $(\vec{B}\cdot\vec{R})$

$(\vec{B}\cdot\vec{T})$ accost

Figure IV-1. Cne-Sigma Tracking Error Ellipses

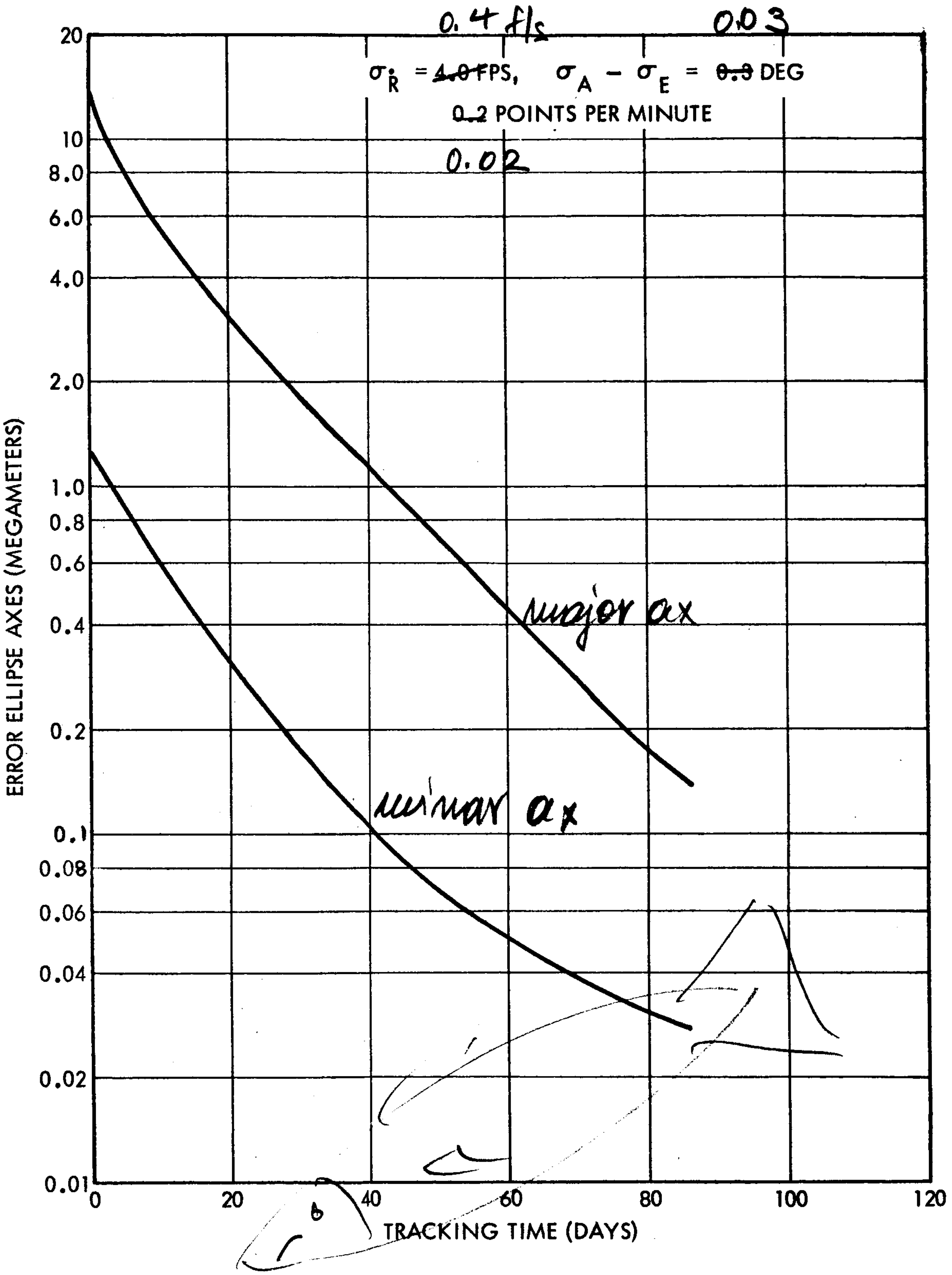

Figure IV-2. Tracking Errors as a Function of Time (no midcourse corrections)

"lower bounds" on the expected tracking uncertainty, as opposed to Figure IV-2 which shows "upper bounds".

In practice, the previous tracking covariance matrix, plus a covariance matrix of execution errors, constitute an a priori covariance matrix for tracking after each midcourse maneuver. Using this data will significantly reduce tracking uncertainties compared with the "upper bound". In Table VI-1 it can be seen that without using a priori data, tracking errors contribute approximately the same as execution errors to the final miss viz, about 0.9 Mm, 1$\sigma$ in each direction. Therefore, we may conclude that with the use of a priori data for tracking, execution errors will dominate over tracking errors Hence, if any additional effort is to be expended to reduce the final miss, the effort should be concentrated on reducing midcourse maneuver execution errors rather than tracking errors. In particular, the use of additional stations early in the mission does not appear to be called for.

Table IV-3 shows how accurately the spin axis can be determined from tracking. The technique is to estimate the velocity vector just before a particular midcourse correction by using tracking data before the correction, and also to estimate the velocity vector just after that correction using tracking data after the correction. The difference between those measurements is the velocity correction which was actually fired. By comparing the actual vector correction with the commanded vector correction, one can estimate both magnitude and attitude errors in the execution of the midcourse correction.

Tracking after the last midcourse correction--from about 80 days to Mars Encounter or later--will be used both to estimate the miss at the target and to measure the AU. Figures IV-3 and IV-4 show how well thses quantities can be determined from this tracking data. The final prediction of impact parameter uncertainty indicated--less than 100 km--is probably optimistic due to the fact that we have not simulated all possible systematic errors which tend to degrade this accuracy. Accuracy better than 1/4 Mars radius should be obtainable, however. Similarly, the estimated error in AU will probably be about $1:10^5$ rather than the more optimistic value indicated in Figure IV-4.

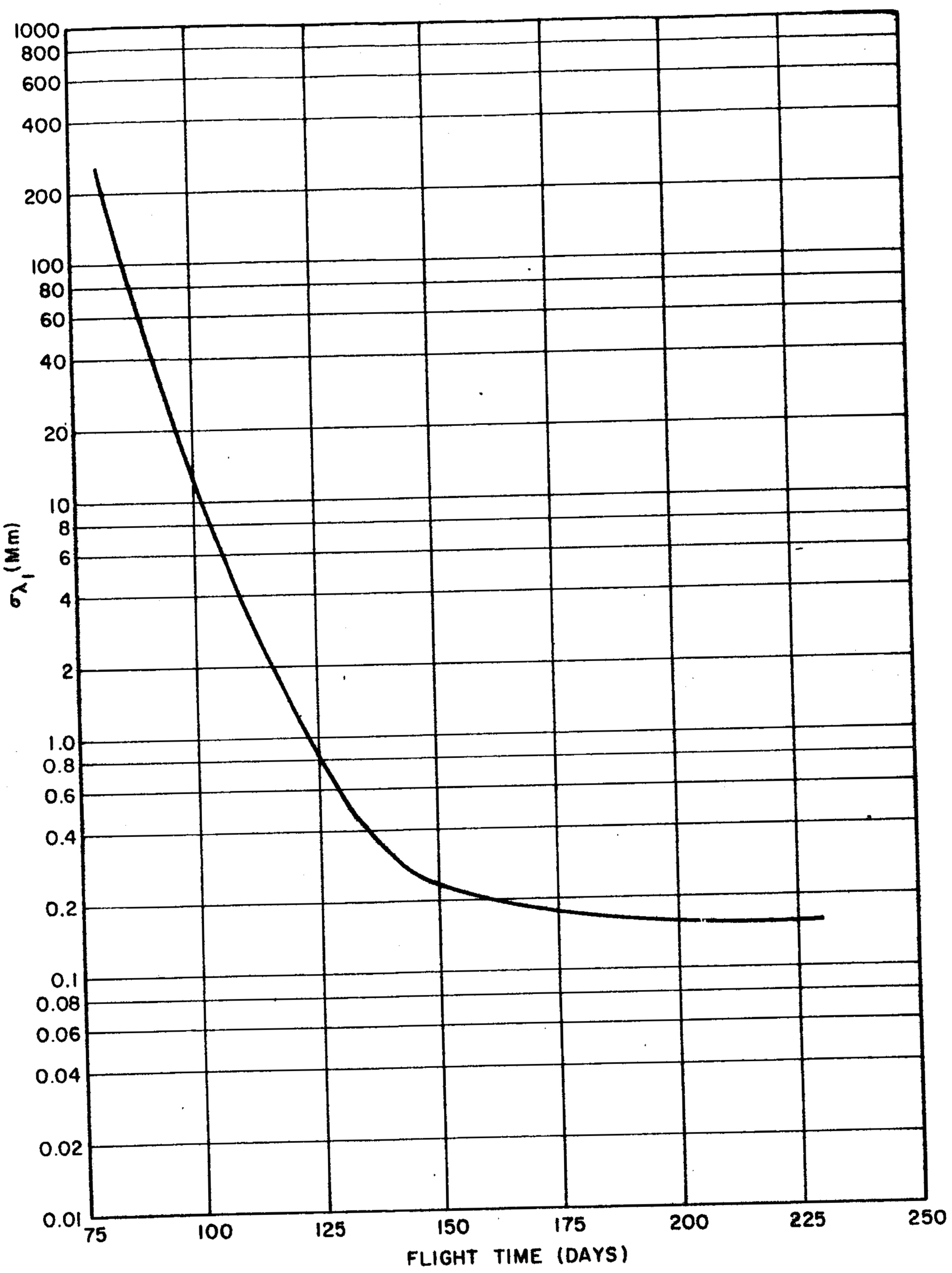

Figure IV-3. Standard Deviation Caused by the Uncertainty in Tracking Including the effect of AU: Semi-major Axis, $\sigma_\lambda$, of Dispersion Elipse in Impact Parameter Plane (Mm) V Flight Time in Days

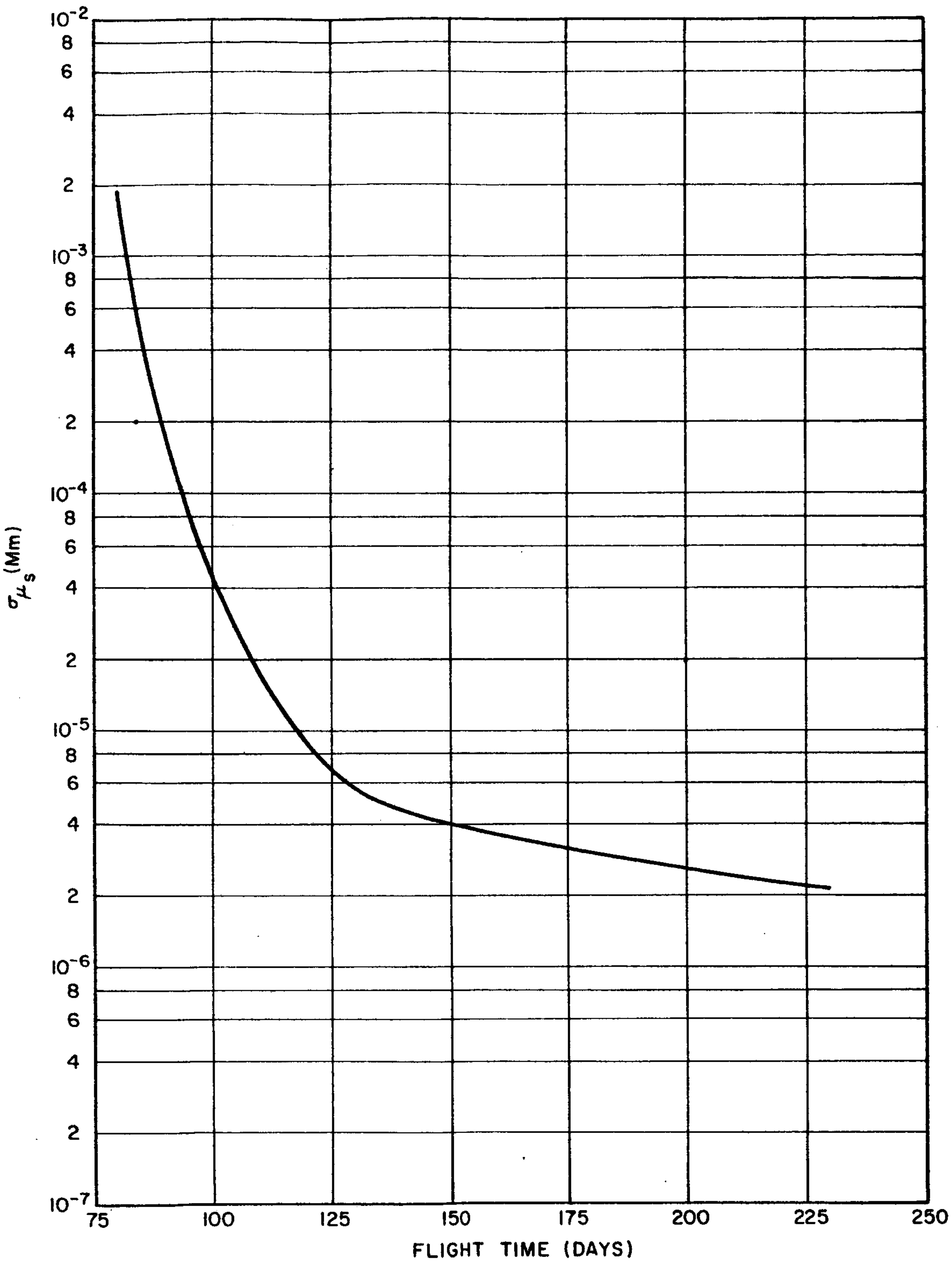

Figure IV Standard Deviation from Uncertainty of Sun's Gravitational Constant, $\sigma_{\mu_s}$, versus Time in Days

# V. THE ASTRONOMICAL UNIT AND PHYSICAL CONSTANTS

There are a number of systematic errors, as opposed to random errors, which affect the accuracy of any interplanetary mission. Most prominent of these is the uncertainty in the astronomical unit (AU). These errors and the resultant misses are discussed below.

## A. ASTRONOMICAL UNIT (AU)

### 1. Uncertainty in AU

Table V-1 shows the measurement of the AU since 1895 expressed in terms of solar parallax. If the recent radar measurements of JPL and Millstone are correct, then the AU will not be a major problem. However, since those results are inconsistent with the most recent results of dynamical methods, it must be assumed that the problem is not satisfactorily resolved as yet, and the inconsistencies in Table V-1 make one hesitate to assert that the knowledge of the AU is better than a few parts in $10^4$. It is quite possible, however, that by 1964 (and probably by 1966), improved data analysis and/or additional data will reduce the uncertainty in the AU to, say, one part in $10^5$. As seen below, this degree of accuracy would make the miss due to the AU near-negligible for purposes of this mission.

### 2. Miss Due to AU

Assessing the effect of the AU is made complicated by the fact that we are not analyzing a single free flight trajectory, but an entire mission in which there is tracking, orbit determination and midcourse guidance to consider. In evaluating the miss, the following computer runs were made:

1) A "nominal" free flight trajectory was selected. Specifically, this corresponds to injection on 20 November 1964 into a trajectory which arrives in the vicinity of Mars on 12 July 1965.

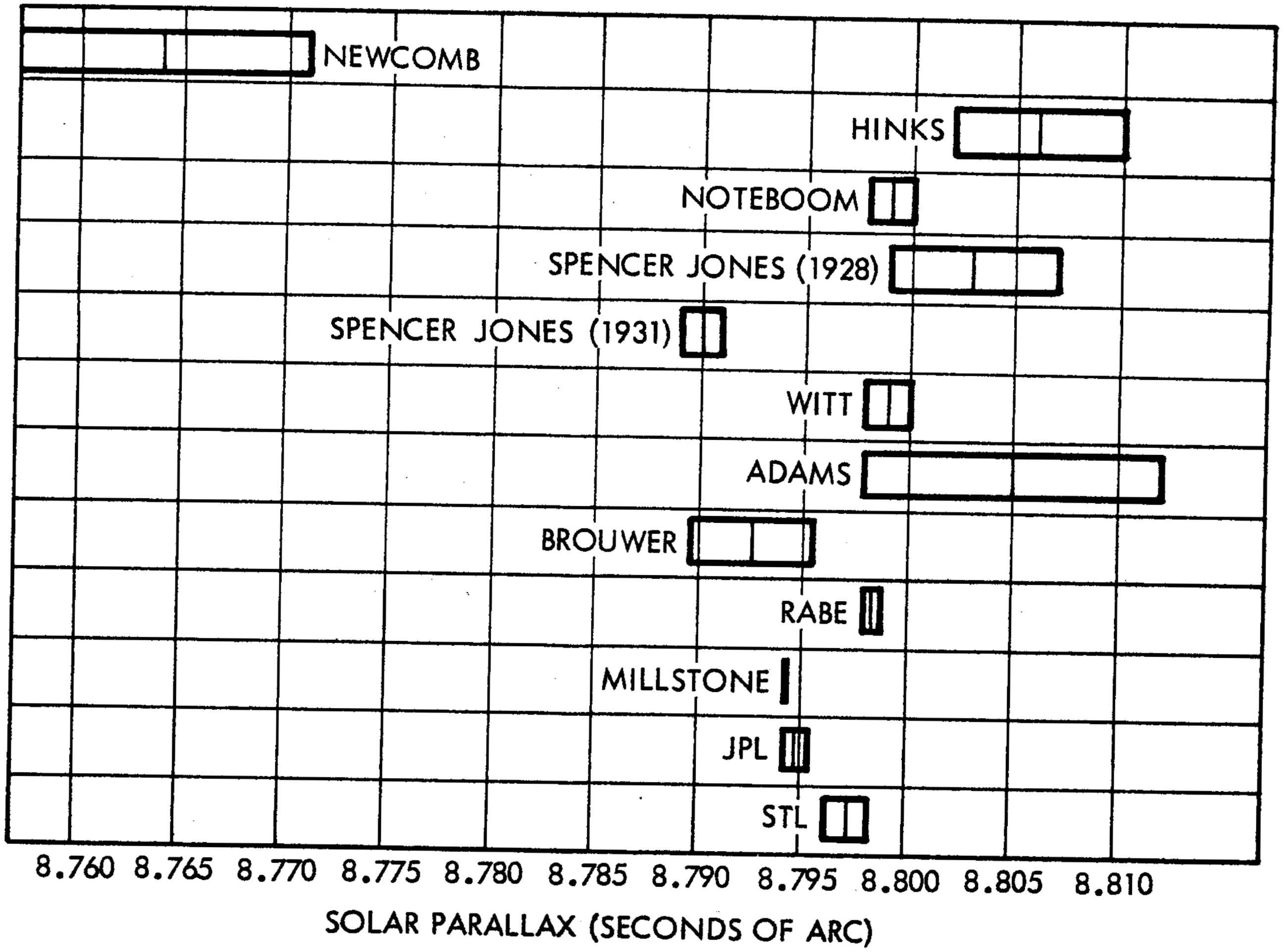

Figure V-1. Measurements of AU in Terms of Solar Parallax

2) Within the computer, the planetary system was perturbed to correspond to a change in the AU of 3:10$^4$. Using the above nominal injection condition, the trajectory was "flown" out to the vicinity of Mars and the miss in the impact parameter plane evaluated.

This analysis provides the miss coefficient which would be applicable if there were no injection errors, and hence no midcourse corrections. To see what happens when midcourse corrections are made, the following additional runs were made:

1) Position and velocity in the unperturbed case were evaluated when the spacecraft was 5 days out (25 November). These values were used as "initial conditions" for a trajectory "flown" in the perturbed planetary system, and the miss in the impact parameter plane evaluated.

2) Similarly, position and velocity were evaluated 80 days out (8 February 1965) from the unperturbed case. These were used as initial condition in a perturbed planetary system.

The interesting fact develops that the AU miss is essentially invariant out to 80 days of the mission and that the miss coefficient is approximately 1.4 earth radii (or 2.5 Mars radii) per one part in 10$^4$ uncertainty in AU.

### 3. Measurement

A Mars mission in 1964 could be used to determine the AU using the same technique as was used on Pioneer V in 1960. Briefly, this technique is to track a body in the sun's field and, on the basis of range rate data from the tracking system, determine the mass of the sun, which from Kepler's third law gives the AU. Improvements in space communication, and the longer tracking interval and consequent increase in data would definitely make for more accuracy than was attained by the Pioneer V experiment. However, midcourse maneuvers during the course of the flight could seriously affect the accuracy of an AU determination made in this way because of the errors introduced in the course of making the maneuvers. Therefore, a different approach, described below, will be used.

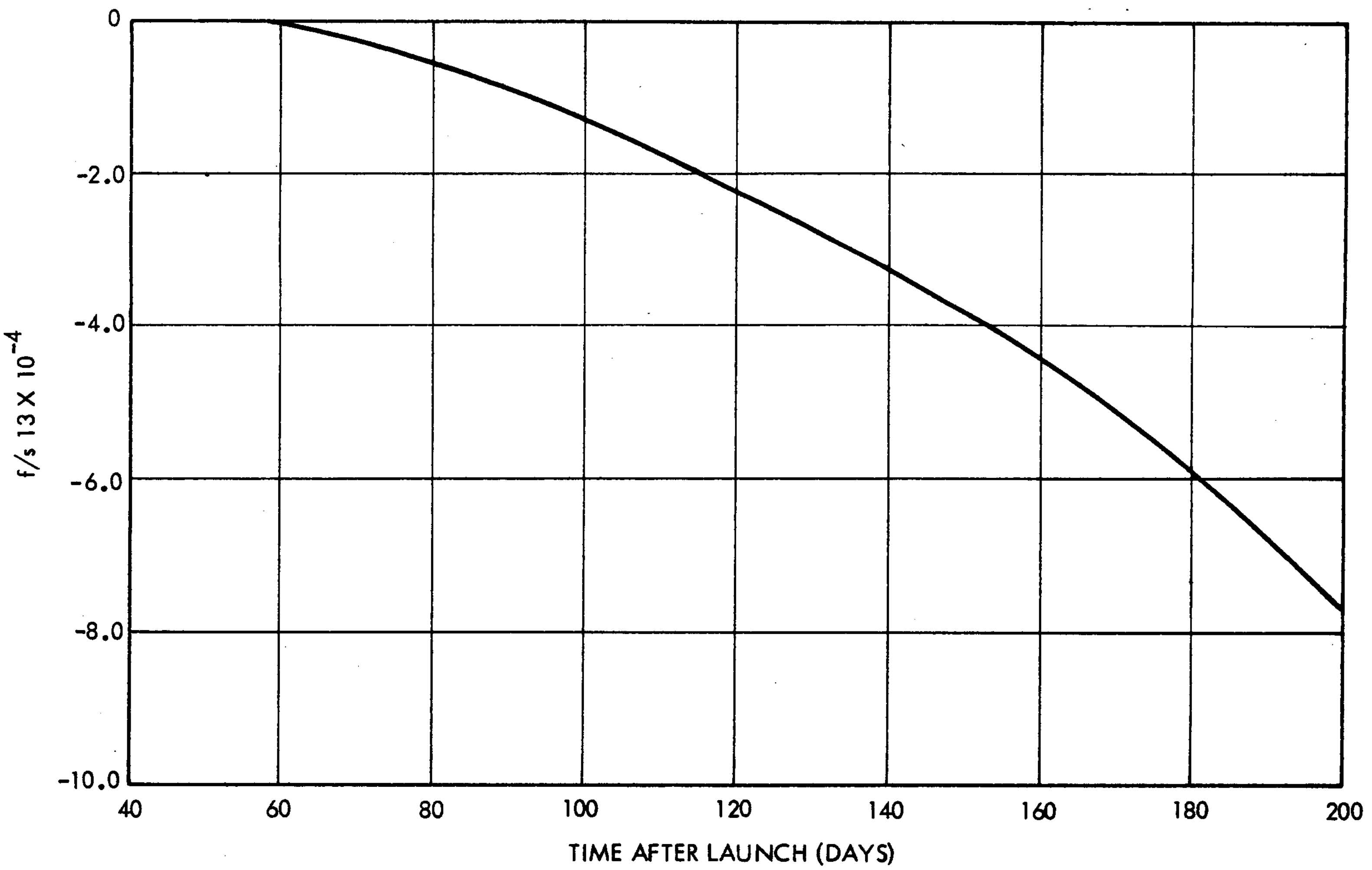

Figure V-1. Change in Range Rate for an Error of Three Parts in $10^4$ Error in AU (1964 Trajectory)

The situation with a Mars probe is different from Pioneer V since it will pass near Mars and the effect of a relatively close passage can be used to advantage in the determination of AU. Figure V-1 shows the change in range rate, ($\dot{R}$), measured from the center of the Earth for a 3 part in $10^4$ change in the AU as a function of time from launch. This curve is typical and has the same general features for all interplanetary flights (see Figure V-2 for the corresponding Pioneer V curve). But after an encounter with Mars, this curve will undergo a radical change, as shown in Figure V-3, that is, the change in range rate will be magnified approximately 100 times.

The reason for this magnification may be understood by the following argument. The predicted impact parameter at Mars is very sensitive to the assumed AU; hence an error in the assumed AU will result in a large change in the impact parameter plane which shows up as a large difference in velocity after encounter with Mars, one component of which is directly measurable by observing the doppler shift. If this one component of difference velocity were exactly known, it would determine exactly one component of the impact parameter, or, more correctly one relation between impact parameter magnitude and direction. If we can assume that the AU is the only thing which caused the impact parameter to be different from our value calculated before encounter, we can conclude that the impact parameter must have been moved along the line which is the characteristic direction of the AU partial derivative in the impact parameter plane. This line, together with the difference doppler measured from the Earth, provides the information necessary to resolve the ambiguity of the vector impact parameter and allows us to solve for magnitude of the change in the AU.

The principal inaccuracies in the determination outlined above are:

1) Accuracy with which the impact parameter prior to the encounter could be determined;

2) Accuracy with which the difference doppler shift could be measured;

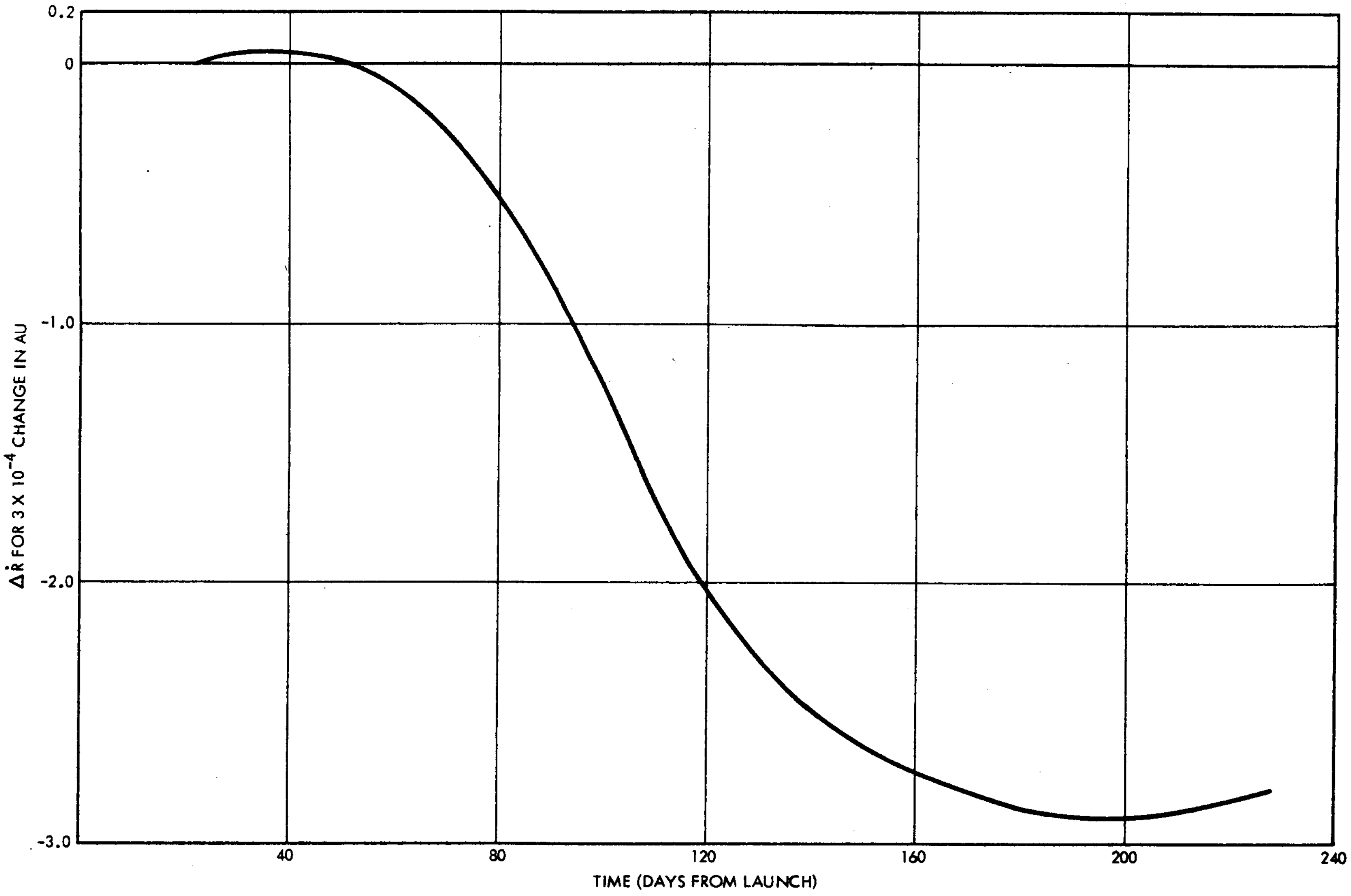

Figure V-2. Change in R with AU Versus Time from Launch for Pioneer V

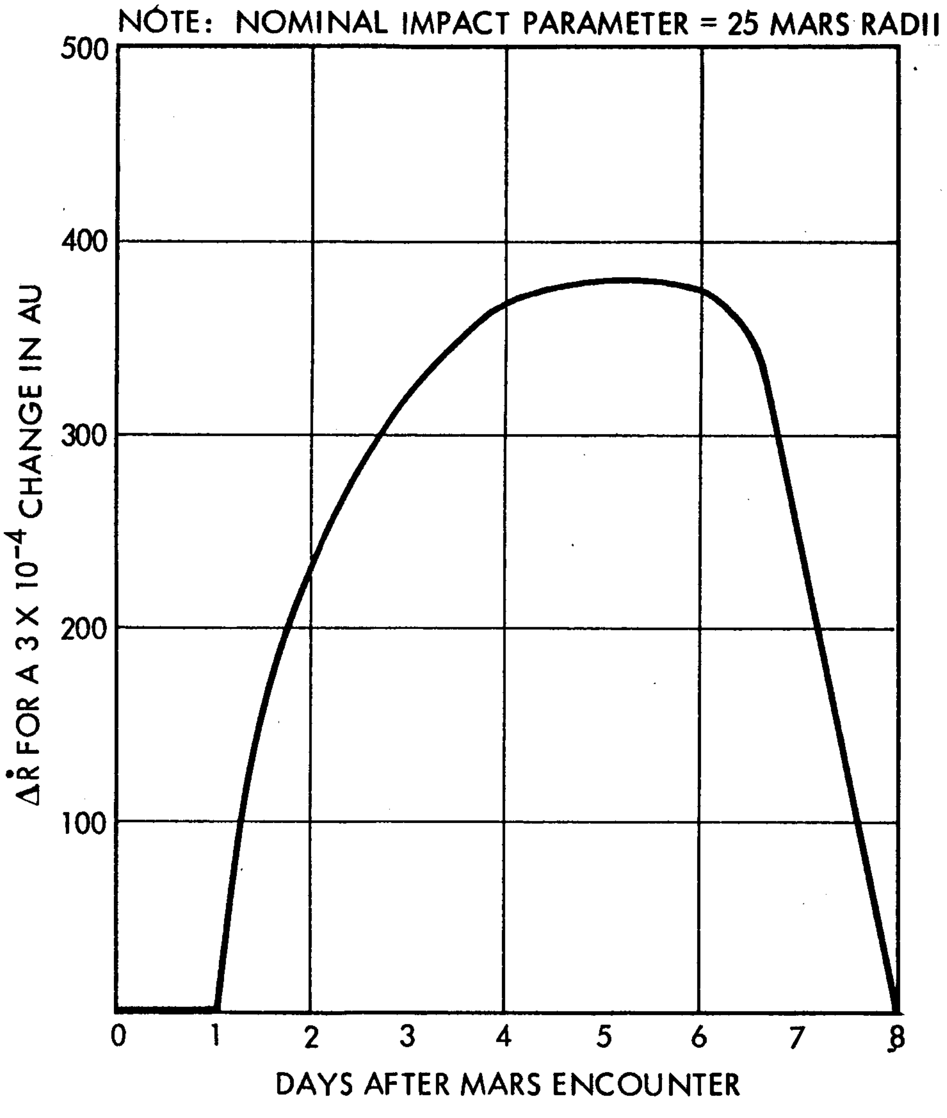

Figure V-3. Effects of a 3 x $10^{-4}$ Change in AU with a 25 Mars Radii Nominal Impact Parameter

3) Influence of the uncertainty in the GM of Mars.

The accuracy of tracking above in the prediction of impact parameter is estimated to be about 2.5 Mars radii (see Section IV) and may be directly connected to uncertainty in AU using the AU partial derivative of 2.5 Mars radii/$10^{-4}$ AU. This yields an expected error in the AU of 1 part in $10^5$.

A measurement of the difference doppler velocity should be easily good to 1 ft/sec which in turn would be 1 percent of the effect for a 1 part in $10^4$ uncertainty in the AU. This contribution would therefore be of the order of 1 part in $10^6$ in the AU.

The mass of Mars will have approximately the same percentage effect on the difference Doppler shift as will the magnitude of the impact parameter, but the uncertainty in the mass of Mars is only 1 part in $10^4$ which would be something like 0.01 ft/sec in difference velocity, and thus is negligible.

The above argument is intended only for purposes of estimating the accuracy of the AU measurement by this method. The actual implementation of the measurement would be a least squares fit to 7 parameters, for example, the 3 positions and 3 velocities after the last midcourse correction and the AU.

## 4. Other Physical Constants

### a. GM of the Earth and Station Locations

The effects of uncertainties in the GM of the earth and in station location are equivalent to errors in position and velocity of the spacecraft at a large distance from the Earth (i.e., an error in $V_\infty$ vector). Therefore, the effects on these errors are essentially cancelled by performing a least squares fit which would simply treat these effects as position and velocity errors of the spacecraft and the midcourse corrections would be computed to eliminate them.

### b. Velocity of Light

The largest velocities which would be observed on a Mars mission would be of the order of $10^5$ ft/sec (largely the velocity of the

Earth in its orbit). Since the uncertainty in the velocity of light is 1 part in $10^6$, this would lead to an error of 0.1 ft/sec, which is negligible.

### c. Integration Accuracy

The errors associated with numerical round off and truncation can be shown to increase approximately as $t^{3/2}$ where $t$ is the total flight time. It is known that for the Pioneer V flight, significance was being lost in the seventh place. Since a Mars flight would be about 2.5 times as long, the effect would be four times worse and would probably effect the sixth place, or of the order of 0.1 ft/sec.

### d. Planetary Ephemerides

The principal difficulty in the reduction of the JPL and Millstone radar data has been the planetary ephemerides. At present the radar data are inconsistent with the ephemerides to approximately the extent of 1 part in $10^5$ in the AU. It seems probable therefore that the inconsistencies in the tabular positions of the planets could cause errors in the order of 0.25 Mars radii.

### e. Ground Oscillator Stability

At the time of the encounter with Mars, the two-way transit time will be of the order of one-half hour. Since we will be attempting to measure velocity to accuracies of 0.1ft/sec, the ground oscillator must not drift more than $\frac{0.1 \text{ ft/sec}}{c}$ or $1 \times 10^{-10}$ in one-half hour.

### f. Solar Radiation Pressure

It is well known that a solar radiation pressure can have an appreciable effect on space probes. For example, STL studies of solar radiation on the RANGER-MARINER* Venus probe for 1962 indicates that for that particular spacecraft configuration is between 9,000 and 6,000 km, depending on the particular trajectory (flight time) involved. However, this effect is to a large extent predictable in advance, with the residual uncertainty amounting to approximately 5 to 10 percent of the total effect. For the Mars mission in question, we estimate that the unpredictable portion of the miss due to radiation pressure will be less than 1,000 km, and this value may be appreciably decreased as better measurements of the solar constant become available.

---

* This work was performed under the RANGER Targeting Studies for Lockheed.

## VI. RELATIVE EFFECTS OF ERROR SOURCES

The error sources that affect the final accuracy of a particular flight can be divided into three categories--midcourse execution errors, tracking errors, and physical-constant errors (the launch errors enter into the error sources as magnitudes of the midcourse correction). Of these sources, the dominant one for 1964 is the AU error. In 1966-67 the AU error should be reduced to about a tenth of its 1964 value. In each case the accuracy is not limited by tracking. Although additional tracking accuracy is always desirable, the three DSIF stations yield sufficient accuracy to accomplish the mission.

### A. EXECUTION ERRORS

The execution error sources consist of magnitude error and attitude error. The magnitude error is a result of the uncertainty in converting firing times to velocity and in starting and stopping the engine. For the first correction, the attitude error is a result of the uncertainty in the attitude of the booster stages and the tip-off error occuring in the separation of the spacecraft from the booster. For the succeeding corrections the attitude error is reduced by tracking before and after the first correction. The firing time error is proportional to the velocity desired and is estimated to be one percent ($1\sigma$). The shutdown error is independent of desired velocity and is estimated to be 0.1 meter per second ($1\sigma$).

The impact parameter errors caused by velocity magnitude errors can be reduced by firing a vernier correction soon after the main correction, but this does not remove the effects of the attitude errors. The final estimate of execution errors after the second vernier in the impact parameter plane is 0.23 Mars radii for B.T. and 0.15 for B.R.

### B. TRACKING

Tracking error enters the system in the prediction of impact parameter and time of flight, and in the measurement of attitude. The tracking errors in the impact parameter plane at the end of the second vernier are 0.23 in Mars radii for B· T and 0.27 for B· R, and the attitude measurement error is 0.17 in B· T and 0.2 in B· R.

## C. PHYSICAL CONSTANTS

The only physical constant which has a significant effect on this mission is the astronomical unit (see Section V). For 1964 it is assumed that a one-sigma uncertainty of one part in $10^4$ exists. The error in impact parameter plane after the second vernier in the 1964 trajectory is expected to be 1.75 Mars radii in B· T and 1.75 in B·R for an error of one part in $10^4$. By 1966, it is expected that the uncertainty in AU will be reduced by an order of magnitude. The resultant AU miss at Mars will then be comparable with the other errors.

## D. COMPARISON OF EFFECTS

Table VI-1 show the "one-sigma" effects of the separate error sources for the 1964 trajectory. The ultimate components of impact parameter are given in units of Mars radii for convenience in visualization. Since the execution errors do not have a Gaussian distribution, the term "one-sigma" does not exactly have its usual significance, but the numbers given are useful for approximate comparisons.

Table VI-1. Final Accuracy

| After Second Correction | B˙T<br>Mm | B˙R<br>Mm |
|---|---|---|
| Spin Axis Measurement (from tracking) | 0.582 | 0.736 |
| Magnitude Execution (one percent (50 m/sec firing) | 4.67 | 2.70 |
| Tracking Error (5-60 days) | 0.753 | 0.163 |
| RSS | 4.76 | 2.80 |
| After Second Vernier | | |
| Spin Axis Measurement (from tracking | 0.582 | 0.736 |
| Magnitude Execution (0.1 m/sec shutdown error) | 0.793 | 0.518 |
| Tracking Error (5-60 days)* | 0.753 | 0.163 |
| (60-80 days) | 0.249 | 0.922 |
| RSS | 1.26 | 1.30 |
| In Mars radii, RSS = | 0.36 | 0.38 |
| AU ($10^{-4}$) | 6.00 | 6.00 |
| RSS | 6.14 | 6.15 |
| In Mars radii ($1\sigma$) = | 1.79 | = 1.79 |
| ($3\sigma$) = | 5.37 | = 5.37 |

---

* The 5 to 60 day tracking is included during the second vernier correction because this approximate method is conservative and still gives good results.

# VII. COMMUNICATION SUBSYSTEM

## A. REQUIREMENTS

The communication requirement for the Able-M bus is to transmit data for a period of 8 months and for distances ranging from that at lift-off to the Mars-Earth distance at arrival. For the trajectory chosen the maximum communication distance is approximately 120 million miles. The communication system is compatible with the NASA Deep Space Instrumentation Facility (DSIF) as projected for the 1964-66 era. At maximum range the system will provide, with 5 db margin, a one bit per second command and telemetry capability using the present DSIF 85-foot antennas and 10 kilowatt transmitter. Should the projected 210-foot antennas and 100 kilowatt transmitter become available during the program, communication rates up to 8 bits per second at maximum with a 5 db margin will be possible.

However, unlike the previous Able-M study in which experimental data was telemetered directly from the spacecraft, there appears to be no real need for high-speed telemetry in the present Able-M bus concept. All experimental results are to be relayed to Earth by the experimental capsule telemetry, leaving only diagnostic data to be handled by the telemetry system on the bus vehicle. With a bit rate of one per second and an antenna gain of 8 db, the transmitter power required at Mars is 25 watts. However, to achieve the required antenna gain at Mars a simple attitude reorientation maneuver must be performed at approximately 155 days. Prior to reorientation, the directional antenna will nevertheless be pointed in the general direction of Earth, thereby allowing for the use of the 2.5 watt driver of the 25-watt power amplifier for about half the flight (110 days). In addition to the directional antenna, an omnidirectional antenna will be provided for use in case of vehicle attitude failure during the boost phase. Also during this phase the 50 mw output of the solid state driver for the TWT will provide communication with the vehicle.

## B. GENERAL DESCRIPTION

The basic communication system to be employed for the Able-M bus is shown in Figure VII-1. This system provides tracking, telemetry and command in an integrated loop. To meet the lifetime requirements of the mission

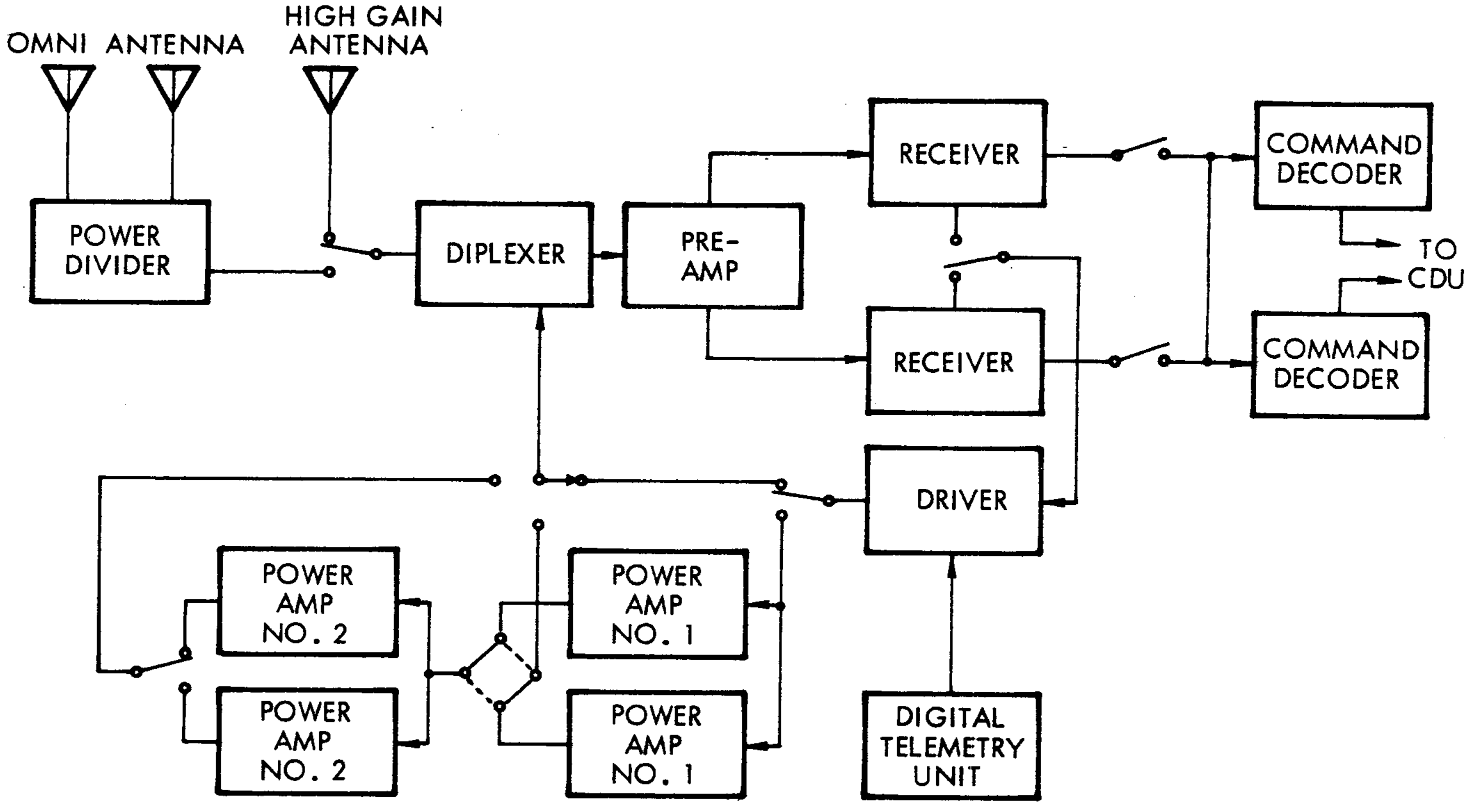
OMNI ANTENNA
HIGH GAIN ANTENNA
POWER DIVIDER
DIPLEXER
PRE-AMP
RECEIVER
RECEIVER
COMMAND DECODER
COMMAND DECODER
TO CDU
DRIVER
DIGITAL TELEMETRY UNIT
POWER AMP NO. 1
POWER AMP NO. 1
POWER AMP NO. 2
POWER AMP NO. 2

Figure VII-1. Communication Subsystem Simplified Block Diagram

with high reliability, virtually the entire communication system has been made redundant. Parallel operation of receivers, transmitters and command decoders insures a minimum likelihood of additional unreliability due to the added redundancy. The single low-noise preamplifier allows the separation of the signal into two redundant paths without incurring a noise penalty due to rf losses.

In operation the DSIF transmitter will impress on the spacecraft receivers a highly stable radio frequence signal. The transmitter frequency is swept through the receiver frequency at which time the receiver locks on the transmitted signal. The phase-lock receivers then permit the generation of a coherent transmitter frequency which is a precise fraction (240/221) of the received frequency. The coherent transponder allows the extraction of accurate doppler information by comparison of the ground transmitter and ground received frequencies. Doppler recovery is especially important in this mission because spacecraft velocity changes will be used to estimate the miss distance at Mars.

Ground commands are phase-modulated on the carrier in such a fashion that the resultant spectrum lies outside the receiver phase-lock loop bandwidth. The commands therefore appear at the output of the loop phase detector as error signals. Thus these signals can be extracted and applied to the command decoders.

The diagnostic information from the various spacecraft subsystems is encoded by the digital telemetry unit. The information emerges in binary code and phase modulates the transmitter driver. The ground receiver demodulates this information. The information format is compatible with teletype and can readily be transmitted between the DSIF sites and NASA headquarters.

## C. TELEMETRY POWER BUDGET

The binary telemetry data is to be encoded onto the rf carrier by bi-phase modulating a sinusiodal subcarrier of frequency $f_m = 1024$ cps and then phase modulating the carrier with this subcarrier. Both the carrier and subcarrier will be coherently demodulated in the ground stations through the use of phase-lock loops. The carrier loop which tracks the carrier frequency spectral line is to be designed for a closed loop noise bandwidth of 3 cps. An examination of the minimum energy trajectory for the Able-M mission has indicated, that, for the two-way doppler rates to be encountered, and for a loop bandwidth of 3 cps, the resulting phase error is less than 0.1 radians at all ground stations, except during the boost phase. The power of the carrier frequency spectral line is given by

$$S_c = J_o^2(\beta)\, S_1 \tag{6.1}$$

where $S_i$ = total received signal power at the antenna, watts

$S_c$ = received carrier power at the antenna, watts

$\beta$ = peak modulation index of subcarrier on carrier, radians.

After coherent demodulation of the subcarrier the resultant binary digits are passed through an averager, which is the optimal filter in the presence of white noise. Since the receiver i-f passband is limited to include only the first order subcarrier sidebands, the signal-to-noise ratio at the output of the averager at the decision time is given by

$$\frac{S_o}{N_o} = \frac{4\, S_i\, J_1^2(\beta)}{\phi_i\, H} \tag{6.2}$$

where $\phi_i$ = receiver noise spectral density referred to the antenna, watts/cps

H = bit rate, bits/sec.

Equation (6.2) can be considered to result from

1) A received data subcarrier power of $2\, J_1^2(\beta)\, S_i$
2) Equivalent noise bandwidth of demodulator and averager of H/2.

The desired accuracy of the telemetry link is assumed to correspond to a bit error probability of $10^{-3}$. This accuracy requires a signal-to-noise ratio ($S_o/N_o$) equal to 9.5 db. This value could be reduced through the use of error detecting and correcting codes, but this is not considered justifiable for this application.

The peak modulation index ($\beta$) utilized for the link was chosen consistent with the following requirements:

1) The performance margin will be approximately the same in the carrier and subcarrier loops for the required data rate. This margin can be changed in the actual design if desired to provide a higher bit rate.

2) Smaller values of $\beta$ will be preferred due to minimization of energy content of higher order subcarrier harmonics.

The telemetry power budget of Table VII-1 reflects the performance of the link for a spacecraft transmitter power of 25 watts and spacecraft antenna gain of 8 db. The ground stations (DSIF) possess an 85-foot antenna with a gain of 52.8 db at 2300 Mc. For the 1 bit/sec data rate, these system parameters provide a 5 db margin in each loop at Mars distance with a peak modulation index of 0.8 radians.

In Table VII-1 the required signal-to-noise ratio for threshold in the carrier loop is given as 6 db. Knowledge and experience regarding the capabilities of phase-coherent devices in the presence of noise has indicated that this is reasonable level of performance to be expected from the Able-M telemetry receiver.

## D. COMMAND POWER BUDGET

The modulation technique for the command link will differ slightly from the telemetry link. The sinusoidal subcarrier which is phase modulated onto the r-f carrier will be frequency modulated (FSK'd) with the binary command data. This will allow non-coherent detection of the subcarrier with an existing command decoder. The carrier will be coherently demodulated by a phase-lock loop of noise bandwidth equal to 10 cps. For the doppler rates to be encountered, the resulting phase error is well within 0.1 radian for a loop of this bandwidth. The subcarrier will appear as an instantaneous phase error at the input to the loop filter. The subcarrier frequency is 125 cps and the subcarrier frequency deviation due to the binary data is ±25 cps. The received command signal at r-f or i-f can be represented by

Table VII-1. Able-M Telemetry Power Budget

| | | |
|---|---|---|
| 1. | Transmitter Power | 25 watts |
| 2. | S/C Transmission Circuit Loss | 1 db |
| 3. | S/C Antenna Gain | 8 db |
| 4. | Space Loss (R = 220 x $10^9$ meters<br>(2300 Mc) = 119 x $10^6$ n mi) | 266.5 db |
| 5. | Polarization Loss | 1 db |
| 6. | Ground Antenna Gain | 52.8 db |
| 7. | Ground Transmission Circuit Loss | 0.3 db |
| 8. | Net Circuit Loss | 208 db |
| 9. | Total Received Power | -164 dbm |
| 10. | Receiver Noise Spectral Density ($50^{\circ}$K) | $-181.7 \frac{\text{dbm}}{\text{cps}}$ |
| 11. | Carrier Modulation Loss | 1.5 db ($\beta = 0.8$) |
| 12. | Received Carrier Power | -165.5 dbm |
| 13. | Carrier Loop Noise Bandwidth (3 cps) | 4.8 db |
| 14. | Carrier Loop Noise Power | -176.9 dbm |
| 15. | Threshold SNR in Carrier Loop | 6 db |
| 16. | Carrier Performance Margin | 5.4 db |
| 17. | Subcarrier Loss (to Carrier, etc.) | 5.7 db |
| 18. | Received Data Subcarrier Power | -169.7 dbm |
| 19. | Equivalent Noise Bandwidth (1 bit/sec) | -3 db |
| 20. | Subcarrier Loop Noise Power | -184.7 dbm |
| 21. | Required S/N for $P_{BE} = 10^{-3}$ | 9.5 db |
| 22. | Data Performance Margin for 1 bit/sec | 5.5 db |

$$E(t) = E_i \sin \left[ \omega_c t + \beta \sin (\omega_m \pm \Delta\omega) t \right] \tag{6.3}$$

where $E_i$ = magnitude of received signal

$\omega_c$ = carrier radian frequency

$\beta$ = peak modulation index

$\omega_m$ = subcarrier radian frequency

$\Delta\omega$ = radian frequency deviation of binary data on subcarrier.

After coherent carrier phase detection and filtering the subcarrier signal is given by

$$E_s(t) = E_i J_1(\beta) \Big[ (1 \pm 1) \sin (\omega_m + \Delta\omega) t + (1 \mp 1) \sin (\omega_m - \Delta\omega) t \Big] \tag{6.4}$$

As can be observed from Equation (6.4), the presence of a signal at $f_m + \Delta f = 150$ cps represents a one and the presence of a signal at $f_m - \Delta f = 100$ cps represents a zero. The subcarrier demodulator consists of bandpass filters at 100 cps and 150 cps followed by envelope detectors, low pass filters and a subtractor. This non-coherent reception results in a signal-to-noise ratio of

$$\frac{S_o}{N_o} = \frac{2 J_1^2(\beta) S_i}{\phi_i B} \tag{6.5}$$

where B = equivalent noise bandwidth of receiver. The low pass filters have a Gaussian frequency response and a noise bandwidth equal to the bit rate. For a probability of a bit error of $10^{-3}$ the required value of $S_o/N_o$ for this non-coherent FSK system is 13.8 db.

Table VII-2 gives the power budgets for the command link for ground transmitter powers of 10 KW and 100 KW, which correspond to the DSIF ground station capabilities. The spacecraft has an antenna gain of 8 db and a receiver noise figure of 10 db. The carrier loop margin is shown as 6 db and the data

Table VII-2. Able-M Command Power Budget

| | | 10 KW Transmitter | 100 KW Transmitter |
|---|---|---|---|
| 1. | Total Transmitter Power | 70 dbm | 80 dbm |
| 2. | Ground Transmission Circuit Loss | 0.3 db | 0 db |
| 3. | Ground Antenna Gain | 52 db | 51 db |
| 4. | Space Loss ($R = 220 \times 10^9$ meters (2100 Mc) $= 119 \times 10^6$ n mi) | 265.7 db | 265.7 db |
| 5. | Polarization Loss | 1 db | 1 db |
| 6. | S/C Antenna Gain | 8 db | 8 db |
| 7. | S/C Transmission Circuit Loss | 1 db | 1 db |
| 8. | Net Circuit Loss | 208 db | 208.7 db |
| 9. | Total Received Power | -138 dbm | -128.7 dbm |
| 10. | Receiver Noise Spectral Density | $-164 \frac{dbm}{cps}$ | $-164 \frac{dbm}{cps}$ |
| 11. | Carrier Modulation Loss | 4.0 db ($\beta = 1.27$) | 13.3 db ($\beta = 2.0$) |
| 12. | Received Carrier Power | -142 dbm | -142 dbm |
| 13. | Carrier Loop Noise Bandwidth (10 cps) | 10 db | 10 db |
| 14. | Noise Power at Output of Carrier Loop | -154 dbm | -154 dbm |
| 15. | Threshold SNR for Carrier Loop | 6 db | 6 db |
| 16. | Carrier Performance Margin | 6 db | 6 db |
| 17. | Subcarrier Loss (to Carrier, etc.) | 2.7 db | 1.8 db |
| 18. | Received Data Subcarrier Power | -140.7 dbm | -130.5 dbm |
| 19. | Equivalent Noise Bandwidth (1 cps) | 0 db | 0 db |
| 20. | Noise Power at Output of Subcarrier Demodulator | -164 dbm | -164 dbm |
| 21. | Required S/N for $P_{BE} = 10^{-3}$ | 13.8 db | 13.8 db |
| 22. | Data Performance Margin for 1 bit/sec | 9.5 db | 19.7 db |

performance margin considerably greater. In the actual design the modulation index will be adjusted to provide nearly equal margins for the carrier and data if desired.

## E. SPACECRAFT EQUIPMENT

The spacecraft communication equipment planned for the Able-M bus was shown in Figure VII-1. Transmitter, receiver and command decoder will have redundant counterparts. Spacecraft attitude permits use of the directional antenna throughout the entire flight while the omnidirectional antenna provides back-up capability in case of attitude control failure. Both receivers and decoders will operate continuously. The remainder of the major units may be interchanged upon command. A list of equipment and its important characteristics is given in Table VII-3.

### 1. Transmitter

The choice of transmitter configuration depends primarily on the power required for communication at maximum range. The telemetry power budget (Table VII-1) indicates that 25 watts will be needed at Mars. Only electron tubes such as the triode, traveling wave tube, and amplitron are presently capable of delivering this power level. A particular triode amplifier which will satisfy the present requirements is the P31H triode amplifier made by Resdel Engineering Co. The P31H has an overall efficiency of 30 percent utilizing an ML 7855 ceramic-metal planar triode. It weighs 21 ounces by itself, and when packaged with the power supply, the total weight is 6 pounds. With a minimum gain to 10 db, the P31H demands a drive power of 2.5 watts for full output. The important drawback in using a triode is the relatively short lifetime of the device. Compared to the ten thousand plus hours predicted for TWT's, the 25 watt triode life is estimated at 1000 to 2000 hours. Of course, the triode amplifier would be in operation only about 500 hours since it will be commanded on for brief periods every day after 110 days.

At present there is no light-weight rugged TWT available with the required 25 watt output capability at 2300 Mc. Manufacturers of the TWT's are of course working to extend the power capability of their tubes. In particular the Watkins-Johnson WJ-227 and Hughes 349H are capable of 12 to 14 watts at

## VII-3. Spacecraft Equipment

| | No. Req'd | Weight | | Size (ea) | Power Input | Duty Cycle | Allowable Temperature Range |
|---|---|---|---|---|---|---|---|
| | | Unit | Total | | | | |
| Communication System | | | 45.9 | | | | |
| Dividers | | | | | | | |
| 2-way | 3 | 0.2 | 0.6 | 0.5 x 1.25 x 2 | | | |
| 4-way | 2 | 0.35 | 0.7 | 1.25 x 1.25 x 2 | | | |
| Diplexer | 1 | 1.5 | 1.5 | 2 x 3.5 x 5 | | | |
| Coupler | 1 | 0.3 | 0.3 | 0.5 x 1.25 x 3.5 | | | |
| Receiver | 2 | 5.0 | 10.0 | 100 $in^3$ | 3.0 w | Continuous | 0 to 40°C |
| Decoder | 2 | 2.5 | 5.0 | 100 $in^3$ | 1.0 w | Continuous | -40 to 60°C |
| Digital Telemetry | 1 | 4.0 | 4.0 | 150 $in^3$ | 1.2 w | Continuous | 0 to 40°C |
| Driver | 1 | 0.9 | 0.9 | 50 $in^3$ | 1.0 w | Continuous | |
| Power Amplifier No. 1 | 2 | 2.5 | 5.0 | 8.3 x 1.6 x 1.2 | 16 w | Continuous | |
| Power Amplifier No. 2 | 2 | 6.0 | 12.0 | 8-9/16 x 5 x 3-1/8 in | 100 w | Intermittent, 110 - 240 days | |
| Antenna-directional | 1 | 1.0 | 1.0 | (130 $in^3$) | | | |
| Antenna-omni | 1 | 0.4 | 0.4 | | | | |
| Switches | 5 | 0.8 | 4.0 | 2 x 2 x 3.63 | | | |
| Cables and Connectors | 1 | 0.5 | 0.5 | | | | |

band center and could be optimized at 2300 Mc. One version of the 349H has been scaled to 20 watts over the 3.0 to 3.6 Gc band with an efficiency of 25 percent. However, the tube life would be adversely affected with a probable reduction from 20,000 to 10,000 hours. The TWT would be a desirable solution to the transmitter problem because of its high efficiency, relaibility and ruggedness. However, the decision would be dependent on the ability of a manufacturer to scale a tube to the required power level and frequency with a minimum expenditure of time and money.

The Raytheon QKS 997 amplitron is available with a 25 watt minimum capability at precisely 2300 Mc. The device efficiency is 60 percent (not including heater), the power gain is 20 db, and the weight only one pound. However, there are three problems associated with using an amplitron in the Able-M bus. The first concerns the unknown lifetime of the device which is an important consideration for a system which must survive for 8 months. Although the manufacturer predicts lifetimes comparable to those of TWT's, the additional back bombardment of the amplitron cathode raises questions as to the justification for these predictions.

The second problem is the need for a very special power supply for reliable operation. The amplitron, while operating in the signal-locked mode, may be triggered into a noncoherent or noisy mode by power supply or signal input transients. Restoration of normal drive, for example, will not return the tube to normal operation. Instead the power supply voltages must be reduced and then gradually increased until coherent operation is restored. This phenomenon was actually observed at STL during tests of a Raytheon amplitron.

A third questionable amplitron characteristic is the large stray magnetic field. Although there are no magnetic experiments aboard the Able-M bus, a large stray field is generally undesirable. Although this field can probably be reduced to 1 gamma by shielding with no increase in tube weight, this is a major effort and no results are available yet.

The choice of a driver for the final power amplifier must also be predicated on high efficiency, light weight and high reliability. Efficiency and reliability are vital since this lower power amplifier must function continuously virtually the entire 8-month mission. A solid-state transmitter developed at STL which could supply the 2.5 watts was considered. However, even though the reliability of this transmitter is in excess of 10,000 hours, the efficiency is not much better than 10 percent. Certain TWT's on the other hand, exhibit efficiencies of 20 percent not including DC/DC converters. In particular the Watkins-Johnson WJ-237 and Hughes 314H traveling wave tubes are nominally 2 watt tubes and operate in this frequency range with minimum efficiencies of 20 percent. Furthermore, measurements of the 314H at STL have verified the fact that the tube will supply up to 3 watts at band center. The predicted life of both tubes, based on cathode loading, is at least 40,000 hours. With 33 db of gain at saturation the TWT as a power amplifier requires only slightly more than a milliwatt of drive.

The 2-watt TWT would be an appropriate driver for either the triode or amplitron as a final stage. If a 25-watt TWT were available, then only a low power (milliwatts) driver would be needed. For the early part of the flight the TWT output would be limited to about 2.5 watts by voltage controlling the beam current. The gain would also be reduced in approximately the same ratio. However, the tube efficiency will suffer by such operation. In one test of the 349H, Hughes reduced the output power by 6 db, the gain dropped 4 db, and the efficiency went from 28 percent to 19.6 percent. The effect of reducing the output power by 10 db as required for Able-M would of course have to be similarly measured and evaluated before this mode of operation could be recommended.

The overall transmitter block diagram is shown in Figure VII-2. The output from the receiver at 115 Mc is phase modulated with the telemetry information. At this frequency a deviation of 1/20 radian will result in a one radian deviation at the output frequency. The power amplifier following the modulator generates 0.5 watt to drive the varactor multiplier. The x 20 multiplier will have an output of 50 mw or a conversion loss of 10 db. The multiplier will use four idler circuits at the second, fourth, eighth and sixteenth harmonics of the input frequency. The techniques involved in building high-harmonic multipliers have been previously studied at STL. One example is a x19 multiplier which produced a 1786 Mc output at 20 mw when driven by 200 mw at 94 Mc. High-harmonic multiplier circuits have been found to be easier to build and are more stable than a chain of several multipliers in cascade. The former

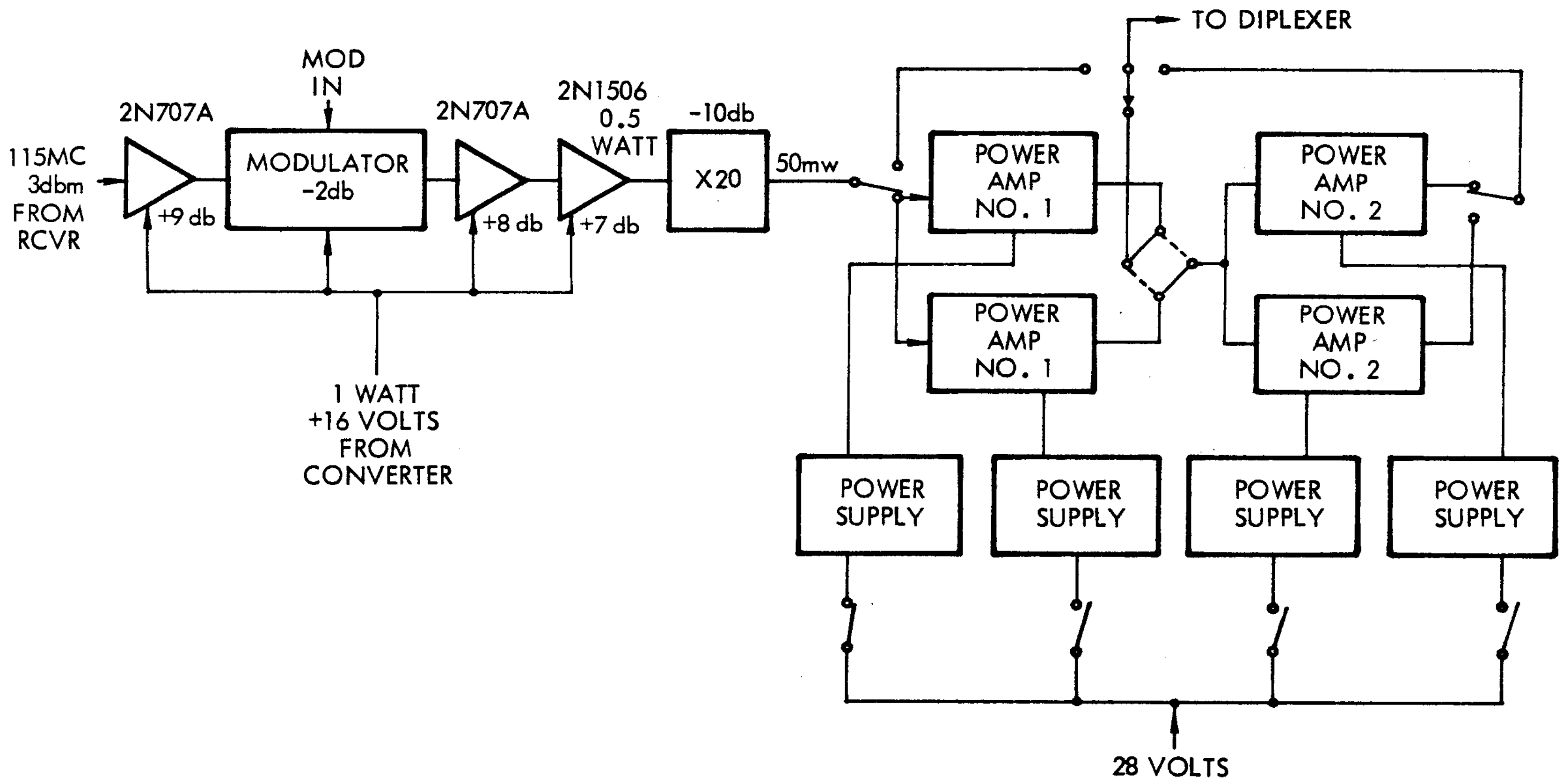
TO DIPLEXER
MOD IN
2N707A
2N707A
2N1506 0.5 WATT
-10db
115MC 3dbm FROM RCVR
MODULATOR -2db
X20
50mw
+9 db
+8 db
+7 db
POWER AMP NO. 1
POWER AMP NO. 1
POWER AMP NO. 2
POWER AMP NO. 2
1 WATT +16 VOLTS FROM CONVERTER
POWER SUPPLY
POWER SUPPLY
POWER SUPPLY
POWER SUPPLY
28 VOLTS

Figure VII-2. Transmitter Block Diagram

are especially to be preferred when the power level is low enough to prevent excessive varactor dissipation as in the present case.

Following the low power driver are power amplifiers Nos. 1 and 2. If, from further study and experimentation, the amplitron or triode prove suitable as power amplifier No. 2, then power amplifier No. 1 should be one of the nominal 2-watt traveling wave tubes discussed above. Should a 25-watt TWT capable of satisfactory operation at 2.5 watts become available, then only a single pair of power amplifiers in parallel redundancy would be required.

As shown in Figure VII-2 the inputs of the pair of power amplifiers No. 1 are permanently connected together through a power divider. The outputs may be directed, through a 4-pole transfer switch, either to the output selector switch or to the inputs of the power amplifier No. 2. The output of either amplifier No. 2 can then be connected to the output selector switch which selects one of three power levels -- 50 mw, 2.5 watts or 25 watts. The 50 mw level from the solid-state driver will be used during the boost phase while the vehicle is in the Earth's atmosphere. Then the 2.5 watt TWT output will provide sufficient power to about 110 days out, after which point the 25-watt amplifier will be employed. The duty cycle of the transmitter for Able-M is depicted in Figure VII-3.

### 2. Receiver

The principal considerations in designing a receiver for this mission were:

1) Compatibility with DSIF transmitting and receiving frequencies.

2) Provision of a coherent transponder with the appropriate frequency ratio (240/221) for two-way doppler measurement.

3) Efficient reception and demodulation of the command information.

4) Avoidance of self-lock and other spurious response phenomena.

The last item was given especially heavy weight in the decision. The block diagram of the triple-conversion phase-lock transponder is shown in

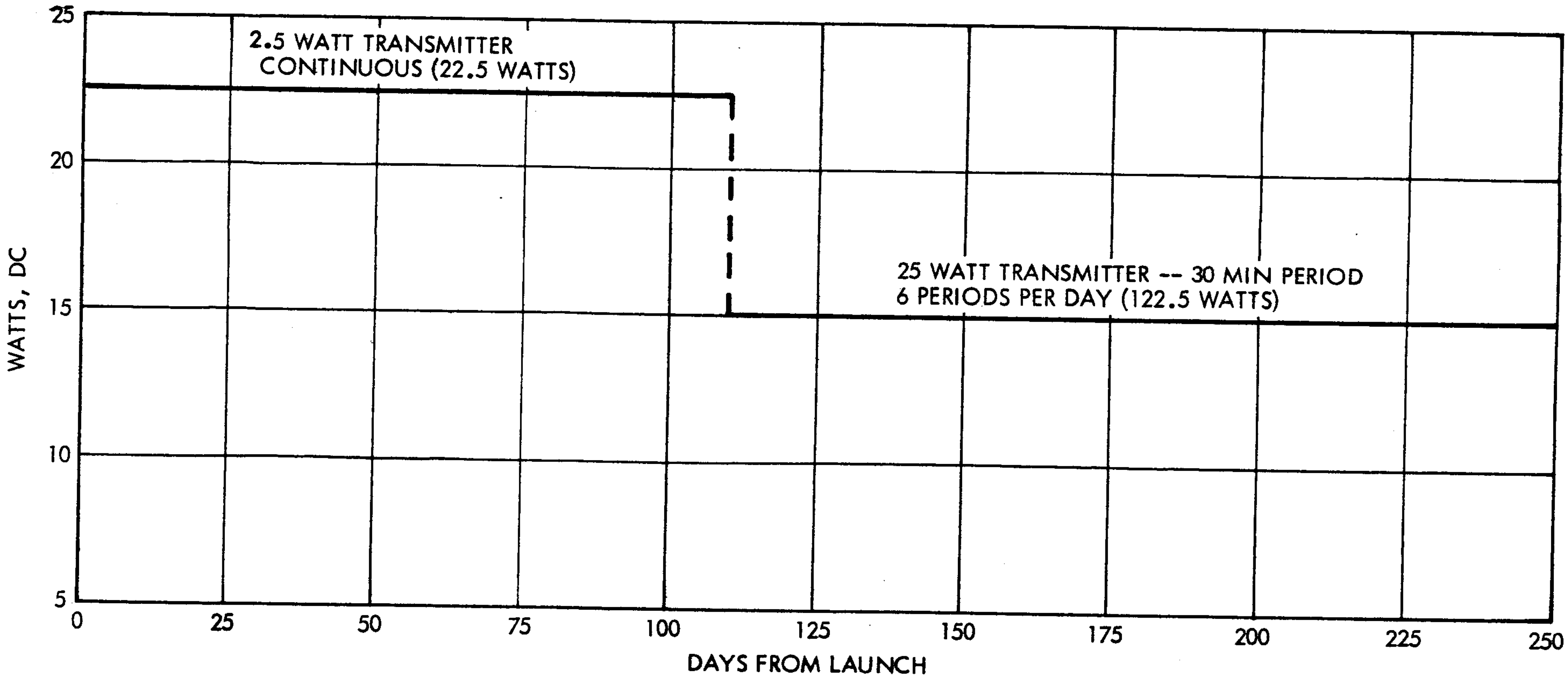

Figure VII-3. Able-M Power Duty Cycle

Figure VII-4. The receiver is a modification of the design employed on the ABLE series at a lower frequency. Approximately 80 receivers of the ABLE design have been produced to date, 25 of which have been flown on space missions with no record of failure.

In Figure VII-4 the received frequency, 221 $f_1$, is mixed with the locally generated signal 216 $f_1$. The difference frequency 5 $f_1$ is amplified and filtered by a crystal filter in the first i-f amplifier. Then the i-f output is further reduced in frequency in the second mixer to $f_1$. The second i-f amplifier includes a crystal filter and a limiter. In the third mixer the second intermediate frequency $f_1$ is mixed with the voltage-controlled oscillator (VCO) frequency $f_2$ and the difference $f_2 - f_1$ selected at the output. After amplification in the third i-f amplifier, the signal is finally applied to the phase detector. The other phase detector input is the locally generated reference oscillator signal, $f_2 - f_1$. The outputs of the VCO and reference oscillator are doubled, and then mixed in the fourth mixer to produce an output at $2f_1$. This is subsequently amplified, doubled and applied to the second mixer, and, after tripling and multiplication by 18, drives the first mixer.

The output of the phase detector is amplified, filtered by the loop filter and returned to the VCO control input to complete the feedback loop. The feedback controls the VCO frequency and phase such that the coherent 216/221 ratio is maintained at the first mixer and the two inputs to the phase detector are in quadrature.

The receiver is of the triple-conversion type and so designed as to minimize the possibility of self-locking. Also drifts in the reference oscillator are cancelled and do not appear in the transmitted signal. The combination of the receivers and the common preamplifier should provide an acquisition sensitivity of -148 dbm in the narrow-band mode. The receiver can be operated with either a 500 cps or 10 cps bandwidth. Phase-lock loop acquisition is best accomplished by sweeping the ground transmitter through the receiver frequency. A frequency sweep of 30 kc should be adequate to cover the range of frequency uncertainty.

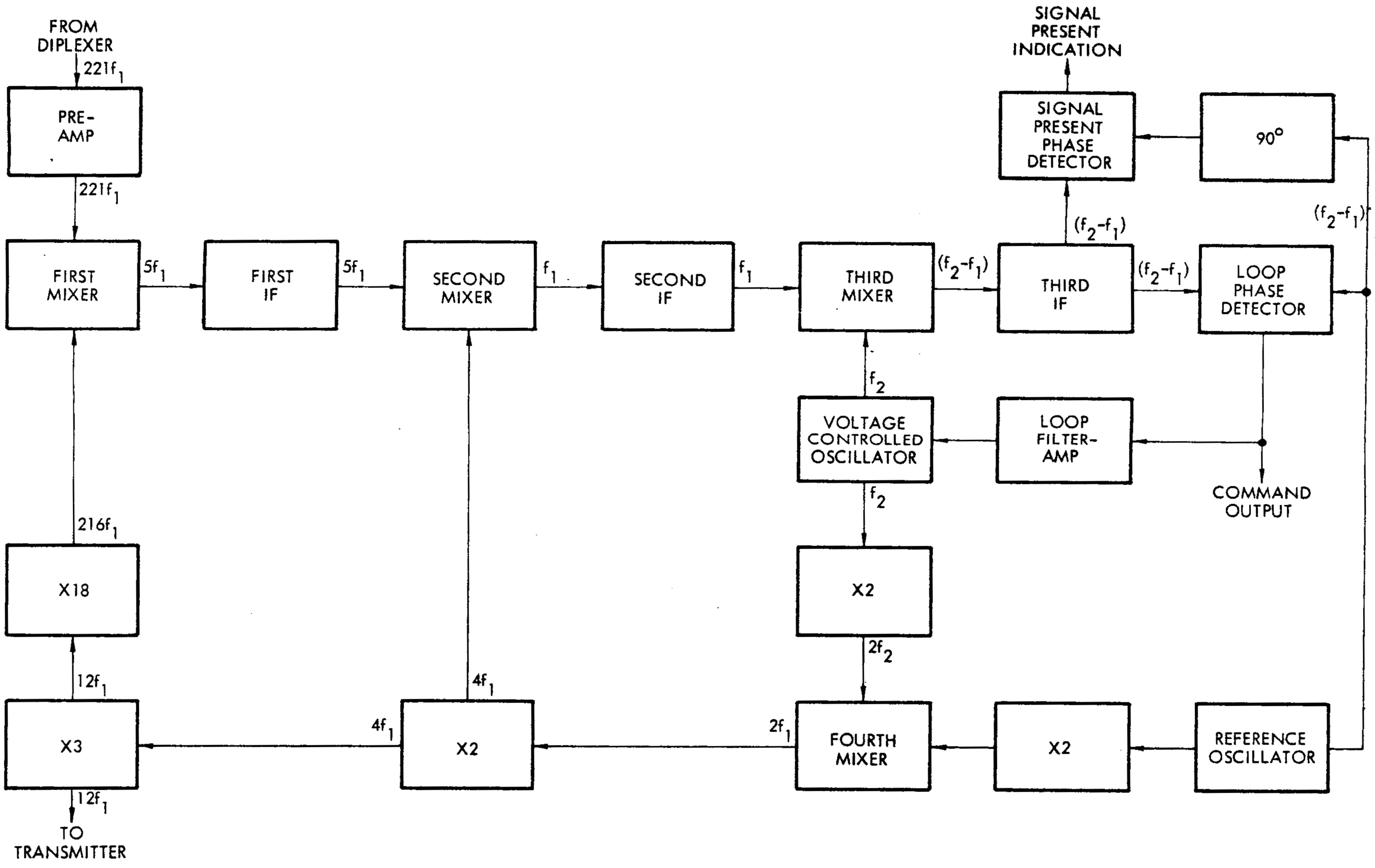
FROM DIPLEXER
221f1
PRE-AMP
221f1
FIRST MIXER
5f1
FIRST IF
5f1
SECOND MIXER
f1
SECOND IF
f1
THIRD MIXER
(f2-f1)
THIRD IF
(f2-f1)
SIGNAL PRESENT PHASE DETECTOR
SIGNAL PRESENT INDICATION
90°
(f2-f1)
LOOP PHASE DETECTOR
(f2-f1)
COMMAND OUTPUT
LOOP FILTER-AMP
VOLTAGE CONTROLLED OSCILLATOR
f2
f2
X2
2f2
FOURTH MIXER
2f1
X2
REFERENCE OSCILLATOR
X2
4f1
4f1
X3
12f1
12f1
TO TRANSMITTER
X18
216f1

Figure VII-4. Receiver Block Diagram

Ahead of the first mixer in each receiver is a single transistor preamplifier which allows low-noise distribution of the incoming signal from the antenna to the two receivers. The preamplifier incorporates two newly-developed Texas Instruments transistors, each of which are rated at 9 db gain and 7.5 db noise figure at 3000 Mc. The transistors are combined in a tuned rf amplifier providing at least 10 db of gain and a substantial measure of preselection as well. The noise figure of the preamplifier at 2300 Mc should be about 5 db.

### 3. Antenna Group

The Able-M bus antenna group consists of a high-gain antenna, an omnidirectional antenna, power dividers, a coupler, a switch, and a diplexer. Interconnection is as depicted in the block diagram of Figure VII-5. The power dividers and couplers are used to obtain the desired power division and phase among the various antenna feed points. The switch allows selection upon ground command of one of the two antennas. The diplexer permits simultaneous operationof the receiver and trasnmitter with a single antenna. Under normal conditions, communications between spacecraft and ground is effected via the high-gain antenna. An omnidirectional antenna is provided, however, which is useful during the earlier phases of the flight or in case trouble is encountered in the orientation control system.

The high-gain antenna is of the circular horn type and is mounted concentric with the rocket-nozzle heat shield on the aft end of the spacecraft as shown in Figure VII-6. Internal radila vanes are used for equalizing the E-plane and H-plane beamwidths. The outer end of the antenna structure slopes backward from the heat shield in order to be removed from the rocket plume. The antenna is excited in a circularly polarized $TE_{11}$ mode by four probes located near the base and fed in phase rotation. The radiated energy is directed along the aft spin axis and is circularly polarized. Control of beamwidth and beam circularity is obtained by adjusting the aperture diameter and the vane width.

The radiation pattern, when adjusted to vary approximately as $Cos^4$ $\theta$, yields the optimum gain as is demonstrated in Figure VII-7. From these

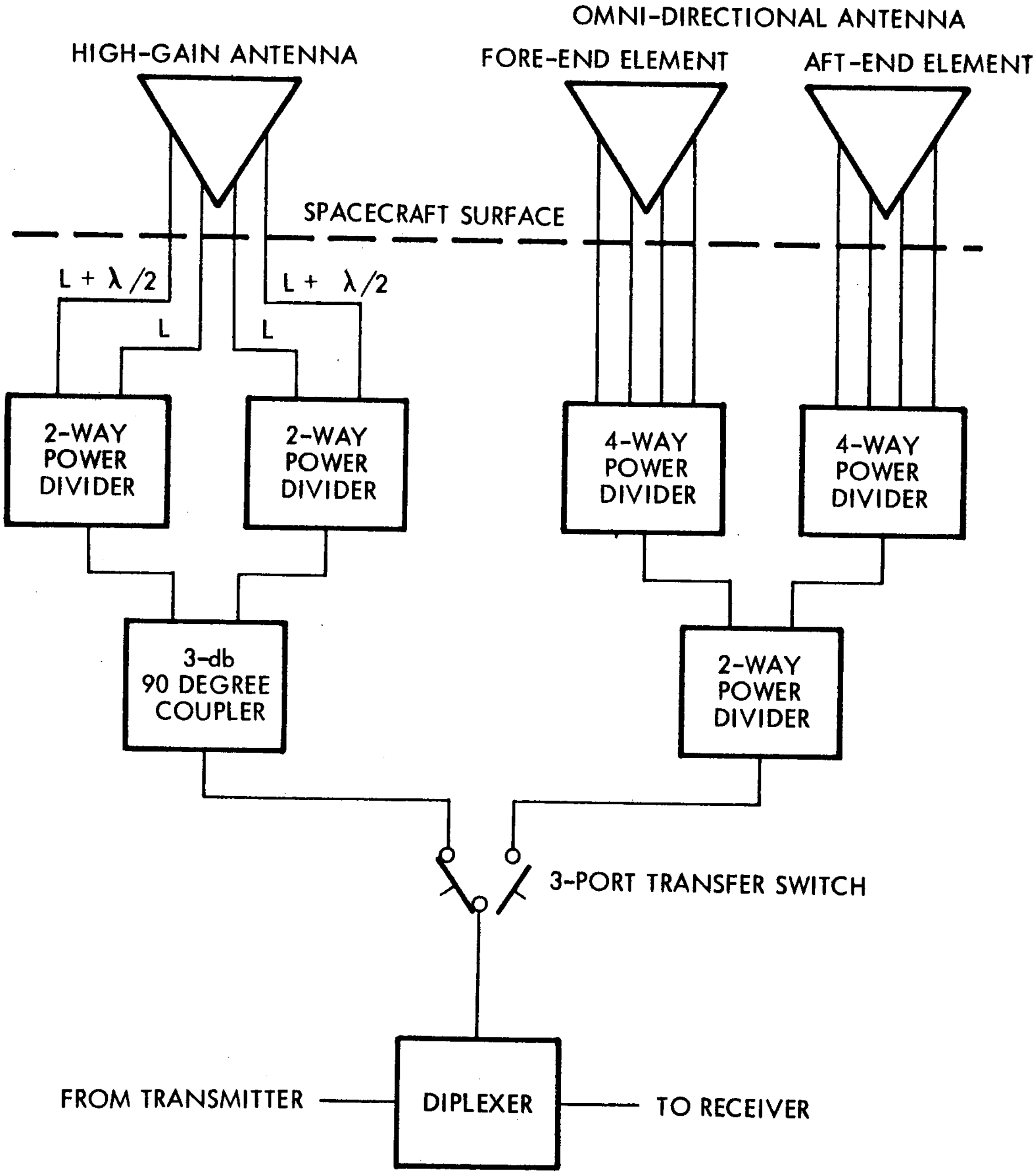
OMNI-DIRECTIONAL ANTENNA
HIGH-GAIN ANTENNA
FORE-END ELEMENT
AFT-END ELEMENT
SPACECRAFT SURFACE
L + λ/2
L
L
L + λ/2
2-WAY POWER DIVIDER
2-WAY POWER DIVIDER
4-WAY POWER DIVIDER
4-WAY POWER DIVIDER
3-db 90 DEGREE COUPLER
2-WAY POWER DIVIDER
3-PORT TRANSFER SWITCH
FROM TRANSMITTER
DIPLEXER
TO RECEIVER

Figure VII-5. Block Diagram of Antenna Group for Able-M Bus Spacecraft

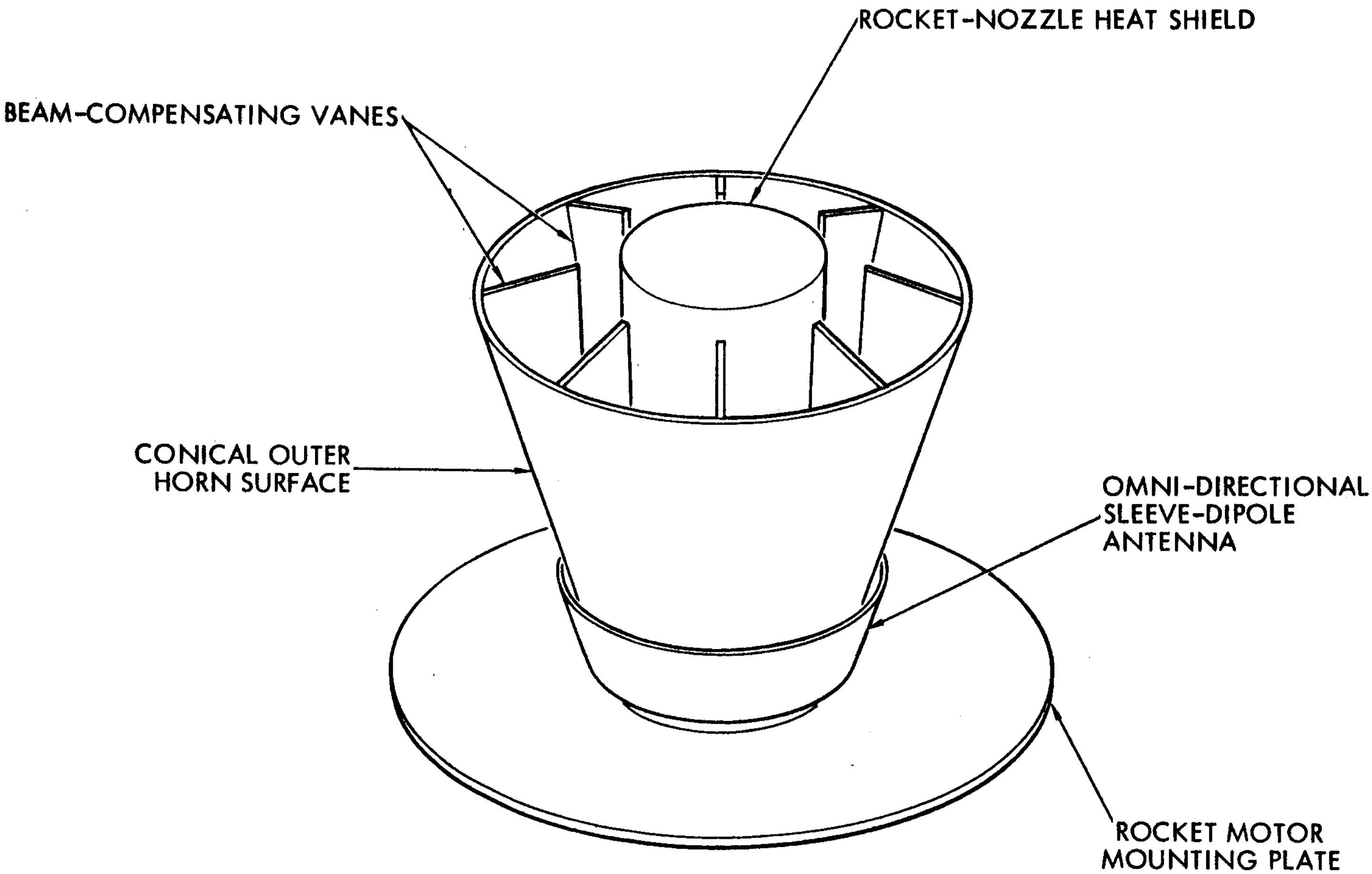
ROCKET-NOZZLE HEAT SHIELD
BEAM-COMPENSATING VANES
CONICAL OUTER HORN SURFACE
OMNI-DIRECTIONAL SLEEVE-DIPOLE ANTENNA
ROCKET MOTOR MOUNTING PLATE

Figure VII-6. Sketch Showing High-Gain Horn Antenna and Omni-Directional Sleeve-Dipole Antenna for use on the Able-M Bus Spacecraft

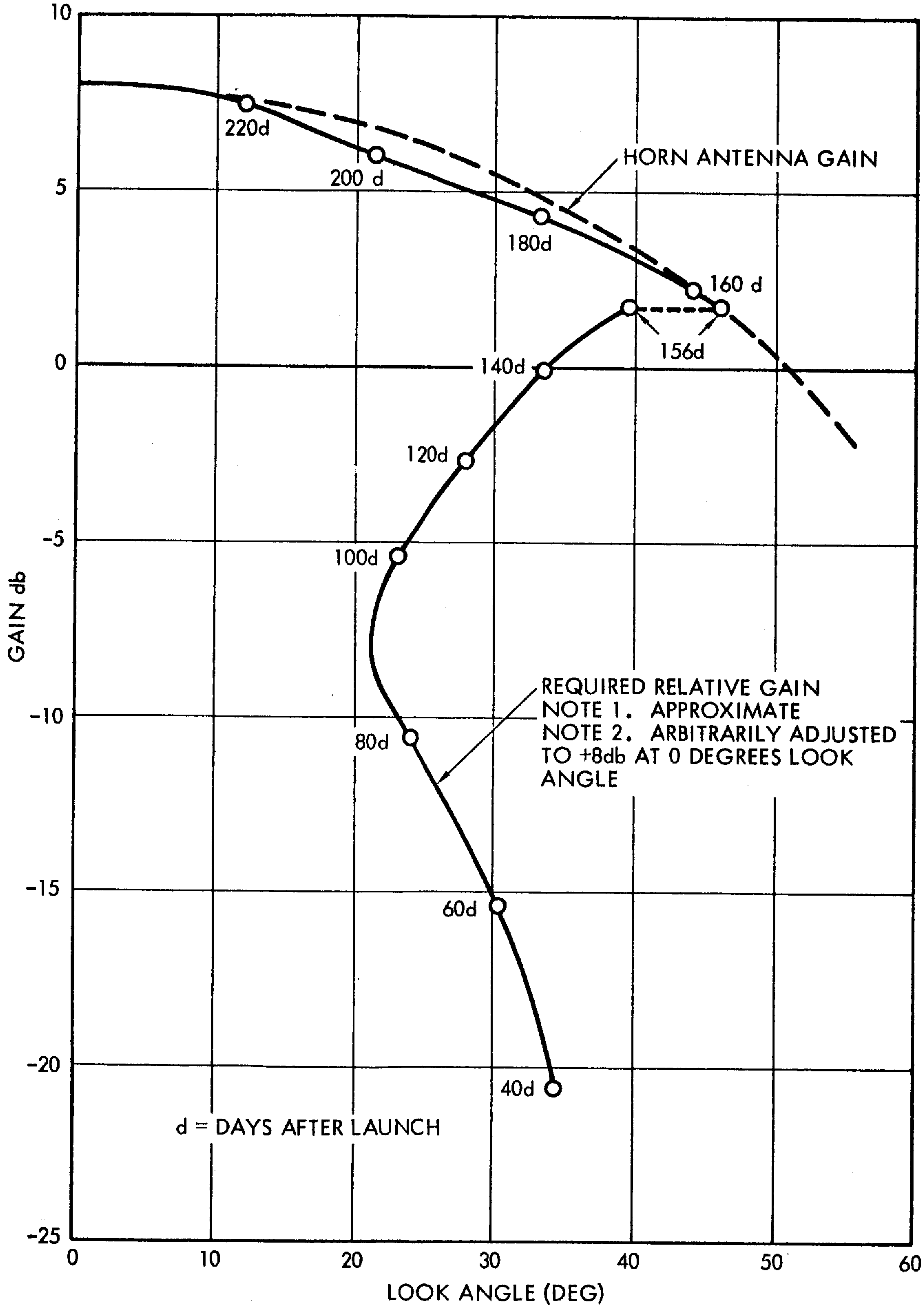

Figure VII-7. Horn Antenna Gain Versus Look Angle and Relative Gain Versus Look Angle for the Able-M Bus Spacecraft

curves it is seen that the signal strength remains essentially constant after reorientation at 156 days and until passage of Mars. Before reorientation the gain is in excess of that required. These curves are based on a minimum-energy trajectory and will differ for other trajectories. The lock angles used are with respect to the aft spin axis.

The omnidirectional antenna consists of two elements, one mounted on each end of the spacecraft. Each element has approximately hemispherical coverage, with the exception of a null along the spin axis, so that the combination of the two yields coverage throughout both hemispheres. Each element consists of a cylindrical sleeve approximately one half wavelength long; one is mounted around the horn, as shown in Figure VII-6, on the aft end and the other around the heat shield on the fore end. Each sleeve is excited in the TEM mode by four in-phase inputs at the base; the four feed-points are necessary to preclude the existence of higher-order modes. The radiation is linearly polarized parallel to a plane which includes the spin axis.

The power dividers are of the coaxial type employing nominally a single-section quarter-wavelength matching transformer. However, a two-section quarter-wavelength matching transformer can be used to minimize the VSWR at the two specific frequencies of interest, i.e., the transmit and receive frequencies, if necessary.

The 3-db 90-degree coupler is of stripline construction. It is constructed so as to yield a coupling of 3 db at both the transmit and receive frequencies.

The diplexer consists of two bandpass filters which connect the transmitter and receiver to the common antenna terminal. The filters each have four sections, or resonators, of the coaxial cavity type. Aperture or loop coupling is used to couple the cavities.

### 4. Digital Telemetry Unit (DTU)

The basic requirement for the telemetry unit of the communication subsystem is to accept diagnostic and status data from the spacecraft and status data from the spacecraft (bus) subsystems, convert it to digital form and apply it to the transmitter. Approximately 50 performance measurements will be needed and these will require a data rate of about 0.5 bits/sec, not including data from a miss distance indicator. Based on considerations of efficient modulation, high accuracy and ease of data handling, a digital PCM telemetry system has been chosen. Furthermore, it is planned to use a telemetry unit based on the design developed for the 698AM program by STL.

The DTU accepts both analog and digital measurements and processes these into a time-multiplexed PCM format. The analog inputs are converted to a 6-digit binary number while the digital inputs can have 7 digits. Each analog output signal will be normalized to a 0-3 volt range. Each input to the DTU corresponds to an 8-bit word in the output format. One bit of each word is always a one so that the ground demodulator can maintain bit synchronization. There are 32 words to the frame and four words in the frame are each time shared by 16 measurements. The output of the DTU is a 1024 cps subcarrier which is encoded with the time-multiplexed PCM. Each time a binary "one" occurs in the format the phase of the subcarrier is reversed. A "zero" causes no phase reversal.

A simplified block diagram of the digital telemetry unit is shown in Figure VII-8. The basic elements are the clock, programmer, multiplexer, analog-digital converter, combiner, and bi-phase modulator. The elements here are similar to the design used in the 698AM telemetry except for the interfaces and concepts of redundancy. The clock is a 1024 cps tuning fork oscillator which supplies timing pulses to the programmer and a sine wave to the bi-phase modulator. The programmer provides gating logic for the multiplexers, timing pulses for the analog-digital conversion, and sampling pulses for frame synchronization. The combiner combines the output of the A-D converter with digital inputs to form a composite time-multiplexed PCM signal which then modulates the subcarrier. The frame synchronization word is also inserted in the combiner.

Because of weight considerations, it is more efficient (by 2 pounds) to apply redundancy within the DTU rather than use two units. Therefore, both the programmer and A-D converter have redundant counterparts since these units have the greatest number of in-line components. The overall reliability

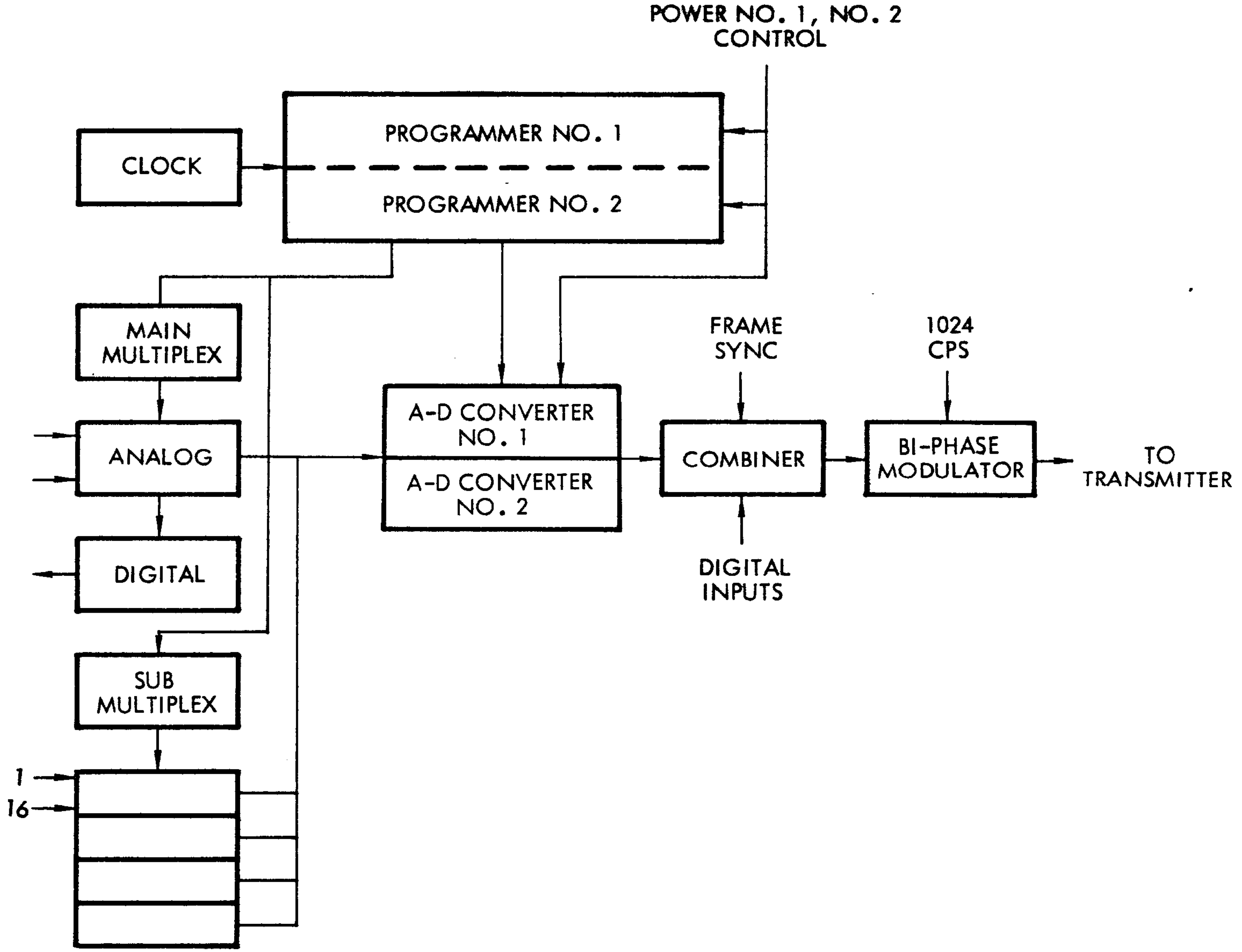
POWER NO. 1, NO. 2 CONTROL
CLOCK
PROGRAMMER NO. 1
PROGRAMMER NO. 2
MAIN MULTIPLEX
ANALOG
DIGITAL
SUB MULTIPLEX
1
16
A-D CONVERTER NO. 1
A-D CONVERTER NO. 2
FRAME SYNC
COMBINER
DIGITAL INPUTS
1024 CPS
BI-PHASE MODULATOR
TO TRANSMITTER

Figure VII-8. Digital Telemetry Unit

of the DTU for a period of 8 months and a space factor k = 2 is calculated to be 0.988. This figure is based on the fact that repetitive circuits can use much lower component failure rates, e.g., 20 x $10^{-9}$ per hour for transistors, and over half the circuits in the DTU are repetitive.

### 5. Command Decoder

Each of the two command decoders must accept approximately 20 discrete commands. Commands are routed to one or the other decoder based on an address code transmitted with the command. The command system should provide security against the insertion of false commands either by internal or external noise or purposeful generation of unauthorized commands. Finally, compatability with DSIF and other ground equipment must be assured. Considering these requirements, a digital system similar to those developed by STL for the Able-series and 698AM programs has been selected. Approximately 20 decoders of this type have been built, and three of these have operated in space for a total of 4000 hours without a failure.

The Able-M command (Figure VII-9) system will employ a frequency shift keyed (FSK) subcarrier at 125 cps. The subcarrier will phase modulate the command transmitter. A subcarrier frequency of 150 cps will represent a binary "one" while 100 cps will signify a "zero". The command word will consist of a 3-bitaddress and a 6-bit command and its binary complement. The complement is used to provide an error detection capability. The decoder output will be pulses designed to drive an 8 x 8 SCR matrix which in turn closes magnetic-latching relays. This mechanization provides a capability of receiving and executing 64 commands.

To minimize the expenditure of time and money, a command structure similar to that used on a previous program has been adopted. This consists of 31 pulse periods: 1 sync, 3 address, 3 address complement, 6 command complement, 6 command, 6 command complement, 6 command. Each pulse period will be one second long and the repetition rate will be one pulse per second. This command structure provides for addressing up to eight decoders and offers high resistance to the insertion of false commands. In order to establish synchronization, each command transmissionwill be preceded by a train of zeros to allow signal present circuitry within the decoder to enable the decoder for command reception.

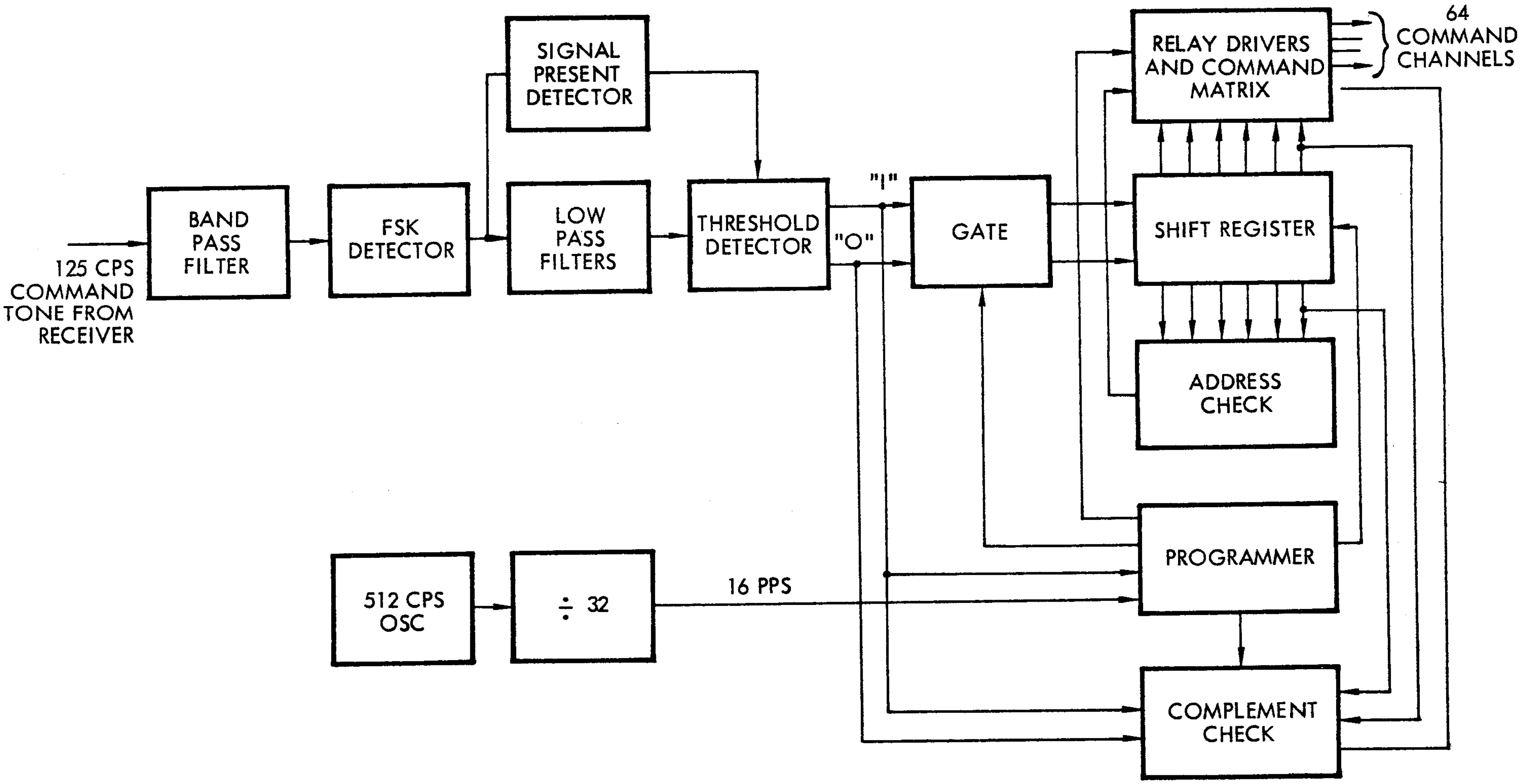
125 CPS COMMAND TONE FROM RECEIVER
BAND PASS FILTER
FSK DETECTOR
SIGNAL PRESENT DETECTOR
LOW PASS FILTERS
THRESHOLD DETECTOR
"1"
"O"
GATE
RELAY DRIVERS AND COMMAND MATRIX
64 COMMAND CHANNELS
SHIFT REGISTER
ADDRESS CHECK
PROGRAMMER
COMPLEMENT CHECK
512 CPS OSC
÷ 32
16 PPS

Figure VII-9. Command Decoder Block Diagram

To meet the reliability requirements of the mission a redundant connection of the two command decoders will be employed. Either of the decoders can drive the output SCR matrix. The decoder outputs will be filtered, detected and summed so that in the event of failure of either receiver both decoders will derive an input from the remaining receiver. A signal present relay in the receiver will disable the output if only noise is present.

# VIII. MISS DISTANCE MEASUREMENT

Fundamentally, the question of measuring miss distance is a trade-off between tracking accuracy and instrumentation complexity. To be of substantial value to the mission, the miss distance indicator should be better than tracking, which is, as shown in Section IV above, accurate at least to ± 0.25 Mars radii and probably much better.

Perhaps the most recent measurement of the Mars radius is quoted in a report by D. L. Lamar titled "Optical Ellipticity and Internal Structure of Mars." * The figure quoted here is 3388 ± 10 km at the solid surface of the planet and measured at the equatorial plane. The polar radius is probably about 37 km less. Since the atmosphere is about 80 km thick, a measurement of the polar diameter including the atmosphere would correspond to a measurement of the solid surface diameter at the equator.

A number of techniques for measuring miss distance were considered. Radar at the maximum possible range of 15,000 n mi is, of course, out of the question, and lasers are not sufficiently well developed for use in the 1964 missions. A very interesting technique would be to use the spacecraft as a receiver of 100 kw signals from Goldstone reflected off the surface of Mars. ** However, optical and infra-sensors appeared the most feasible and direct approach. Since it is possible that the spacecraft will pass the dark side of Mars, a preliminary analysis was made of an infra-red sensing device.

The assumptions made in this very preliminary design were:

1) Sensing the angular size of Mars is the only practical means for measuring miss distance.

---

* JPL Report RM-3127-JPL, June 1962.

** Such a space experiment is presently under study by the Radio and Propagation Laboratory at Stanford University under the direction of Professor Eshelman. Work by this laboratory and by STL show that this technique can be used, even at the present time, at 400 mc using the Stanford 150 foot antenna and 300 kw transmitter.

2) The probe spin rate is sufficiently high so that translation during a single spin revolution may be neglected.

3) The spin rate will be known accurately.

4) The sensor should function regardless of the attitude of the spacecraft.

The infra-red thermistor bolometer seems the simplest method of determining the distance of closest approach to the planet. It would be desirable for the measurements to be made at two wavelength bands; 1) at 14-17 microns, which would correspond to the maximum flux due to $CO_2$ molecules and hence would include the Martian atmosphere, and 2) a shorter wavelength region (6-11.5 microns) which would give a measure of the surface diameter since this region presents a window through the $CO_2$ and $H_2O$. The reflected radiation is also completely negligible at these wavelengths ($>5$ microns). These two measurements would have the additional advantage of yielding a better figure for the thickness of the Martian atmosphere. In addition, if the total relative intensities of the radiation at these two wavelengths could be measured, the surface temperature could be determined by fitting these values to the appropriate blockbody radiation curve without the necessity of an absolute energy calibration. The properties of Earth, Mars and Venus are shown in Figure VIII-1.

## A. SENSING SYSTEM

The sensing end of the miss distance measuring device is shown in Figure VIII-2 for a single sensor. Another sensor could very easily be added. A thermistor bolometer is mounted in the focal plane of a telescope having a small field of view (approximately 1 degree total). The optical axis of the telescope is rotated by means of constant-speed revolving mirror so that it sweeps out a plane in space; and the telescope-mirror combination is mounted such that this plane contains the vehicle spin axis. As shown in Figure VIII-2, the field of view is blocked during half of each mirror revolution by the spacecraft and the limitations of the viewing window.

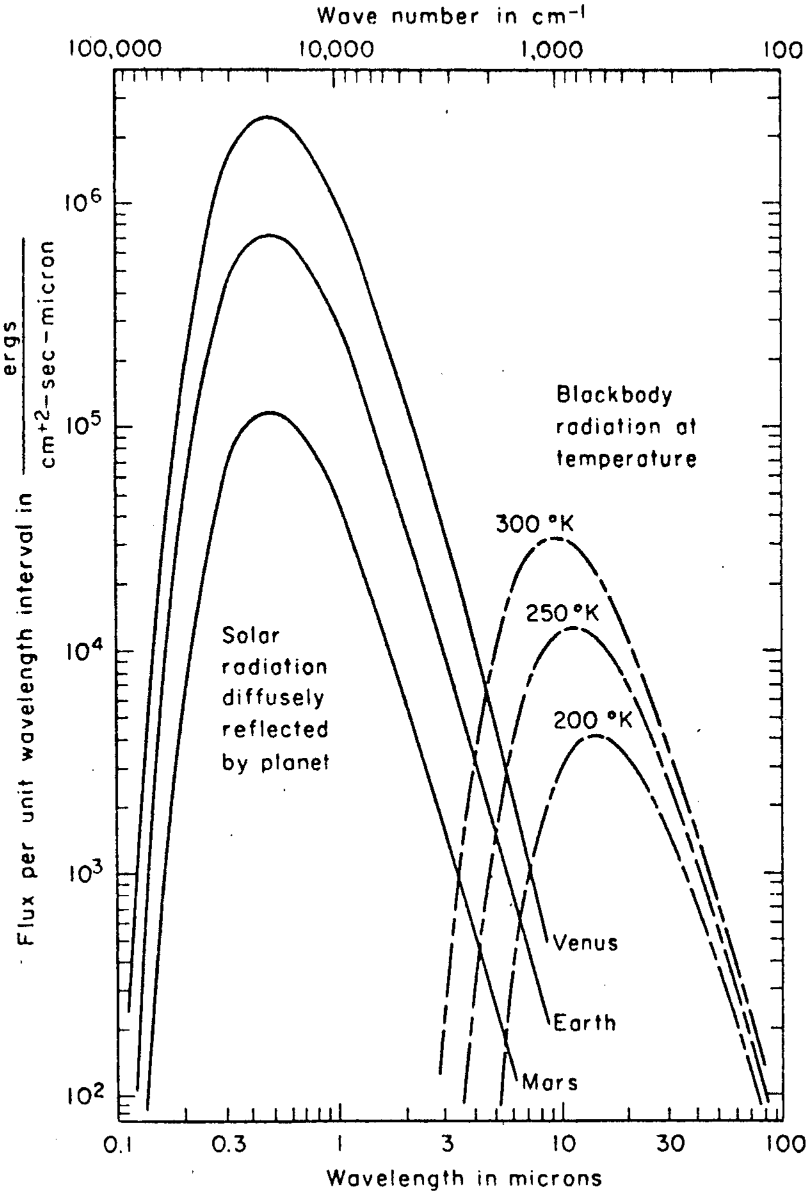

Plot of flux of reflected solar or emitted planetary radiation as a function of wavelength or wave number. The emitted radiation is merely blackbody radiation at the specified temperature (emissivity of one). The reflected or scattered solar radiation takes into account the change of solar constant due to average distance from the Sun, and assumes an albedo (diffuse reflectivity) of 0.7 for Venus, 0.4 for Earth, and 0.15 for Mars. The distribution of the solar spectrum is taken to be that of a 5783°K blackbody. (Calculated by N. T. Divine, RAND Corp.)

Figure VIII-1. Plot of Flux-Reflected Solar on Emitted Planetary Radiation

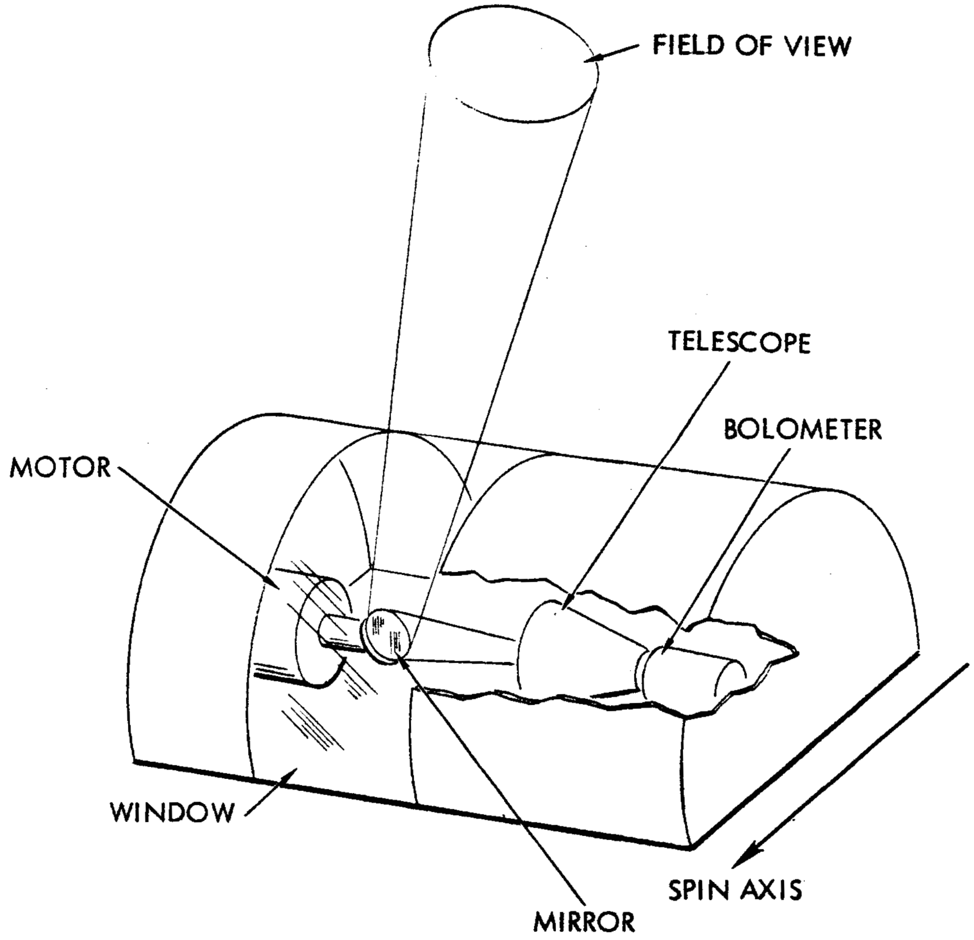
FIELD OF VIEW
TELESCOPE
BOLOMETER
MOTOR
WINDOW
SPIN AXIS
MIRROR

Figure VIII-2. Sensor Elements of Miss Distance Indicators

The rate of mirror rotation is much greater than the vehicle spin rate so that during one spin revolution, the field of view of the telescope sweeps out the entire $4\pi$ steradians surrounding the vehicle. When the field of view crosses the target planet, a pulse is seen on the output of the thermistor bolometer. The width of this pulse is a measure of the diameter of the cap of the spherical planet cut by that scan . Thus, the pulse of maximum width occuring during a single spin revolution is a measure of the planet angular diameter as seen from the vehicle. (The sun will probably not be seen by the sensor or, if it is, it can easily be rejected.) It has been tacitly assumed in the above paragraph and also in the section to follow that the spin axis does not intersect the planet. However, the present scheme can be extended to include the case with increased circuit complexity or the blocked period can be estimated from earlier and later data.

## B. PROCESSING ELECTRONICS

A block diagram of the signal processing circuitry is shown in Figure VIII-3. An AC amplifier following the thermistor bolometer amplifies the pulses obtained by scanning the field of view across the planet. These pulses are then clipped since it is the width of the pulse which carries distance information. The clipped pulses enable an "and" gate and one of the counters, which had contained zero count, counting clock pulses until the end of the signal pulse. The outputs of each counter are converted to analog signals and continually compared in the comparator circuitry. When the end of the signal pulse is reached, the sequencing logic acts upon the comparator output and clears the counter to receive future clock pulses by means of the steering network.

The circuitry is now prepared to accept the next signal pulse and the above sequence of events is repeated until a reset pulse, indicating that the vehicle has completed a spin revolution, is received by the sequencing logic. At this time, the sequencing logic clears the counter with the lower total count and then enables the sample and hold circuit so that it retains the output of the uncleared counter. This counter is then cleared and the circuitry is ready for another measuring cycle. It can be seen that the output of the sample and hold circuit

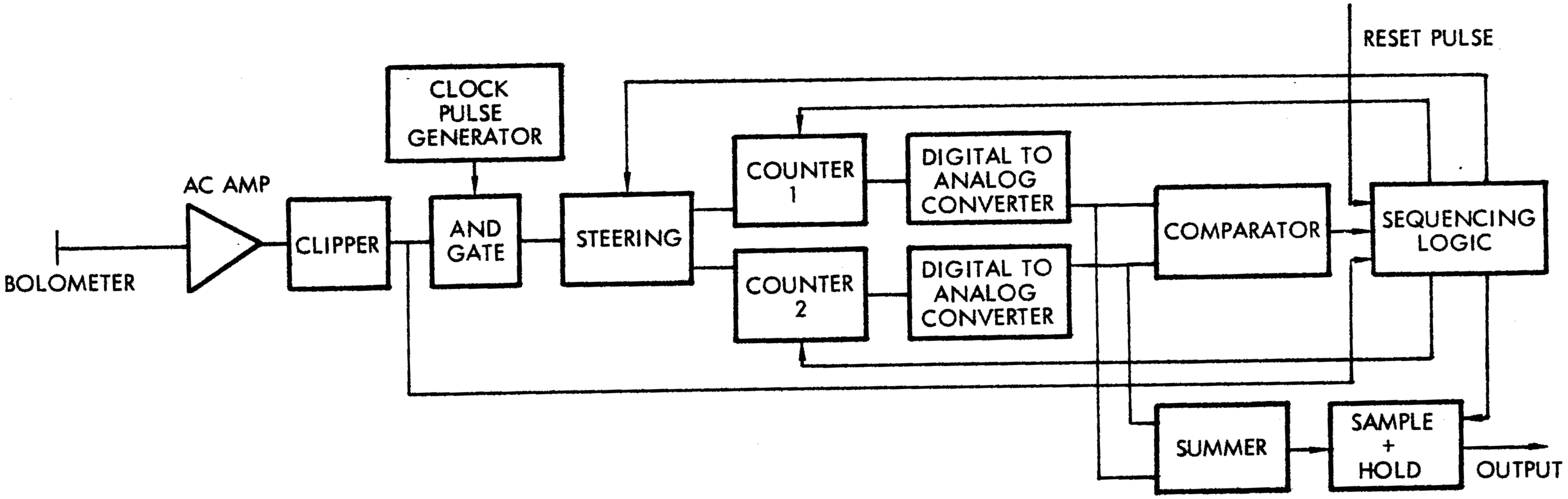

BOLOMETER
AC AMP
CLIPPER
CLOCK PULSE GENERATOR
AND GATE
STEERING
COUNTER 1
COUNTER 2
DIGITAL TO ANALOG CONVERTER
DIGITAL TO ANALOG CONVERTER
COMPARATOR
SEQUENCING LOGIC
RESET PULSE
SUMMER
SAMPLE + HOLD
OUTPUT

Figure VIII-3. Block Diagram of Electronics for Miss Distance Indicator

is a measure of the angular diameter of the planet as seen from the vehicle. This signal may be recorded for later transmission to earth and the miss distance may then be computed from the maximum diameter measured. Also available from this device are the velocities of approach and recession of the vehicle with respect to the planet.

## C. ACCURACY

It appears comparatively easy to build the sensor to work to an accuracy of about 1 percent on the angular diameter measurement if the maximum distance of closest approach is 15,000 n mi and 0.5 percent or less at 1,000 n mi. Since the diameter of Mars is apparently known to within about a small fraction of a percent, improving the accuracy of the sensor is desirable. (It is possible that the tracking accuracy may actually assist in determining the Mars diameter should the sensor achieve the predicted accuracy.)

## D. SIZE, WEIGHT, AND POWER

The telescope, mirror, mirror drive motor, and bolometer are contained in a box, external to the spacecraft, of dimensions 3" by 2" by 1". The electronics are contained in a box of dimensions 4" by 4" by 1".

The weight of the entire unit will be less than 1.5 lbs. The power consumed by the subsystem will be about 5 watts; however, this power consumption is not crucial since the unit is only required to operate for a period of, at most, a few hours.

## EQUIPMENT LIST

1. DIVIDER
2. DIPLEXER
3. COUPLER
4. RECEIVER
5. DECODER
6. DIGITAL TELEMETRY UNIT
7. DRIVER
8. POWER AMPLIFIER NO. 1
9. POWER AMPLIFIER NO. 2
10. SWITCH

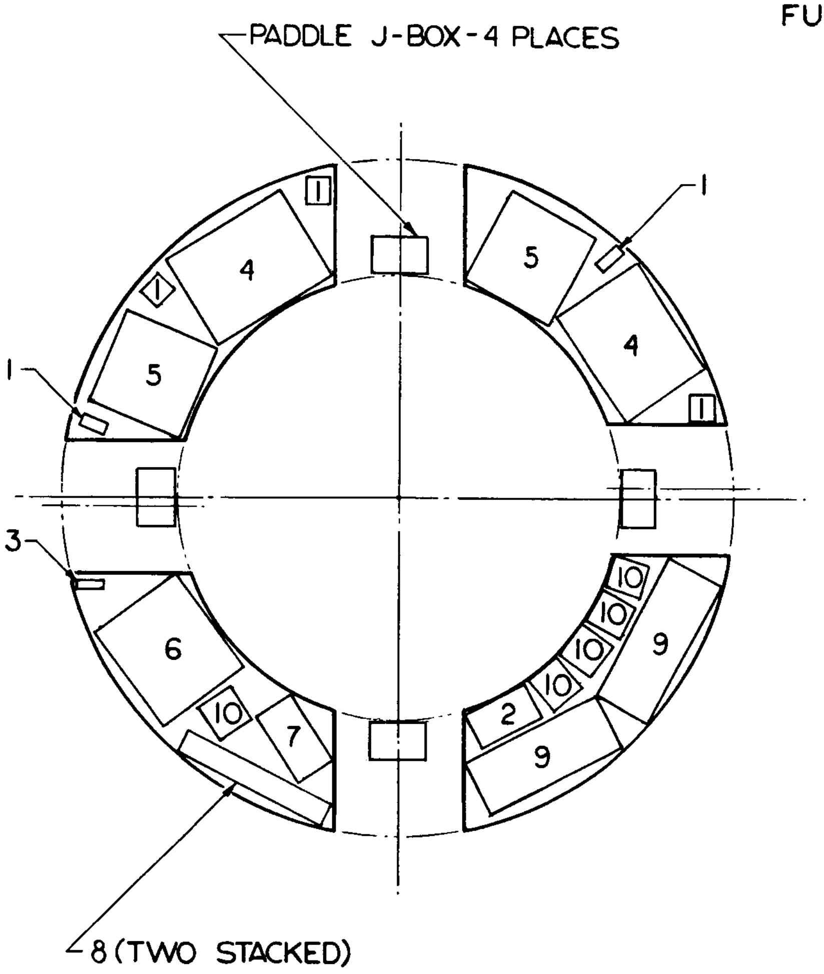
PADDLE J-BOX-4 PLACES
1
5
4
1
1
1
5
4
1
3
6
10
7
8 (TWO STACKED)
2
10
10
10
10
9
9

PLAN VIEW OF EQUIPMENT PANEL

FUEL

OMI

COV
CHA

A

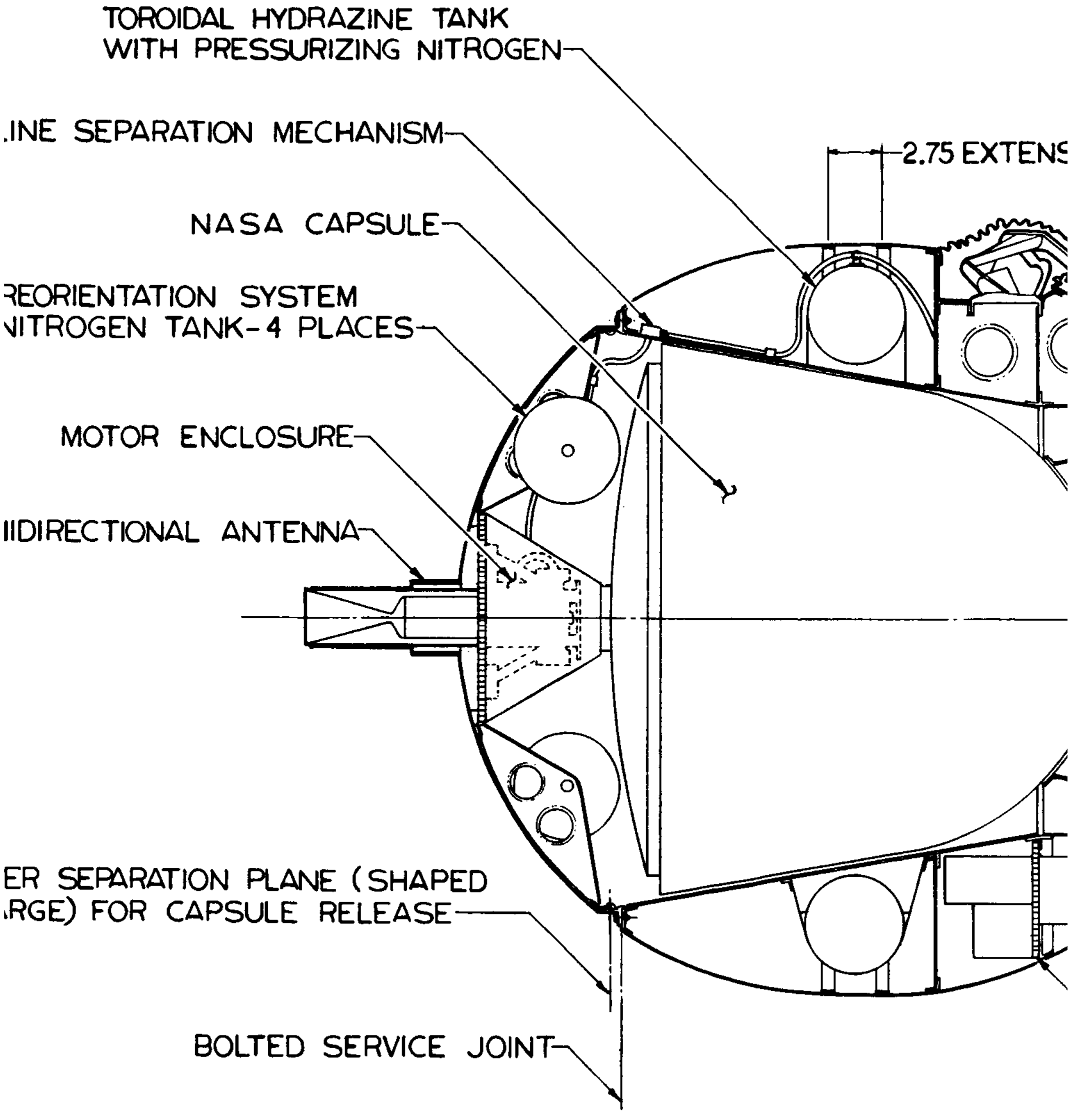
TOROIDAL HYDRAZINE TANK
WITH PRESSURIZING NITROGEN
INE SEPARATION MECHANISM
2.75 EXTENS
NASA CAPSULE
REORIENTATION SYSTEM
NITROGEN TANK-4 PLACES
MOTOR ENCLOSURE
IIDIRECTIONAL ANTENNA
ER SEPARATION PLANE (SHAPED
RGE) FOR CAPSULE RELEASE
BOLTED SERVICE JOINT
0

BLE-M BUS AND NASA CAPSULE

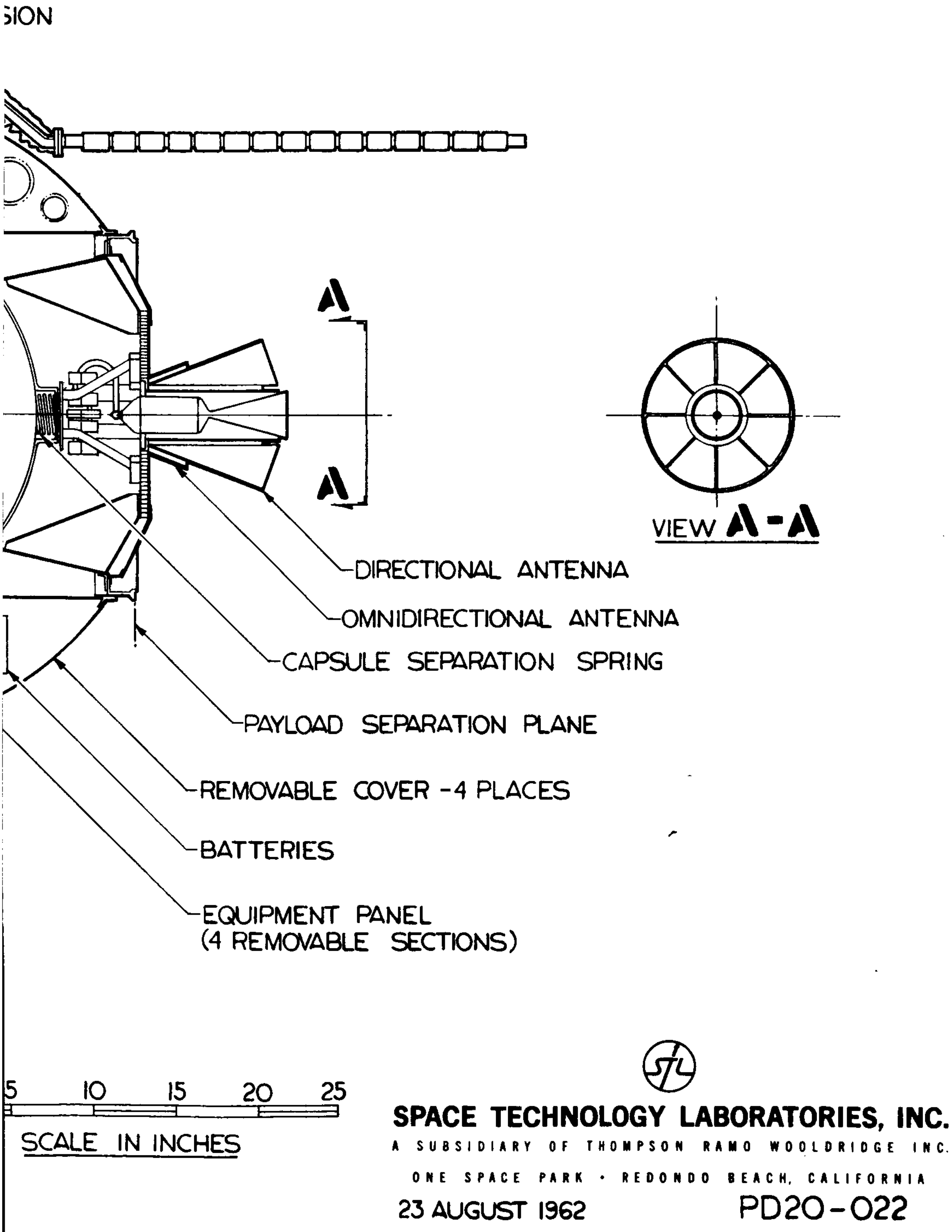
SION
A
A
VIEW A-A
DIRECTIONAL ANTENNA
OMNIDIRECTIONAL ANTENNA
CAPSULE SEPARATION SPRING
PAYLOAD SEPARATION PLANE
REMOVABLE COVER -4 PLACES
BATTERIES
EQUIPMENT PANEL
(4 REMOVABLE SECTIONS)
5 10 15 20 25
SCALE IN INCHES
STL
SPACE TECHNOLOGY LABORATORIES, INC.
A SUBSIDIARY OF THOMPSON RAMO WOOLDRIDGE INC.
ONE SPACE PARK • REDONDO BEACH, CALIFORNIA
23 AUGUST 1962
PD20-022

Figure IX-1. Mars Encounter Spacecraft

3

# IX. MARS ENCOUNTER SPACECRAFT DESIGN

The modifications required of the Able-M spacecraft to make it suitable for Mars Encounter Mission have been investigated. Although not all areas have been studied in equal detail, the major changes required have been identified and accounted for. However, specific details which depend upon the trajectory selected, such as solar array output, thermal control, reliability and lifetime, have not been analyzed.

The Mars Encounter Spacecraft (Figure IX-1) which contains the NASA Mars landing capsule, is a modified Able-M spacecraft and utilizes most of the components from the the Able-5 vehicle. The basic concept of a spinning vehicle with a spherical shell using the Able-5 temperature control blades, hydrazine motors fore and aft for vernier corrections, and four unfolding solar paddles remains unchanged. The main difference between the Able-M and this encounter vehicle is the internal configuration.

The Able-M spacecraft had a large, centrally located, spherical hydrazine tank. This space is used for the entry capsule of the proposed Mars Encounter Spacecraft. The forward portion of the spacecraft is a cover which, when separated from spacecraft, allows the Mars entry capsule to be ejected away from the spacecraft bus. The hydrazine is carried in a toroidal tank which surrounds the capsule. Since the diameter of the capsule and toroidal tank is larger than that of the Able hydrazine tank, a new equipment shelf, somewhat lower on the spacecraft, replaces the Able equipment shelf. The batteries are mounted on the bottom of this shelf.

The two Able-5 four-start monopropellant hydrazine engines, one forward and one aft, provide midcourse corrections. A horn antenna is mounted around the aft nozzle with an omnidirectional antenna outside of the horn. Another omnidirectional antenna is mounted around the forward nozzle. The cold gas reorientation system is taken directly from Able-M and is sized for a single reorientation manuever after about 150 days for the 1964 mission. Nitrogen for this system is stored in four spherical tanks located on the forward cover of the spacecraft. The monopropellant motor assemblies are identical to those used on the Able-5 vehicles. Using the existing hydrazine motor assemblies and installing the NASA capsule required that the spacecraft be lengthened by 2.75 inches over the Able-M envelope. This approach was followed rather than a redesign of the motor assemblies in order to avoid an extensive development and test program of a new hydrazine motor system.

The installation of a jettisonable capsule in the space formerly occupied by the hydrazine tank requires a redesign of the major portion of the structure. The booster adapter structure, the tank support structure, and the aft motor support structure are taken from Able-M. A conical sheet metal structure surrounding the capsule, extends forward from the tank support structure to the forward cover service joint. The toroidal tank and equipment platform attach to this conical structure. The forward cover, which supports the forward motor assembly and reorientation nitrogen tanks, holds the capsule in place against a spring. The forward cover is separated from the spacecraft by firing a shaped charge just forward of the service joint and the capsule is ejected by the compressed spring.

The spacecraft power supply system, including the solar cell paddles and batteries is identical to the one used on the Able-M vehicle. The thermal control system, employing rotating blades, is also identical to the one used on Able-M. Able-M bus plus NASA capsule weight breakdown is given in Table IX-1.

## Table IX-1. Able-M Bus Plus NASA Capsule

### Weight Breakdown

| | |
|---|---|
| NASA Capsule | 94.0 |
| Structure | 93.0 |
| Temperature Control | 21.4 |
| Communication and Data Handling (Including antenna system) | 46.7 |
| Power Supply System | 104.3 |
| Reorientation System | 12.5 |
| Damper | 1.0 |
| Propulsion System | 34.2 |
| Dry Weight Subtotal | 407.1 lb |
| Hydrazine (for 750 ft/sec) | 44.0 |
| Start Fuel | 0.2 |
| Nitrogen for Pressurizing | 1.2 |
| Payload Gross Weight | 452.5 lb |